CHEMO-MECHANICS OF DUST AND MUD ON PROTECTIVE SURFACES

BY
Ghassan Hassan H. Abdelmajid

A Thesis Presented to the
DEANSHIP OF GRADUATE STUDIES

KING FAHD UNIVERSITY OF PETROLEUM & MINERALS

DHAHRAN, SAUDI ARABIA

In Partial Fulfillment of the
Requirements for the Degree of

MASTER OF SCIENCE

In

MECHANICAL ENGINEERING

May 2016

KING FAHD UNIVERSITY OF PETROLEUM & MINERALS

DHAHRAN- 31261, SAUDI ARABIA

DEANSHIP OF GRADUATE STUDIES

This thesis, written by **Ghassan Hassan Hajhamed Abdelmajid** under the direction thesis advisor and approved by his thesis committee, has been presented and accepted by the Dean of Graduate Studies, in partial fulfillment of the requirements for the degree of **MASTER OF SCIENCE IN MECHANICAL ENGINEERING.**

Dr. Syed Ahmed M. Said
(Advisor)

Dr. Zuhair Mattoug Gasem

Department Chairman

Dr. Bekir Sami Yilbas

(Co-Advisor)

Dr. Salam A. Zummo
Dean of Graduate Studies

عمادة الدراسات العليا
DEANSHIP OF GRADUATE STUDIES

Dr. Nasser M. Al-Aqeeli

(Member)

25/5/16

Date

Dr. Numan Abu-Dheir

(Member)

Dr. Mazen Mohammad Khaled

(Member)

بسم الله الرحمن الرحيم

To my dear brother FARIS, May Allah bless his soul, his memory will reside in me perpetually

For my parents Hassan & Zeinab, and my beloved brothers, Ghofary &Tuga for their affection, love, endless support and prayers of day and night which helped me to achieve such success.

ACKNOWLEDGMENTS

First of all, praise be to Allah almighty, most beneficent and merciful.

I acknowledge, King Fahd University of Petroleum and Minerals (KFUPM) for offering me this opportunity to accomplish my Master of Science in Mechanical Engineering. I would like to express my sincere gratitude to my advisor Dr. Syed A.M.Said for his guidance, enthusiasm, encouragement and the imparting of his knowledge and expertise. My appreciation and thanks are also extended to my co-advisor Dr. Bekir Sami Yilbas for his invaluable assistance and immense knowledge. I convey my thanks to my committee members for the help and valuable assistance.

I would like to thank Dr. Asif Matin and others who contributed to this research in any way, shape or form. Finally, I express my gratefulness to my parents, family and friends for endless love, supplication. I couldn't have made this work without you all.

TABLE OF CONTENTS

ACKNOWLEDGMENTS VI

TABLE OF CONTENTS VII

LIST OF TABLES X

LIST OF FIGURES XI

ABSTRACT XIV

ملخص الرسالة XV

CHAPTER 1 INTRODUCTION 1

1.1 Research motivation 4

1.2 Objectives of research 5

1.3 Thesis Overview 5

CHAPTER 2 LITERATURE REVIEW ..... 7_Toc450639690

2.1 Introduction 7

2.2 Effect of dust on PV modules output power 8

2.3 Effect of dust deposition on PV modules output in Saudi Arabia and the Middle East 9

2.4 The impact of the wind on Dust deposition 11

2.5 Humidity and dust adhesion 12

2.6 The effect of adhesion force and cohesion force on dust particles and surfaces 16

CHAPTER 3 MUD CHEMISTRY 20

3.1 Introduction 20

3.2 Nature of water chemistry 22

3.3 Influence of dissolved ions on water 22

3.4 Mechanisms for Soil-Water interaction 23
3.4.1 Hydrogen bonding 23

3.5 Effect of power of hydrogen (PH) 23

3.6 Exchange capacity and common Ions in mud and clay minerals 24

3.7 Decomposition process 25
3.7.1 Dissolution 25

3.8 Mud drying 26

CHAPTER 4 EXPERIMENTAL STUDY 29

4.1 Introduction 29

4.2 Dust collection 31

4.3 Mechanical testing 32
4.3.1 Mud pellets preparation 32
4.3.2 Tensile testing for dry mud pellets 32
4.3.3 Scratching test 37
4.3.4 Sample preparation for scratching test 38

4.4 Microstructure characterization 40
4.4.1 Sample preparation (Specimens coating) 40
4.4.2 Scanning electron microscopy (SEM) 42
4.4.3 X-Ray Diffraction (XRD) 44
4.4.4 Atomic force microscopy (AFM) 44
4.4.5 3D optical microscope 46
4.4.6 Energy Dispersive Spectroscopy (EDS) 47

4.5 Chemical investigation group 49
4.5.1 Fourier transform infrared spectroscopy (FTIR) 49
4.5.2 PH measurement 52

CHAPTER 5 RESULTS AND DISCUSSION .... 53_Toc450639732

5.1 Characterization of Dust Particles: 53

5.2 Characterization of Mud Solution and Dry Mud: 57

5.3 Mechanical Properties of Dry Mud: 67

CHAPTER 6 CONCLUSIONS AND RECOMMENDATION.................. 76_Toc450639738

6.1 Conclusions 76

6.2 Recommendation.. 78

REFERENCES.. 79

APPENDICES 85

APPENDICES A 85

APPENDICES B 86

APPENDICES C.. 89

APPENDICES D 93

VITAE 97

LIST OF TABLES

Table 2.1 The effect of rainfall on PV modules performance 11

Table 2.2 The dust effect on PV modules covers in different locations 15

Table 2.3 Different studies on particles adhesion measurements 19

Table 3.1 Decomposition of soil and minerals with decomposition 26

Table 4.1 The input parameters used during the scratching test 38

Table 5.1 Elemental composition of the dust particles (wt%). 54

Table 5.2 Inductively coupled plasma spectroscopy (ICP) data 58

Table 5.3 Elemental composition of the mud crystals 62

Table 5.4 Elemental composition of dry mud residues on glass surface (wt%). 62

Table 5.5 Adhesion work obtained from the tangential force measurements.................. 71

LIST OF FIGURES

Figure 1.1 The process of environmental dust deposition on the protective surfaces 3

Figure 2.1 Relation between humidity and adhesion [7] 14

Figure 2.2 Optical performance vs relative humidity, during exposure to dust. 14

Figure 3.1 The process description of dust water interaction. 20

Figure 3.2 The zones of ion-water interaction [66]. 22

Figure 3.3 Dust particles reactions with molecules of polarized water 23

Figure 3.4 The charges located on the mud particles edges 24

Figure 3.5 The effect of the cation size on the cation migration into a mud interlayer 27

Figure 3.6 The effect of water evaporation on dust particles during mud drying 27

Figure 3.7 The process of dust-water interaction.. 28

Figure 4.1 The process flow chart.. 30

Figure 4.2 The dusty and clean photovoltaic modules 31

Figure 4.3 The assembly of non-fractured mud pellet sample... 33

Figure 4.4 The mechanical drawing for mud pellet specimen used for tensile testing..... 34

Figure 4.5 The load variation with the displacement... 35

Figure 4.6 The micro-electric machine for the mud pellets tensile testing....................... 36

Figure 4.7 The mud pellet specimen for tensile testing 36

Figure 4.8 The specimen surface during scratching test 37

Figure 4.9 Scratching test machine.. 39

Figure 4.10 Dry mud solution samples used in scratching test.. 39

Figure 4.11 The gold sputter coater machine used to coat the mud pellets fractured...... 41

Figure 4.12 The mud specimen fracture surface with gold coating................................ 41

Figure 4.13 Shows the scanning electron microscopy components 43

Figure 4.14 The X-Ray Diffraction (XRD) machine.. 45

Figure 4.15 The samples used in XRD characterization.. 45

Figure 4.16 3D optical microscope made by Bruker Company 47

Figure 4.17 The gold coated sample used for SEM and EDS analysis............................ 48

Figure 4.18 The SEM image for scanned area (100 µm) for the elemental analysis...... 48

Figure 4.19 FTIR testing system... 50

Figure 4.20 The analysis process of FTIR testing method 51

Figure 4.21 The pH meter device used for mud solution pH measurements.................. 52

Figure 5.1 SEM micrograph of dust particles.. 55

Figure 5.2 XRD diffractogram for dust particles... 56

Figure 5.3 Temporal variation mud pH of mud solution... 58

Figure 5.4 SEM micrograph of mud crystallized structures... 59

Figure 5.5 The FTIR experimental test data.. 60

Figure 5.6 SEM micrograph of mud surface 63

Figure 5.7 SEM micrograph of dry mud cross-section.. 64

Figure 5.8 SEM micrograph of dry removed glass surface 65

Figure 5.9 AFM micro-images of glass surface after dry mud removed......................... 66

Figure 5.10 Friction coefficient for dry mud solution, as received glass surface and dry mud removed surface.. 68

Figure 5.11 Tangential force obtained from scratch tests.. 69

Figure 5.12 Optical image of the fractured pellet surface after tensile tests.................... 72

Figure 5.13 The data obtained from tensile testing for sample (1) 73

Figure 5.14 The data obtained from tensile testing for sample (2) 74

Figure 5.15 The data obtained from tensile testing for sample (3) 75

ABSTRACT

Full Name : Ghassan Hassan Hajhamed Abdelmajid

Thesis Title : Chemo-Mechanics of dust and mud on protective surfaces

Major Field : Mechanical Engineering

Date of Degree : May 2016

Environmental dust and mud formed from dust particles in humid air ambient influence significantly optical characteristics of photovoltaic panel cover glasses. In the present study, characterization of dust environmental particles and chemo-mechanics of dry mud formed from dust particles are examined. Analytical tools including scanning electron microscope and atomic force microscopes, energy dispersive spectroscopy, particle sizing, and X-ray diffraction are used to characterize dust particles. Micro/nano tribometer is incorporated to measure tangential force and friction coefficient during dry mud removal from glass surface. Tensile tests are carried out to assess the binding forces of dry mud pellets, which compose of adhesion and cohesion forces. Mud residuals on dry mud removed glass surface are examined and optical transmittance of the glass is measured. It is found that dust particles possess alkaline and alkaline earth metals, which dissolve in water condensate while forms mud solution, which has pH in the order of 0.75. Mud solution forms a thin liquid film at the interface of dust particles and surface. Upon drying mud solution, crystals are formed, which increased adhesion work required to remove dry mud. The Optical transmittance of dry mud removed glass samples is reduced because of dry mud residues at the surface.

ملخص الرسالة

الاسم الكامل: **غسان حسن حاج حمد عبد الماجد**

عنوان الرسالة: **الخصائص الكيميائية والفيزيائية لزرات الغبار المتراكم علي الأسطح الوقائية لأنظمة التوليد بإستخدام الطاقة الشمسية**

التخصص: **الهندسة الميكانيكة**

تاريخ الدرجة العلمية: مايو 2016

تعتبر الطاقة الشمسية من أهم مصادر توليد الطاقة المتجددة, ولكنها تتأثر ببعض العوامل الطبيعية كدرجات الحرارة والرطوبة بالأضافة إلي سرعة الرياح والغبار الجوي . تنخفض كفاءة الأداء للخلايا الشمسية المستخدمة لتوليد الطاقة الكهربائية بتكون طبقات طينية رقيقة ,ناتجة من تراكم زرات الغبار العالقة في الغلاف الجوي الرطب علي سطح اغطيتها الزجاجية ; مما يؤدي إلي إنخفاض كفاءة التوليد بشكل ملحوظ. تتطرقت هذة الأطروحة لدراسة خصائص جزيئات الغبار والقوى المؤثرة عليها من المنظورين الفيزيائي والكيميائي. أستخدمت العديد من التقنيات التي بدورها ساهمت في تحديد خصائص الغبار المتراكم الكيميائية والفيزيائية كمجهر المسح الإلكتروني ومجهر القوى الذرية والتحليل الطيفي وتشتت الطاقة بالأضافة إالي حيود الأشعة السينية. قيس كل من معامل الإحتكاك والقوى المماسية اللازمة لفصل جزيئات الطين الجاف المتراكم من الاسطح الزجاجية للخلايا الشمسية باستخدام جهاز الترايبوميتر. أجري إختبار الشد لحساب قوى الألتصاق والتماسك بين حبيبات الطين الجاف الناتج من تراكم زرات الغبار الجوي. أجريت بعض الدراسات علي حبيبات الطين المتبقية علي أسطح الأغطية الزجاجية وأثرها علي نفاذية الزجاج للأشعة الشمسية. وجد أن المحلول الناتج من إذابة زرات الغبار في الماء ذو طابع قلوي بدرجة حموضة 0.75 فقط. وجد أن بعض البلورات الملحية تتكون أثناء تبخر الماء من محلول الطين مما يزيد من قوي الألتصاق بين الحبيبات والأسطح الزجاجية للخلايا الشمسية.

1

CHAPTER 1

INTRODUCTION

The demand for energy has been increasing significantly at high rate due to lifestyle, development in technology, industrialization as well as the growth of global population with a rate more than 2% [1]. Energy production need to be cost-effective, sustainable and environmentally friendly, which focuses to utilize sustainable resources and maintain effective energy consumption. The sun is a major source of earth’s energy which emits 38 x 10^{19} megawatts in the form of heat and light [2]. The cost effective utilization of this source of renewable energy remain challenging and hence more research and development should be carried at out in this regard.

Effective solar energy harvesting is of tremendous importance, as a solution for the increasing demand of power consumption that is coupled with the depletion of fossil fuels resources. The sector of renewable energy needs to provide a considerable share of future development in order to take advantage of incident solar radiation as a source of clean energy without involving any emission product. The fields of solar energy applications have grown steadily especially in electric power generation sector. Several factors motivated the use of renewable energy such as global warming reduction, low maintenance requirement and cost effectiveness for remote areas with no electric grid connections.

Photovoltaic solar energy technologies and their applications have received global research attention and becoming an interesting area for financial investments[1] and [2]. The power output from solar energy systems depends on several environmental factors such as wind velocity, rainfall, ambient temperature and dust accumulation on the system protective surfaces. The nature of dust accumulation and its effect on the PV module performance needs current attention. The literature review indicated the importance of the influence of dust deposition on protective surfaces in the energy production [5]

The effect of dust and aerosol minerals on anthropogenic still not obvious, because of uncertainties of product microscopic levels such as particles distribution, shape and size [6]. On the other hand, the effect of dust soiling on solar PV modules has a great impact on light transmission, through protective covers of solar active materials. This soiling process on solar panels - because of airborne dust- happens due to dry dust deposition because of gravitational settling and wet particles deposition. Such soiling absorbs and reflects incident solar radiation leading to a reduction of light transmittance. The process of dust and minerals movement, soiling and its effect on solar panels performance are summarized in the figure (1.1).

Various problems are associated with dust deposition on solar energy protective surfaces such as a reduction in the output energy yield, difficulty in predicting the power output due to dust deposition losses, time and cost associated with cleaning solar protective surfaces. Self-cleaning or cost effective removal of dust particles is still remaining challenging. The dust particles absorb water vapor in the humid air environments and forms mud at the surfaces and become hard to remove. Therefore, reducing the amount of accumulated dust on the solar energy protective surfaces is of immense importance. This study focuses on the dust deposition effect and the dust particles characteristics of dust accumulation photovoltaic modules surfaces; Located in Dhahran, Saudi Arabia which has a hot and humid environmental conditions with frequent dust storms[7].

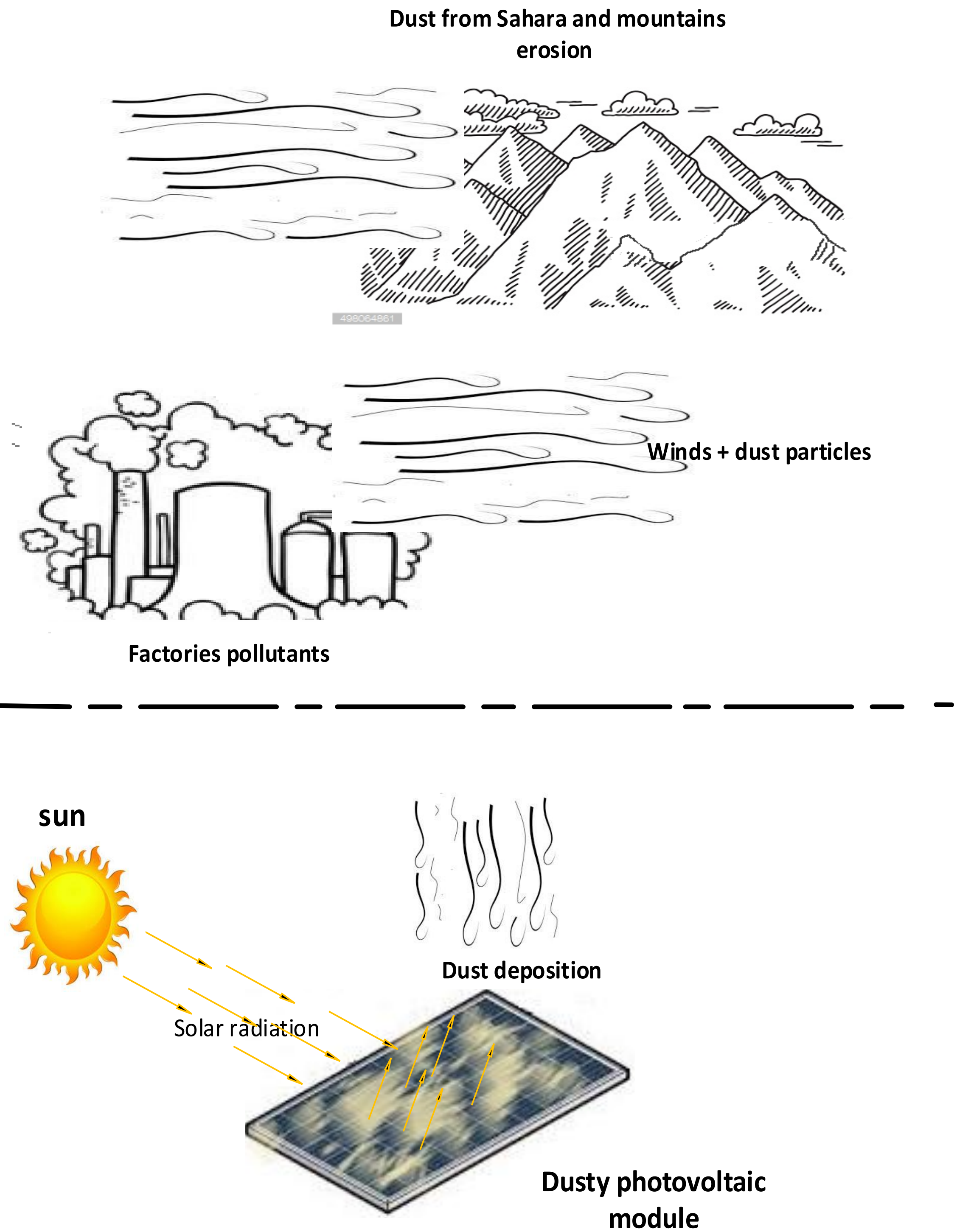

Figure 1.1. The process of environmental dust deposition on the protective surfaces

1.1 Research motivation

Recent changes in climate results in severe and frequent dust storms around the world, particularly in Saudi Arabia. Dust settlement onto the surfaces located to open environments causes irrecoverable damages on surfaces and lowers the system performance, such as those associated with solar thermal and solar photovoltaic applications. There are many surface treatment methods being reported in the literature for minimizing the dust effect on the surface characteristics and surface performance [31, 32]. However, self-cleaning or cost effective removal of dust particles from such surfaces still remains challenging. Moreover, the dust particles absorb water vapor in humid air environments and form mud at the surface. Once the mud is dried at high-temperature conditions under the solar radiation, it becomes difficult to remove from the surfaces. This is because of the fact that the adhesion force between the dry mud and surfaces is not only governed by the physical forces, such as van der walls forces, but chemically induced forces, such as forces due to ionic and covalent bonding. Although some studies on adhesion of particles on the surface are reported in the literature [27] and [30]; the physical and chemical phenomena still needs further exploration. Therefore, the current study considers the cohesion and adhesion forces of dry mud on PV glass surfaces in the perspective of chemo-mechanics properties.

1.2 Objectives of research

The literature review indicated the magnitude and importance of the effect of dust accumulation on protective surfaces such as photovoltaic modules glass covers. Such effect is very significant in the MENA region and it needs to be mitigated for the effective harvest of solar energy in this region. Hence, the overall objective of this research is to study the characteristics (Chemo-mechanics properties) of dust and dry mud in Dhahran area in efforts to come up with effective mitigation techniques. The specific objectives of this study include:

a) Determining the cohesion, adhesion and interfacial forces between dust and dry mud particles.
b) Assessing the effects of dust and dry mud particles interaction with a protective surface, such as PV module glass covers.

1.3 Thesis Overview

In this thesis, six chapters encapsulate the contents of the conducted research. Chapter one is an introduction to energy consumption and the potential of utilizing solar energy to meet some of the energy requirements. A historical review of solar energy production and environmental factors (especially dust deposition) which affect its performance will be presented. Also, the problem statement, as well as contributions to solar energy development.

The second chapter discusses the solar energy production, reviewing the development of solar energy harvesting. The main focus is to review the influence of environmental factors (the dust accumulation in particular) on the photovoltaic modules output power. A comprehensive literature review regarding the dust deposition effects and particles force interactions was reported and summarized using tables and figures. From this chapter, it was demonstrated that previous work studied the impact of dust on the modules performance and the ways to clean without a focus on the dust from chemo-mechanics prospective.

In the third chapter, the instruments and experimental methods developed for testing and characterizing the adhesion and cohesion force of the dust as well as particles interaction are discussed. The testing equipment is classified into two groups, mechanical analysis (tensile test machine and scratching test machine) and microstructure analysis (SEM, EDS, XRD, 3D imaging, etc.). The experimental procedures using these instruments have been illustrated in details using some figures and explanations.

In chapter four, the fundamentals of mud particles chemo-mechanics are presented. The dust and mud microstructure and the influence of water interaction on the adhesion force due to ion exchanging are discussed. When water attracts the soil particles there are some ions dissolved in the water producing an ionic solution and some undissolved particles remains at solid state. During drying some processes take place such as mud shrinkage, mud desiccation and mud cranking due to residual stress resulted from the ionic bonding which holds the particles and increases the adhesion. These explanations are demonstrated in details using data from literature and some comparisons in terms of figures and sketches.

Chapter five presents the thesis results with detailed discussion for the findings. Finally, the study conclusion is shown in chapter six. The finding has been summarized and some possible future work in listed at the end of this chapter.

CHAPTER 2

LITERATURE REVIEW

2.1 Introduction

The degradation in the performance of PV system is due to environmental and climate conditions. Significant advances have been made to improve PV systems performance within the last few decades, but the impacts of climate conditions (such as dust accumulation and high ambient temperature) on PV system performance still remain as a challenge. The contrast between environmental conditions from location to another around the world has a corresponding different level of impact on the performance of PV module system in different zones [12].

Several Studies have been carried out on the effects of different environmental conditions on the performance of PV system. Mekhilef *et al* [13] reviewed the effects of humidity level, dust accumulation and wind velocity surrounding the PV system. They demonstrated that each condition influences the other condition, and thus, all conditions should be considered together. The effect of dust accumulation on PV module output power during time periods, 1940 to1990 and 1990 to 2010 has been reviewed by Mani and Pillai [14]. They used a suitable maintenance/cleaning cycle for their PV systems that considered the prevalent environmental and climatic conditions. However, in this literature survey; the focus is on the effect of dust deposition on solar panels performance and the impact of other environmental conditions on the level of dust accumulation. Moreover, the impact of adhesion and cohesion forces on dust deposition as well as dust particles interactions is also considered.

2.2 Effect of dust on PV modules output power

The effect of dry mud spots and the dust particles on the output power of Photovoltaic Modules have been studied by numerous researchers. Kurokawat [15] studied the effect of small dirt spot between 5 to 100 mm in diameter on the power output of module surfaces. The power output for 3% un-cleaned area was reduced by 50%.

Elminir et al. [16] studied the effect of dust sediment on 100 samples of glass tested at various azimuth and tilt angles for more than six months exposure to the environment. The sediment of dust particles varied from 15.84 to 4.48 g/m^2 for 0 to 90-degree tilt angle with transmittance ranging from 52.5–12.4%, respectively. Also, the output power decreased by 17.4% at 45-degree tilt angle for one-month exposure.

Jiang et al. [17] investigated the deposition effect of airborne dust on photovoltaic panels surfaces. The main focus was to examine performance analysis of polycrystalline and monocrystalline silicon cells experimentally. Based on the experimental setup, the relative humidity was controlled to 60 % and the PV module temperature was 25 C using controlled air environments while a small fan was used to simulate the air velocity. Based on these conditions, it was observed that deposition of dust grew from 0 to 22 g/m^2 the output efficiency reduction increased from 0 to 26%. Also, it was found that module surface material affected the rate of dust accumulation, for example, for the same concentration of dust, the glass surface modules have slow degradation rate than polycrystalline silicon modules.

Brown et al. [18] used an artificial dust < 70 microns for soiling test to predict the photovoltaic modules performance in Arizona. The photovoltaic modules using anti-soiling hydrophilic coating resulted in 5% performance improvement Coating and other mitigation techniques has been reported later on in this review. Touati et al. [19] observed the effect of dust accumulation on different PV Technologies and its sensitivity to humidity and temperature. The obtained results indicated that mono-crystalline modules the efficiency reduced by 10% due to dust accumulation of 100 days. The authors recommended more durable panels for dust accumulation such as semi-flexible photovoltaic modules.

Rajput et al. [20] studied the influence of dust deposition on the electrical efficiency of monocrystalline photovoltaic modules. The findings revealed that a maximum efficiency of 6.38% for clean modules and a maximum efficiency of 0.64% for dusty modules. Also this results indicated a 92.11% of the reduction in modules power output and the reduction of modules efficiency was 89%.Ghazi et al. [21] presented a review on the effect of dust on flat surfaces in the Middle East and North Africa (MENA) region. The MENA region exhibited the worst dust deposition districts in the world. Sudan has the worse deposition of dust 9 times compared to the United Kingdom (UK). Moreover, dust storms in Baghdad do have a significant impact on the intensity of solar radiation[22].

Boyle et al. [23] did investigate the influence of transmissivity due to normal soiling on the glass covers of photovoltaic panels in the USA. They reported a 2 g/m^2 of deposit dust after 5 weeks of exposure. In addition, every g/m^2 accumulated on the surface reduced the transmissivity of light by 4.1%. The solar radiation transmissivity was not influenced by the incidence angle of irradiance which changed linearly with dust accumulation. The authors compared their results with other published results, and they found a large difference in the rate of dust deposition and its effect on the value of transmissivity. They concluded that the effect of dust accumulation on photovoltaic modules glass covers transmissivity is location dependent.

2.3 Effect of dust deposition on PV modules output in Saudi Arabia and the Middle East

A remarkable reduction in the output power was reported in different regions that suffered from a lack of rainfall and encounter high levels of dust soiling such as MENA region countries. Table (2.1) illustrate the effect of rainfall on the PV modules performance.

Said [24] studied the influence of dust accumulation on photovoltaic and thermal collector performances in Dhahran, Saudi Arabia. The measured efficiency degradation was 7% for photovoltaic panels whereas, the efficiency degradation for the thermal panels were 2% to 7 % during one-month exposure to the environment.

The dust accumulation on a PV system installed in a small village in India caused 32% reduction in the performance when compared to an identical Photovoltaic system with a daily cleaning program. On comparable lines, in Kuwait, after 6 days the accumulation of sand on PV panels reduced the panels power output by 17 % [14]. In Dhahran area, Adinoyi and Said [25] studied the effect of dust deposition on the output power of solar photovoltaic modules. A dust storm in March 2012 reduced the modules output power by 20%. Moreover, six months of exposure without cleaning reduced the power output by 50%. Said and Walawil [7] investigated the effect of dust accumulation on the transmissivity of photovoltaic modules glass covers. They indicated that the adhesion force did increase significantly due to humidity effect. The power output reduced by 6% and the short circuit current by 13% after one month of exposure to the environment.

The possibility of utilizing antireflective coated and textured glass in reducing the dust fouling has been studied by Said et al.[26]. The study indicated that textured and coated surfaces did reduce the effect of dust accumulation on module output compared to plain surfaces. However, texturing the surfaces of photovoltaic panels increased the module temperature which affected the power output.

Rahman et al. [27] studied the effects of different parameters on the performance of photovoltaic modules. They developed an experimental setup to investigate the effect of relative humidity, ambient temperature and dust accumulation. It was found that, when the relative humidity increased by 20%, the power output reduced by 3.16 W due to dust falling on the surface of the solar module for a constant ambient temperature 27 C. For 0.012 g/cm^2 dust sediment, the power output dropped down and the photovoltaic modules efficiency decreased by 1.47%.

Table 2.1. The effect of rainfall on PV modules performance

Author & Location	Rainfall (mml/year)	power output reduction	exposure Period
Mohandes et.al UAE [28]	80-90	10%	35 days
Said et.al KSA [25]	6-10	50%	180 days
Elminir et.al Egypt [16]	18-50	70%	100 days
Elizabeth Palestine[29]	30-40	6%	7 days
Qatar Touati [30]	70-75	10%	180 days

2.4 The impact of the wind on Dust deposition

Wind stream can blow the dust particles from PV module surfaces, which can decrease dust accumulation [31]. In Egypt, Hegazy [32] studied the transmission reduction due to dust deposition on the glass cover of photovoltaic modules. Based on experimental investigation, the glass transmittance observed a high dependence on the dust deposition amount. Moreover, the dust accumulation rate decreased because of the wind action.

However, the wind has a negative effect as well. It can increase dust deposition layers by transferring such particles from one location to another. Increases in dust accumulation generally synchronized with monthly increases in wind speed [33]. Goossens *et al*. [34] studied the effect of wind direction and speed on dust accumulation. They developed a wind tunnel simulation and field experiments simulation. Their results concluded that the direction of the wind with respect to the PV module orientation has an impact on dust deposition and distribution more than wind speed does.

Goossens [35] studied the effects of wind velocity and airborne dust concentration on the PV modules performance. It was concluded that the reflected effect of wind on dust accumulation depends on the range of wind speed. The wind speed was tested in several ranges between 0.6 m/ s and 2.6 m /s. High wind speeds (2.6 m/s) resulted in high dust deposition on a PV modules, which reduced the cell performance. For low wind speed, dust deposition was smaller, and the reduction in cell performance was smaller too. Moreover, the PV modules performance was affected by the size of Martian dust particles and wind velocity variation. Gaier et al [36] studied the degradation of PV modules due to dust particles deposition. It was observed that there was no significant reduction in the modules performance which caused by large particles (greater than75 µm) when the wind velocity with high variation between 89 to 116 m/s. The reduction was observed for dust particles accumulation caused by small particles less than 30 µmin size. This results was confirmed by AlBusairi et.al who concluded that the surface density of the dust accumulation should be negligible at a relative high speed of wind velocity approximately greater than 24 m/s [37].

2.5 Humidity and dust adhesion

The effect of humidity was reported by Mekhilef et al. [13]. They studied the effect of wind velocity, humidity and dust deposition on PV modules output power. They observed that, as relative humidity decreased solar panel efficiency increased. In this part of literature survey, the focus is on the effect of humidity on the dust adhesion force. AlBusairi et.al[25] evaluated the PV modules performance reduction due to outdoor environmental conditions. They observed that dust particles stick to PV modules glass covers due to humidity effect which thus requires powerful and careful cleaning action to get back initial power outputs of modules. For instance, the countries near to the Mediterranean Sea such as Italy and Spain, the registered values of humidity are high, which increase the adherence force of dust particles on the modules surface [38]. Said et.al[7] studied the humidity effect in terms of quantity. It has been reported that increasing in the relative humidity (from 40 to 80%) increased the dust adhesion to 80%. In order to improve the dust adhesion and create sticky dust layers on PV modules surfaces, a high relative humidity was required [37], [39]. Figure (2.1) shows the trend of adhesion with respect to relative humidity where the dust adhesion increased exponentially with the relative humidity.

However, the effect of humidity on dusty glass cover surface is significant below 50%RH as shown in figure (3.1). Brown et.al[40] did an experimental soiling tests to predict the PV modules performance. They concluded that applying an anti-soiling hydrophilic coating to the glass cover reduced the amount of dust soiling on the surface, but there is a measurable effect of %RH was observed, as shown in figure (3.1) which compared the optical performance for glass and optical glass. In general, an increase in absolute humidity value should increase the deposition of dust too [28], [41]**.** Table (2.2) illustrate the dust effect on PV modules covers in different locations.

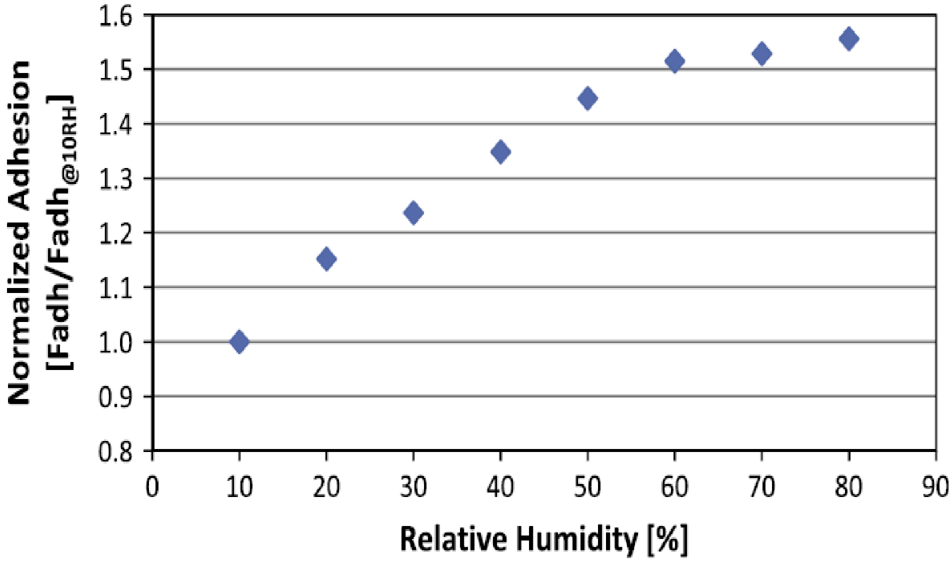

Figure 2.1. Relation between humidity and adhesion [7]

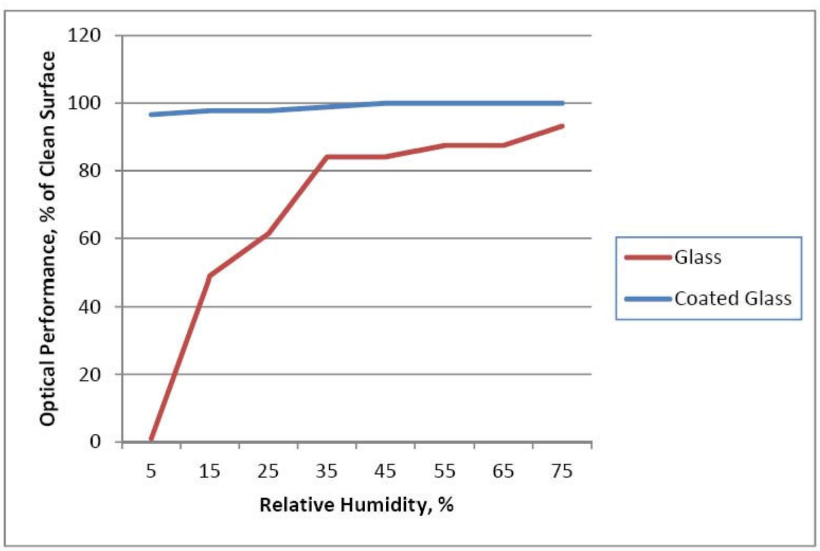

Figure 2.2. Optical performance vs. relative humidity, during exposure to dust, for uncoated glass and glass with an anti-soiling hydrophilic coating [18].

Table 2.2. The dust effect on PV modules covers in different locations

Authors	**Study & location**	**Duration**	**Dust effect**
Said et al. [26]	KSA	Not reported	The average power reduction was 13% for plain glass module
Said and Walwil [7]	KSA	Five weeks	The average power reduction after five weeks of outdoor exposure without any cleaning action was around 6%
Said [24]	KSA	One Month	The average degradation rate of the efficiency was 7% per month
Adinoyi, M.J. and S.A. Said [25]	KSA	Six months	The output power decreases by as much as 50% six months of outdoor exposure without cleaning
Ibrahim et al [42]	Egypt	10 days	Voc decreased by 9% and Isc by 27% after 10 days
Boykiw et al. [29]	Palestine	One week	5 to 6% decrease in the solar panel efficiency in one week
Touati et.al [19]	Qatar	100 days	The efficiency decreased by around 10% after 100 days of dust accumulation
Elminir et.al [16]	Egypt [	One month	the solar module output power decreased about 17.4% per month
Rajput et al. [20]	India	Not reported	a maximum efficiency of 6.38% for clean modules and a maximum efficiency of 0.64% for dusty modules
Piliougine et al [43]	Spain	Two months	After 15 days without rain, the losses are greater than the 4%. And reach up to 15% after 2 months without falling
Pang et al. [44]	China	Not reported	The efficiency decreased by 1.794%
Mohandes et al. [28]	UAE	5 weeks	The output power reduction after 5 weeks was about 10%
Mani [25]	Kuwait	Not reported	The month of May recorded the highest loss (-25%) because of heavy dust accumulation mainly due to presence of dusty rain
Kaldellis [45]	Athens	8 weeks	6.5% power output reduction

Rahman et al. [27]	KSA	Not reported	For 0.012 g/cm^2 dust sediment, the power output dropped down and the efficiency photovoltaic modules decreased by 1.47%.
Boyle et al. [23]	USA	5 weeks	every g/m^2 accumulated on the surface reduced the transmissivity of light by 4.1%

2.6 The effect of adhesion force and cohesion force on dust particles and surfaces

Capillary bridges on the modules surfaces were formed due to the interaction between the dust particle and condensed vapor in the gaps between the particles and the surface. This effect generated meniscus forces which built up the dust layer and increased the adhesion force between dust particles and modules surfaces [46], [47].

Corn [48] studied the adhesion force of solid particles with respect to solid surfaces. It was found that the adhesion force increased with particle size. The contact area between the rough surface and particle or even between particles itself completely different from the real contact area apparent. It can be modified by the surface roughness, the extent of agglomeration of particle and particle shape. Also, the relative humidity of ambient air affects the adhesion force but the influence nature is not obvious.

The adhesion of dust and contact potentials were investigated by Potentials [49]. He reported that the adhesive forces of electrostatically deposited dust were much greater than a similar dust deposited mechanically. Each particle in an electric field takes specific orientation by the dipole moment which produced by the contact potential differences. The coulomb forces between the particles layers producing high adhesive forces by the dipoles orients electrostatically.

McLean [50] presented the cohesion of dust layer and the cohesive force in precipitator electrostatic on the sediment layers of dust in particular . An electrostatic precipitator has a significant cohesive force that influenced the sediment layers because of the electric field of particles air gab by the corona current across the layers. It was found that the electric field flows through the layer had a linear proportional to the cohesive force approximately. Podczeck et al. [51] investigated the influence of relative humidity (changing and constant rate) on the powder particles adhesion. The study indicated that at high relative humidity the adhesion increased slightly while the van der Waals force was 10 times greater than the electrostatic force. The measurement of cohesive forces is difficult to conduct for two individual similar particles having a small size in micrometer and millimeter. These sizes are the most common used in many mercantile systems. E.D. Shchukin et al. [52] is the first one used a cohesive force apparatus. It was improved by Somasundaran [52] in 2005 to measure the various shape, various size and nature of particles chemical structure under various conditions for very low cohesive force around 1 nN. The cohesive force between glass surfaces and dust particles increased with the decreasing in PH and an addition amount of salt results in a significant increase of the cohesive force. Also, the cohesion between dust particles and surfaces is reduced by the interaction of anionic surfactant with polyethylene oxide layer.

The atomic force microscopy (AFM) is another technique used to study the adhesion force between particles and substrates. The adhesive force of particles especially in the humid atmosphere has been investigated by Fukunishi and Mori [53] using AFM .It was concluded that the adhesive force for hydrophobic substrate and glass surface particles, almost remaining constant for different humid atmosphere. On the other; hand the adhesion force between the hydrophilic substrate and the particles of the glass in high capillary condensation boosted significantly. The function of gas fluidizing in the adhesion of iron particles has been observed by Zhong et al. [54] For iron powder the thermo-mechanical analysis due to a soft surface, indicated that the adhesive force of particles with temperature mounting was mainly based on surface viscosity and a minimum velocity of fluidization.

Duri et al. [55] studied the adhesion force of wheat particles experimentally. They normalized the curves of adhesion force distribution using the Weibull clearance to classify the components into hydrophilic and hydrophobic components according to the degree of interaction. The correlation of particles surfaces tension and the allergy of AFM for hydrophobic particles have been reported.

Various models for adhesion force measurements are reported in the literature. Kumar et al [11] studied the role of adhering particles and the size of asperities using such models. The JRK model can be used to characterize the adhesion force for smooth surfaces which increased with adhering particle size raises. Rabinovich model is another model for measuring the cohesion and adhesion force; on which an equation of adhering particle interaction has been developed. Also, their correlations output came in between experimental and theoretical results.

Jarząbek et al. [56] presented a measurement method to determine the particles adhesion of ceramic and the adhesion in composites of ceramic reinforced. Microwires tension was measured for interface investigation using micro tensile tester device and it demonstrated the reduction of Young's modulus and hardness due to the increase of concentration ceramic particles. The results indicated a weak metal matrix interface in 10% Al2O3 samples as compared to 2% Al2O3 composite.

For microscale particles, the adhesion force mostly depends on the material type, freightage density and the structure of surface; in addition to magnetization which has a significant impact on magnetic particles. Knoll et al. [57] characterized the adhesion force of magnetic particles and their effect on the protein surface. The deposit particles have reversible expanding if the separation force was less than particles adhesion force. The test results indicated that the protein surface requires additional force for separation.

Recently, Petean and Aguiar [10] determined the particles adhesive force in rough superficies. They compared experimentally between two models: JKR and Derjaguin, Muller and Toporov (DMT) models. The theoretical values were much higher while the JKR model gave the closest results to the experimental values. Moreover for similar particles, the adhesion force varied due to different values of substrate roughness and the actual contact area which has an important role influencing particles adhesion. This is an overview of recent published researches which consider adhesion and cohesion forces measurements as well as particles interaction with solid surfaces (dust particles in particular). Different techniques and models have been reported such as JKR, JF and Derjaguin Muller and Toporov (DMT) models. Table (2.3) illustrates and summarizes different case studies of particles adhesion measurements and their dates and location

Table 2.3. Different studies on particles adhesion measurements

Author	location	study	Major outcome
M.Corn 1961[48]	Boston, USA	adhesion force of solid particles	the relative humidity of ambient air affects the adhesion force but the nature is not obvious
Podczeck et al. 1996[51]	London, UK	influence of relative humidity on the powder particles adhesion	at high relative humidity, the adhesion force increased slightly
Somasundaran 2005[52]	USA	measurement of cohesive forces between particles	The cohesive force between glass surfaces increased with the decrease in PH
Fukunishi & Mori 2006 [53]	USA	adhesive force of particles especially in humid atmosphere	the adhesive force between hydrophobic substrate and glass surface particles almost remained constant for different humid atmosphere
Zhong et al 2012 [54]	China	function of gas fluidizing in the adhesion of iron particles	the adhesive force of particles with temperature mounting was depends on surface viscosity and a minimum velocity of fluidization
Kumar et al 2013[11]	Germany	the role of adhering particles and the size of asperities	The adhesion increased with adhering particle size raises
Jarząbek et al 2015[56]	Poland	determine the adhesion force of ceramic particles	Reduction of Young's modulus and hardness due to the increase of ceramic particles concentration
Knoll et al 2015 [57]	Germany	Adhesion force of magnetic particles on the protein surface	Protein surface requires additional force for separation
Petean & Aguiar 2015 [10]	Brazil	Particles adhesive force on rough superficies	the adhesion force varied due to different values of substrate roughness

CHAPTER 3

MUD CHEMISTRY

3.1 Introduction

Water interaction with soil particles can take place due to effective adsorption of water molecules by soil surfaces. The interaction between water molecules, dissolved ions and soil particles occur because of unbalanced force field which depends on the particle size and the nature of this interaction will be discussed. When forming mud, a chemical process can take place during drying. How the chemically modified mud undergoes bonding (ionic bonding or other)? How adhesion takes place in the chemically modified region? To answer these questions, the nature of water chemistry, mud chemistry and the interaction in between have to be understood. Figure (3.1) shows the general description of dust water interaction.

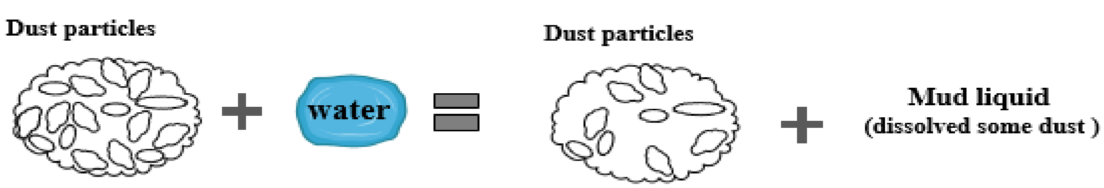

Figure 3.1. The process description of dust water interaction.

The deposition of atmospheric acid generates hydrogen ions to aquatic and terrestrial ecosystems which balanced by chemical weathering. Rudolf et al.[58], Studied the granitic gneiss alteration by deposition of acid and the acidic water lake chemical composition (pH < 5.3) in Switzerland. The lake sediments have been characterized using scanning and transmission electron microscopy, element mapping and X-ray powder diffraction. It observed that non-crystalline iron and aluminum hydroxide were produced from silicates by chemical weathering.

Park et al.[59] Studied the effect of acidic material (H_3PO_4) on the mechanical interfacial properties of red mud and epoxy mixture. The red mud consisted of Fe_2O_3, Al2O3, TiO_2, SiO_2, CaO, and Na_2O was chemically treated with an H_3PO_4 solution. The development of active hydrogen or acidic group on the solution surface decreased the PH of red mud while the acidic value increased. In addition, it was observed that the treatment concentration increased with the improvement of composites mechanical interfacial properties. Pacheco[60], studied the effect of adding sodium carbonate to mineral waste mud extracting from tungsten mine. The results showed that the state of dehydroxylation did not come from calcination of sodium carbonate and waste mud mixture.

During mud drying process there are different interactions take place such as mud shrinkage, desiccation and mud swelling which change the micro-structure of mud. Robert et al.[61] Reported that during mud drying, horizontal cracks take place on mud surface propagated from shrinkage crack and mud peeling was observed above these cracks due to differential stresses. It concluded from the analysis, the peeling phenomenon produced due to tensile stress gradient on the clay surface. Also, they developed a model to calculate the relation between the peeling depth and mud peel curvature radius**.** Shrinkage cracking is significant in controlling of water to soil vertical permeability, nutrients and several soil parameters, it is probably that peeled cracks are of a comparable importance in the horizontal permeability controlling. Lucas et.al [62] evaluated the pattern of mud crack based on the experimental investigation. It was observed that the pattern of desiccation cracks either hexagonal or rectilinear tilting. It resulted that, from the crack pattern geometry after more than 20 generation of drying and wetting, the crack angles reach 120º with 4 generation relaxation time. They developed a model to simulate the crack behavior which observed previous open crack position.

Many studies conducted to avoid mud crack effect e.g. Carreras et al[63] investigated the crack thickness obtained from aqueous alumina thin films drying. Drying shrinkage inside the body developed tensile stresses at the surface which cracking has been generated. To avoid the cracking to method were carried out either by enhancing the mechanical properties or by reducing the stresses (decrease the surface tension or drying slowly). This chapter demonstrates the soil and mud chemistry with an explanation of the physical/chemical processes taking place during dissolving of earth metals (mud forming) as well as those of the processes taking place during mud drying.

3.2 Nature of water chemistry

H_2O (water molecule) has a V-shape arrangement of oxygen and hydrogen nuclei which have a tetrahedral configuration. Pauling 1960[64], Indicated that H-O bonding has 60 % covalent and 40 % ionic and the water bonding was directional due to the high permanent dipole. In water molecules, the positive corner attracts the negative one by sharing a proton to form a hydrogen bonding and each molecule tends to bond with four molecules. There were several models discussed the structure of water based as physical and chemical evidence such as mixture models, interstitial models, distorted hydrogen bond models and random network model (Eisenberg in 1969[65]).

3.3 Influence of dissolved ions on water

The ions hydration takes place due to the dipolar character and uneven charge distribution of water molecules which attracts the solution ions. The ions in soil are not hydrated completely, however, these ions disrupt the structure of water. Frank and wen [66] developed a model to describe ion-water interaction. Three regions were observed: a region of immobilization where the water molecules oriented strongly in the ion field with low kinetic energy, a region of broken down structure with relatively high kinetic energy than immobilization zone and a region with normal water structure which polarized by the ionic field. Figure (3.2) shows the zones of ion-water interaction.

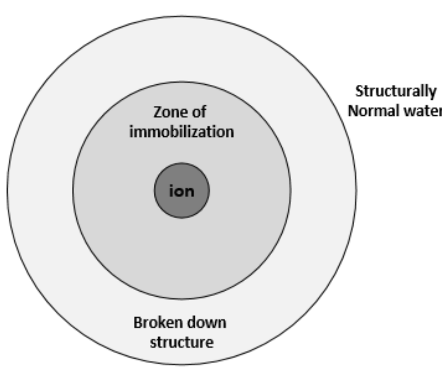

Figure 3.2. The zones of ion-water interaction [66].

3.4 Mechanisms for Soil-Water interaction

Several water adsorption mechanisms were reported by Low [67]. Soil mineral surfaces-mud surfaces, in particular- were strongly attracted by water as shown in figure (3.3), even at low relative humidity, the dried mud adsorbed water vapor from the atmosphere,

3.4.1 Hydrogen bonding

Soil minerals surfaces are composed of hydroxyls and oxygen layers. Hydroxyls attracted the negative corners and oxygen with positive corners which easily generate hydrogen bonding between water molecules. The electron distribution will change due to hydrogen bond formation with surface particles which facilitate additional molecules bonding between layers. The water tetrahedral arrangement would induce by directional bonds properties and be less rigid due to surface energy field reduction and an increase in water force field as well.

3.5 Effect of power of hydrogen (PH)

The Power of Hydrogen can be defined as (PH = - $\log_{10} H^{+)}$. When PH is lower than 7 means a high concentration of H^+ (acid solution) and PH greater than 7 means the low concentration of H^+ . The greater the PH, the higher negative charge of the particle and more tendency for H^+ to attract the solution from the hydroxyl. Hydroxyls OH^- are located on the mud particles edges to dissociate in water.

The PH controls the surface potential and affected the clay suspension behavior. The negative to positive edge interaction was enhances at relatively low PH while stable dispersion or suspension required large PH. For example smectite and silica – as shown in figure (3.4) as clay minerals, the total particle charge was high relative to OH ending sites.

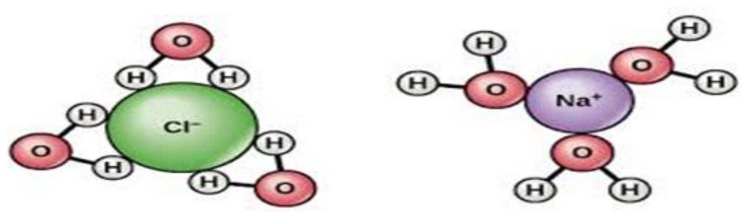

Figure 3.3. Dust particles reactions with molecules of polarized water

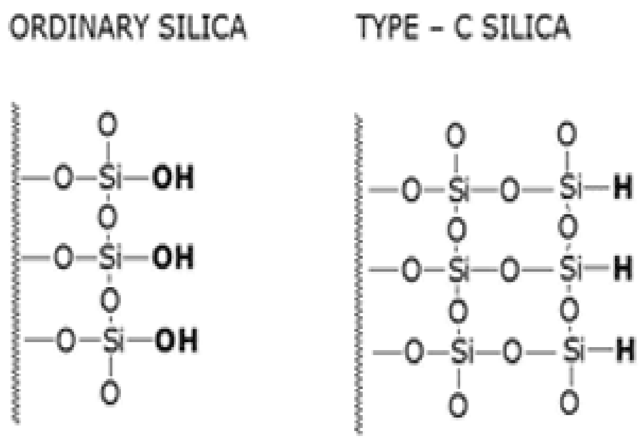

Figure 3.4. The negative and positive charges located on the mud particles edges to dissociate in water

3.6 Exchange capacity and common Ions in mud and clay minerals

The adsorb cations in the sedimentary soil are magnesium, calcium, potassium and sodium. Sodium is the most dominant cation in many saline soil and marine clays as adsorbed cation while chloride, nitrate, phosphate and sulfate are the common anions[68].

The source of exchange capacity depends on compositional and environmental factors and is related directly to the density of surface charge. The sources of exchange capacity are:

a) Broken down exchange which decreases with particle size increase.
b) An isomorphous replacement which is a mineral exchange capacity source.
c) Replacement: where the different cations were replaced by hydrogen.

The replaceability of cation depends on several conditions such as ion size, valence and ion relative abundance. The large cations are displaced by relatively small cations typically as per the following replaceability series:

$$Na^{+} < K^{+} < Cs^{+} < Mg^{+2} < Ca^{+2} < < Cu^{+2} < Fe^{+3} < Al^{+3} < Th^{+4}$$

Thus, Al cation with high replacing power can be displaced by Na^{+} ion if the concentration of sodium in the solution is relatively high than aluminum concentration[69].

3.7 Decomposition process

Decomposition process is the process induced by biological and chemical reactions between water molecules and soil particles. The most common processes causing decomposition are a dissolution, Ion exchange, hydration, dehydration, hydrolysis and oxidation[68].

3.7.1 Dissolution

Soil or mineral components are partially dissolved in the solution during chemical reactions. The dissolution of the soil or mineral clearly will change the chemical composition of original rock and the solution where the dissolved solids particles have been added. The dissolution of calcite (CaCO3) and halite (NaCl), are shown in equations below. In the first example, halite reactions take place with molecules of polarized water which separate chloride and sodium into single ions which surrounded by hydration sheaths and dissolved in the water molecules. The carbonation process takes place in calcite (CaCO3) dissolution, where the carbon dioxide attracted and dissolved in water producing carbonic acid. The dissolution process for calcite (CaCO3) and halite (NaCl) are expressed by the following equations:

$$NaCl + H_2O \longrightarrow Na^{+1} + Cl^{-1} + H_2O \quad (1)$$

$$H_2O + CO_2 \longrightarrow H_2CO_3 \quad (2)$$

$$H_2CO_3 + CaCO_3 \longrightarrow Ca^{+2} + 2(HCO_3)^{-1} \quad (3)$$

The other most common processes which cause decomposition of soil and minerals with decomposition products and reactions equation are shown table (3.1).

Mud has the properties of absorbing certain ions and holding them in an exchangeable condition. The mud structure (e.g. silicate) does not affected by exchange reaction. Cation exchange is more famous than anion exchange. The most common exchangeable cation are K^+, Ca^{+2}, Na^+ , H^+, NH^{+4}, Mg^{+2}.

Table 3.1. The processes causing decomposition of soil and minerals with decomposition products and reactions equation [58]

Decomposition process	Examples	Decomposition products
Dissolution	$NaCl + H_2O \rightarrow Na^{+1}_{(aq)} + Cl^{-1}_{(aq)} + H_2O$ $H_2CO_{3(aq)} + CaCO_3 \rightarrow Ca^{+2}_{(aq)} + 2(HCO_3)^{-1}_{(aq)}$	Dissolved solids including Ca^{+2}, Mg^{+2}, Na^{+1}, K^{+1}, H_4SiO_4, CO_3^{-2}, SO_4^{-2}
Ion exchange	$KAlSi_3O_8 + H^{+1}_{(aq)} \rightarrow HAlSiO_3 + K^{+1}_{(aq)}$ $NaAlSi_3O_8 + H^{+1}_{(aq)} \rightarrow HAlSi_3O_8 + Na^{+1}_{(aq)}$	Dissolved solids including Na^{+1} and K^{+1}
Hydrolysis	$2KAlSi_3O_8 + 2H^{+1}_{(aq)} + 9H_2O \rightarrow Al_2Si_2O_5(OH)_4 + H_4SiO_{4(aq)} + 2K^{+1}_{(aq)}$ $Mn_2SiO_4 + 4H_2O \rightarrow 2Mn(OH)_2 + H_4SiO_{4(aq)}$	Clay minerals such as kaolinite, illite, smectite Other hydroxides
Hydration	$CaSO_4 + 2H_2O \rightarrow CaSO_4 \cdot 2H_2O$ $Fe_2O_3 + H_2O \rightarrow 2FeO \cdot OH$	Hydrated and hydrous oxide minerals
Oxidation	$2Fe^{+2}{}_2SiO_4 + 4H_2O + O_2 \rightarrow 2Fe^{+3}{}_2O_3 + 2H_4SiO_{4(aq)}$ $4Fe^{+2}S^{-2}{}_2 + 15O_2 + 8H_2O \leftrightarrow 2Fe^{+3}{}_2O_3 + 8S^{+6}O^{-2}{}_{4(aq)} + 16H^{+1}_{(aq)}$	Oxide mineral and dissolved solids, e.g., SO_4^{-2}, H_4SiO_4
Chelation	Not reported	Dissolved metals contained in organic ring complexes (chelates)

3.8 Mud drying

The dissolved ions (Na^+, K^+, Ca^{+2}) attract mud and clay minerals structure. These ions penetrate the mud layers and hold them together as shown in figure (3.5). The ions stay in the mud structure during water evaporation holding them and increasing the adhesion force. Figure (3.6) shows the cation attraction process. At high amount of Na^+ and K^+ cations, the mud structure remains intact due to the small size of Na^+ and K^+ cations. These cations can easily penetrate the mud interlayers and hold the platelets of mud together, due to electrostatic double layers which increase the mud particles adhesion. During drying the dissolved ions rearranged themselves forming crystals (the negative charge ions attract the positive charge ions). The crystals formed with a net charge (positive or negative) which make a physical bonding to the undissolved dust particles.

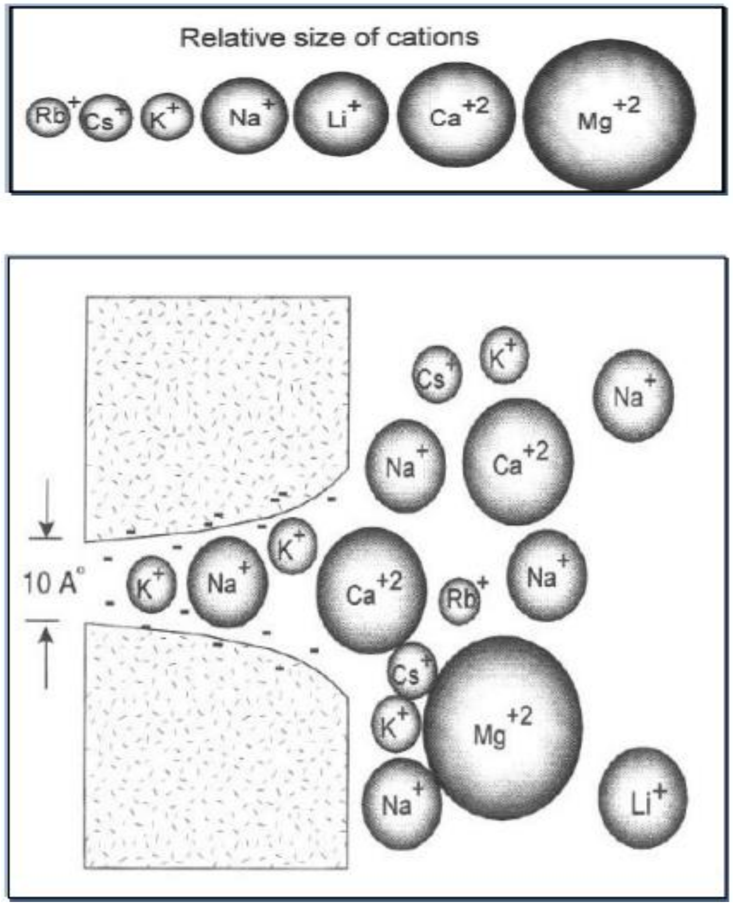

Figure 3.5. The effect of the cation size on the cation migration into a mud interlayer

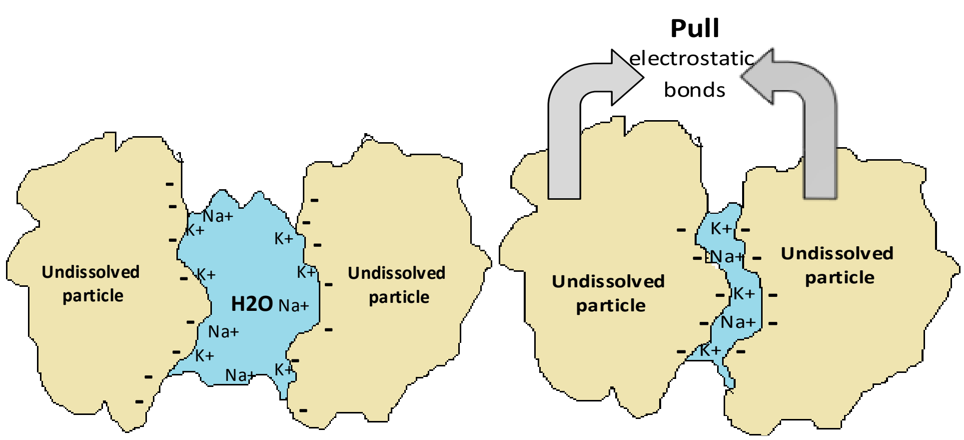

Figure 3.6. The effect of water evaporation on dust particles during mud drying

Figure (3.7) summarizes the process of dust- water interaction and mud formation according to the following steps:

a) Soil and dust particles surfaces are composed of hydroxyls and oxygen layers, so hydroxyls attracted the negative corners and oxygen with positive corners which easily generated hydrogen bonding between water molecules.

b) Dust particles reactions take place with molecules of polarized water which separate single ions (Na^+, K^+, Ca^{+2}) surrounded by hydration sheaths and dissolved in the water molecules forming oxygen and hydroxyls (KOH, NaOH, etc) stretch.

c) Solid undissolved dust particles have pendant hydroxyl (- OH) groups which can form bonds or strong polar attractions to mud solution and inorganic surfaces

d) During drying, the dissolved ions (Na^+, K^+, Ca^{+2}, Cl^-, SiO^-) attract mud structure due to electrostatic and ionic bonding force. These ions dissolved in the mud solution particles holding them together and forming crystals in between. It stays in the mud structure during water evaporation increasing the adhesion force

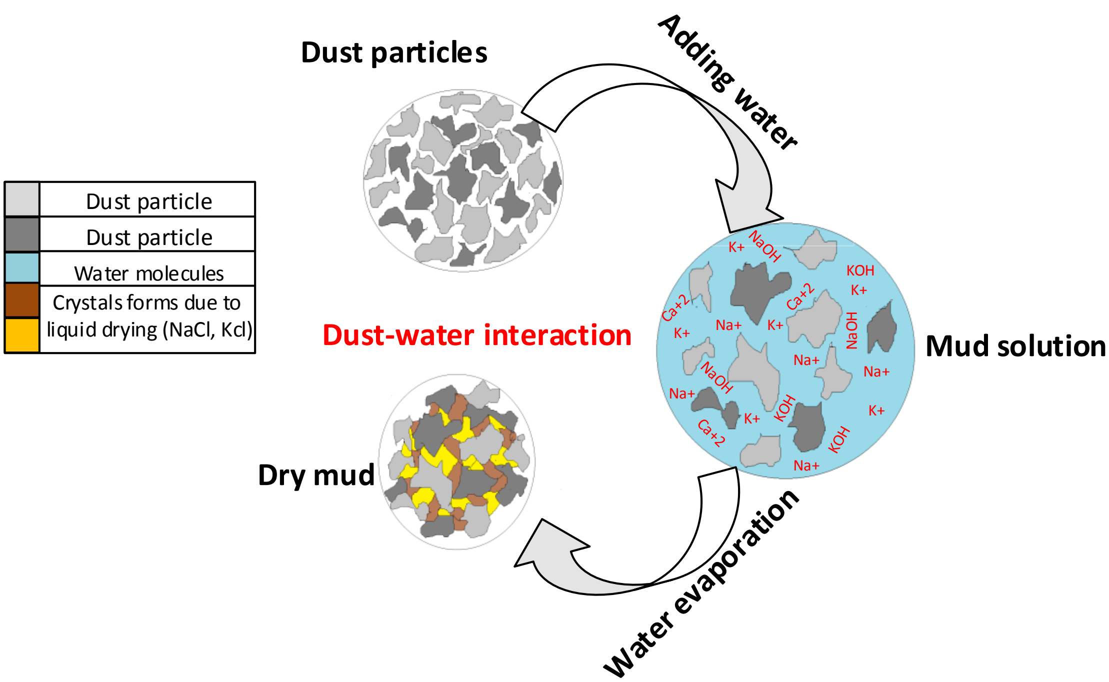

Figure 3.7. The process of dust-water interaction

CHAPTER 4

EXPERIMENTAL STUDY

4.1 Introduction

The investigation of dust and dry mud Chemo-mechanics on solar protective surfaces undergoes several experimental techniques - mechanically and chemically- in order to achieve accurate results. The experimental methods and equipment used in determining the adhesion and cohesion forces are presented in this chapter. Figure (4.1) shows the flow chart of the Chemo-mechanics investigation process.

Experimental techniques used for the chemo-mechanics tests were divided into three main groups. The first group was mechanical equipment used for mechanical testing such as tensile testing machine and scratching testing machine. The second group was the instruments used for microstructure characterization which included scanning electron microscopy, Atomic Force Microscopy (AFM), compound analysis (X-ray diffraction), elemental analysis (energy dispersive spectrometry) and three-dimensional imaging. The third group was the chemical investigation instruments used for chemical examination of dust and dry mud solution such as Fourier transform infrared spectroscopy (FTIR) and power of hydrogen (PH) measurements.

Many sample preparation techniques were used to prepare the samples for testing. These techniques included: cutting the specimens, mounting and gold coating required for mechanical, chemical and microstructure analysis testing. Two types of samples were prepared carefully to ensure accurate results. These were dry mud samples for tensile testing to determine the combination of adhesion-cohesion force and dry mud solution samples where thin layer of these samples were placed in a polycarbonate surfaces to measure the axial force.

Mechanical testing, microstructure characterization and chemical testing are described in detail in the following sections.

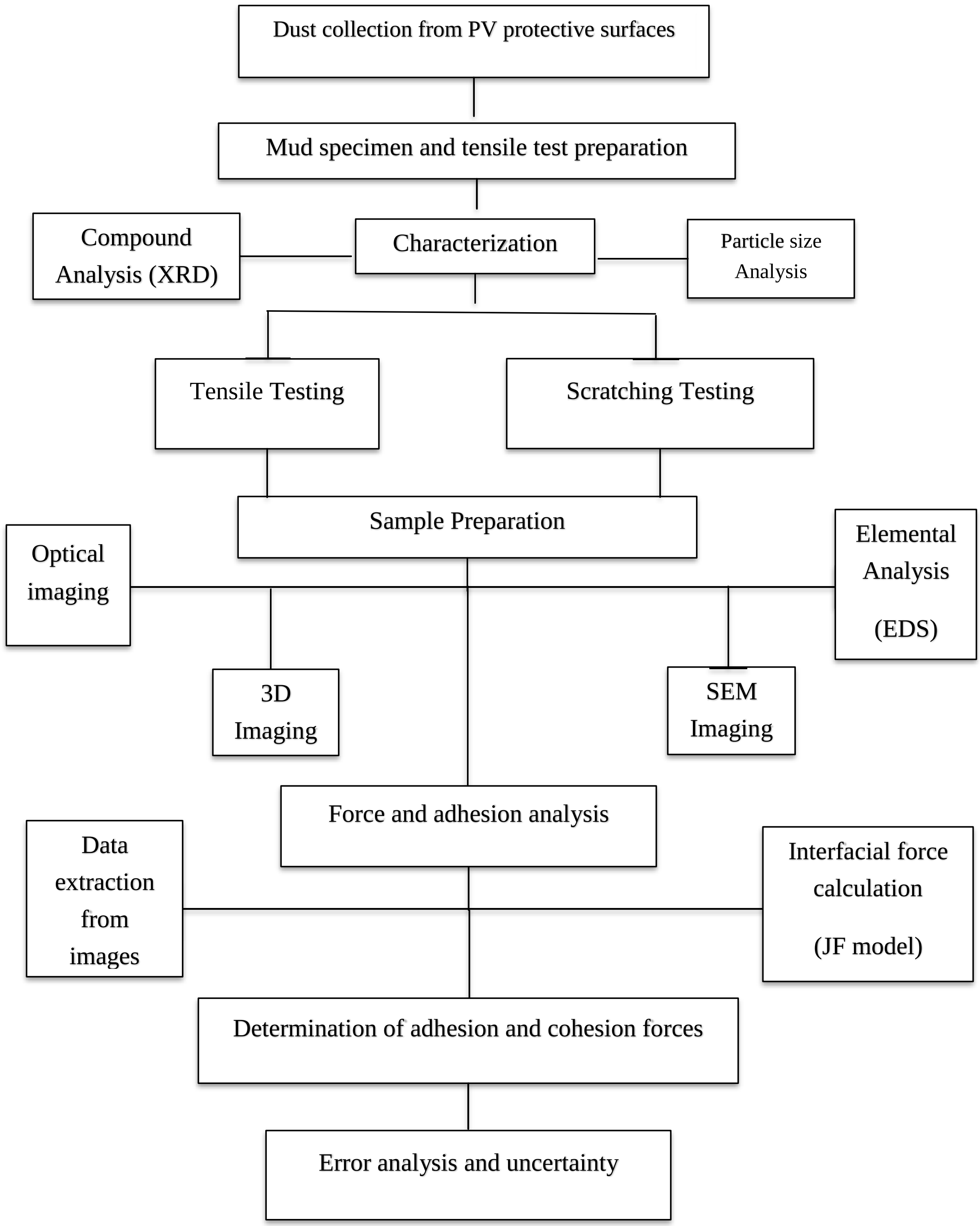

Figure 4.1. The process flow chart

4.2 Dust collection

The Dust was collected from glass cover of photovoltaic modules exposed to the outdoor environment, located in King Fahd University, Dhahran (26°16′N 50°09′E). The PV module setup from which dust is collected is shown in figure (4.2). It was important to collect dust particles that were adhering to a real solar protective surfaces to ensure that we are dealing with the adhered dust particles despite of wind velocity, rainfall and modules inclination.

It was observed that dust sticks to PV modules glass covers because of humidity which thus requires sturdy but careful cleaning action to restore modules to their initial efficiency and power outputs [31]. A careful procedure was adopted for dust removal that avoided scratching or damaging of the glass cover. This small scratches would affect the transmissivity and the module output efficiency at the long term.

Figure 4.2. The dusty and clean photovoltaic modules

4.3 Mechanical testing

4.3.1 Mud pellets preparation

Dust particles absorb water vapor in humid air environments and form mud at the surfaces. Once the mud is dried at high-temperature conditions under solar radiation, it becomes difficult to remove it from the surface. To represent this behavior and perform tensile testing; mud pellets were prepared using the following steps:

a) An electronic sensitive weighing scale was used to measure the masses in kilogram of the mixture (dust and water).
b) Three grams (3g) of dust were mixed thoroughly with four grams (4g) deionized water (DI water) using a mixing rod until a homogenous solution was obtained.
c) The mixture was put in a circular plastic holder which has specified dimensions on horizontal surface to dry at room temperature (around 25Cº) it usually takes four to five days for the pellets to completely dry.
d) Finally, the plastic holder shape (with a 40 mm diameter and 5 mm thickness) taken a way and the dry mud pellets were ready for tensile testing and characterization.

4.3.2 Tensile testing for dry mud pellets

There are two forces act on mud pellets (physical force and chemical induced force). The physical force is measured using tensile testing method.

A circular aluminum holder was designed and manufactured with specific dimensions (having a diameter equal to the mud pellet diameter) to hold the mud pellet during the tensile testing. The aluminum holder was designed with removable rods to have appropriate shape for other test rather than tensile testing.

The mud pellet was glued to the aluminum holder surface using a strong adhesive (3M Scotch-Weld). Figure (4.3) represents the layer of dry mud pellet glued to the aluminum holder while figure (4.4) shows the mechanical drawing for the mud pellet specimen.

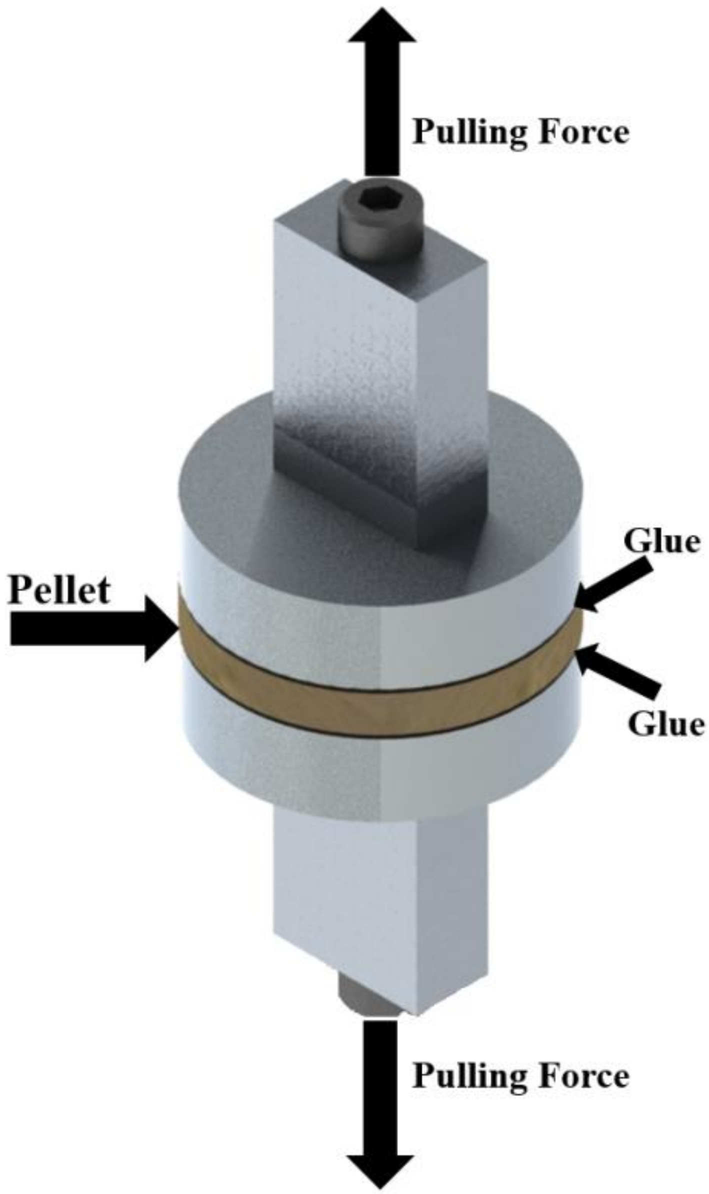

Figure 4.3. The assembly of non-fractured mud pellet sample

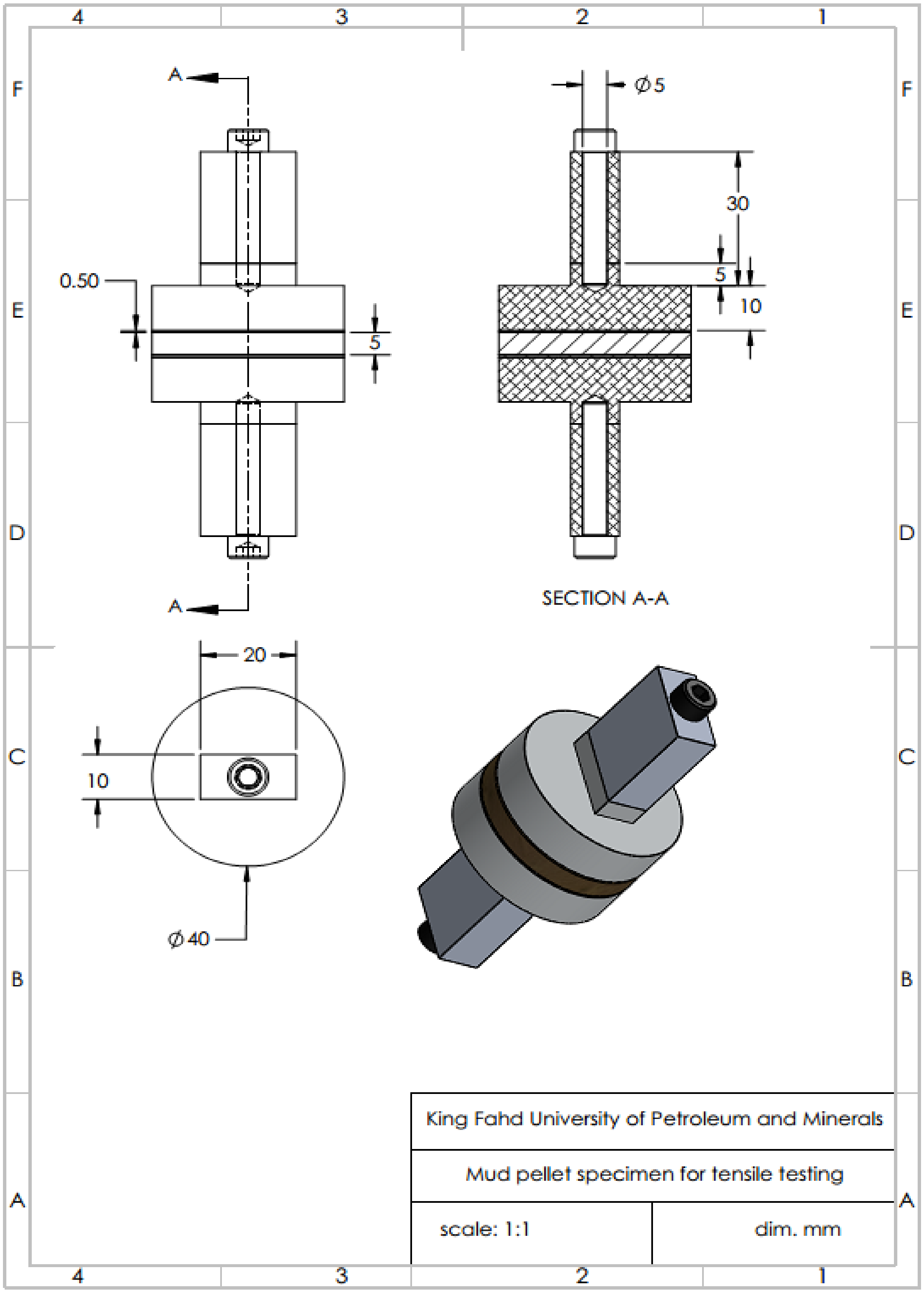

Figure 4.4. The mechanical drawing for mud pellet specimen used for tensile testing

Micro-electric force machine is used to test minuscule material (mud pellets samples) where expected failure occurs after few micrometers. Such condition is expected to be encountered with mud pellets; hence a micro-electric force machine is used for mud pellet tensile testing, such machine is shown in figure (4.6).

The mud pellet was well connected to the rods, figure (4.7) shows a rial picture for the mud pellet specimen used for tensile testing. Test records were obtained from the data acquisition system connected to the machine. The system records the amount of force possible to move the rod 0.001 µm along vertical axis every 0.001 second. All the data were recorded till the specimen crack. . Micro/nano tensile equipment (BOSE, Model: 3220) was operated under constant displacement rate 0.005mm/s with the maximum load of 200N and the maximum displacement of 6.5 mm.

The total tensile force in newton multiplied by the final relative displacement in millimeters as shown in figure (4.5) determines the actual work required to separate the mud particles from each other. The area under the curve represents the amount of cohesive and adhesive force.

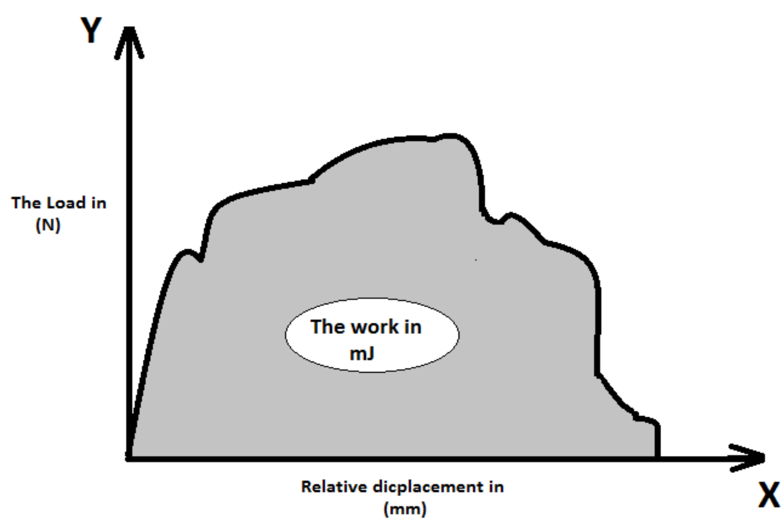

Figure 4.5. The load variation with the displacement

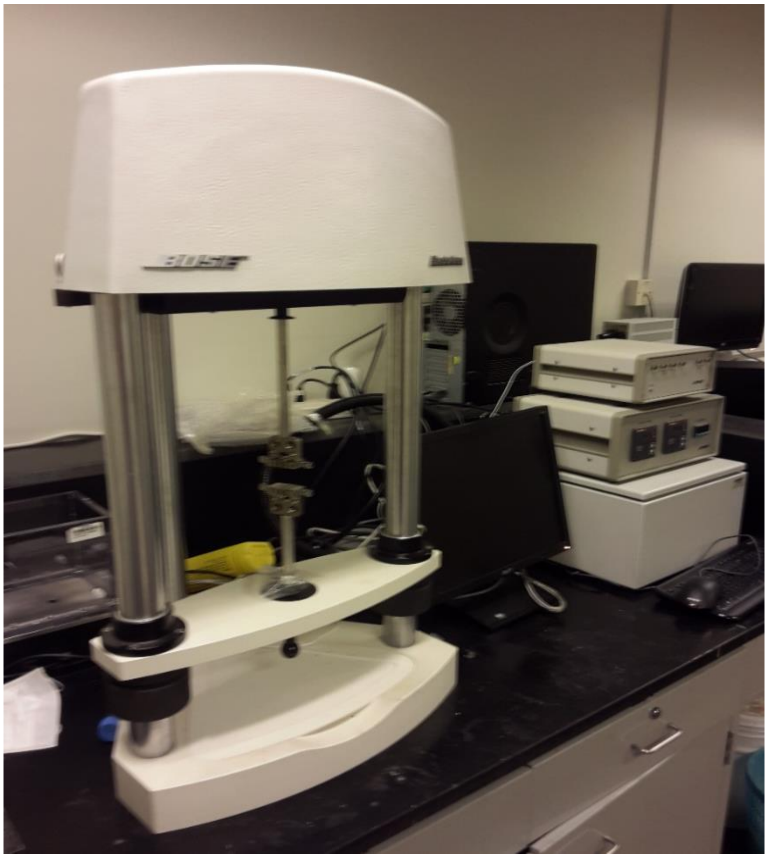

Figure 4.6. The micro-electric machine for the mud pellets tensile testing

Figure 4.7. The mud pellet specimen for tensile testing

4.3.3 Scratching test

Functional behavior of a coating material is critical to its adhesion to the specimen surface. Scratching test is an effective method, fast analysis method which is widely used to obtain critical loads that are functions of adhesion properties of coating. In scratching method stylus is moved over the specimen surface (as shown in figure (4.8)) with a linearly increasing load until failure occurs at critical loads (Lci). Tangential forces (Fx) and normal force (Fz) are recorded. The failure events are examined by an optical microscope. Acoustic Emission (AE) is also measured during the test.

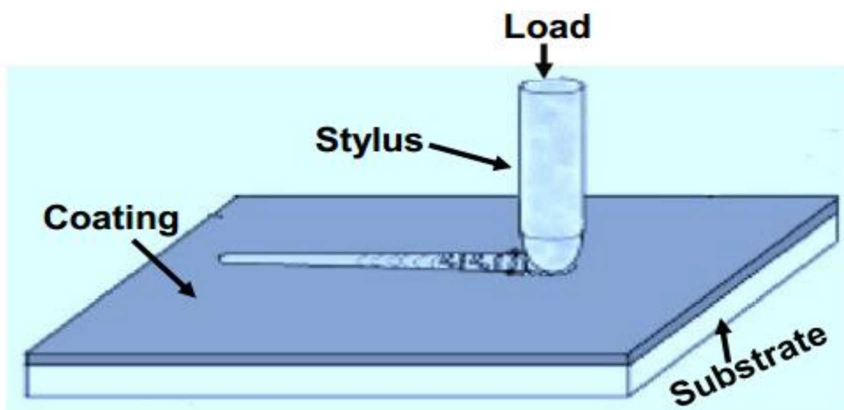

Figure 4.8. The specimen surface during scratching test

Critical load (Lc) is a function of coating-substrate adhesion, loading rate, stylus tip radius, internal stress in coating, mechanical properties of specimen surface and coating, coating thickness, flaw size distribution of coating interface and the friction between stylus tip and coating. Coating Failure during Scratch Test occurs due to cohesive failure (occurs by tensile stress behind the stylus) or adhesive failure (Due to compressive stress). The coating separates from the substrate either by cracking and lifting (Buckling) or by full separation. Practical scratch adhesion value of coating is defined as the lowest critical load at which a coating fails. It is an important parameter related to coating-substrate adhesion that could be used for comparative evaluation of coatings. A similar situation arises when mud solution settles on the surface of PV module protective glass cover as a coating layer. Hence, the above described procedure was used to determine the dust adhesion properties. Figure (4.9) shows the scratching test machine that was used to measure the critical scratching load, friction coefficient and penetration depth.

4.3.4 Sample preparation for scratching test

A polycarbonate surface was used as a substrate for the mud solution layer coating. A fresh dust was mixed thoroughly with DI water with a ratio 1:3 grams using ultrasonic mixture to get homogenous solution. After one hour, the solid particles were settled at the bottom due to density variation and the mud solution remained at the top of the container.
Small droplets of mud solution were put on the glass surface forming a thin layer of coating. After one to two days the mud solution samples got dry under room temperature and it ready to perform scratching test, elemental and compound analysis. Figure (4.10) shows the dry mud solution samples used in scratching test.

The friction coefficient and tangential force for adhesion work calculations are measured using the linear micro-scratch tester (MCTX-S/N: 01-04300). During the experiments, the equipment was set at the contact load of 0.03 N and end load of 5 N. The total length for the scratch tests was 10 mm and the scanning speed was kept at 5 mm/min with the loading rate of 5 N/s. Table (4.1) lists the input parameters for the scratching test. Five different samples had been examined.

Table 4.1. The input parameters used during the scratching test

Scratch parameters	
Linear Scratch	Position Y (mm) : 89.938
Type : Progressive	+ Instrument : MCTX S/N: 01-04300
Begin Load (N) : 0.03	+ Hardware settings
End Load (N) : 2	Fn contact : 0.03 N
Loading rate (N/min) : 1.18	Fn Speed : 5 N/s
	Fn Remove speed : 10 N/s
AESensitivity : 6	Approach speed : 2 %/s
Scanning load (N) : 0.03	Dz sensor in standard range
Speed (mm/min) : 6	
Length (mm) : 10	Date : 2/10/2016
Position X (mm) : 95.216	Hour : 1:51:40 PM
Indenters	
Type : Rockwell	Material : Diamond
Serial number : I-172	Radius (μm) : 100

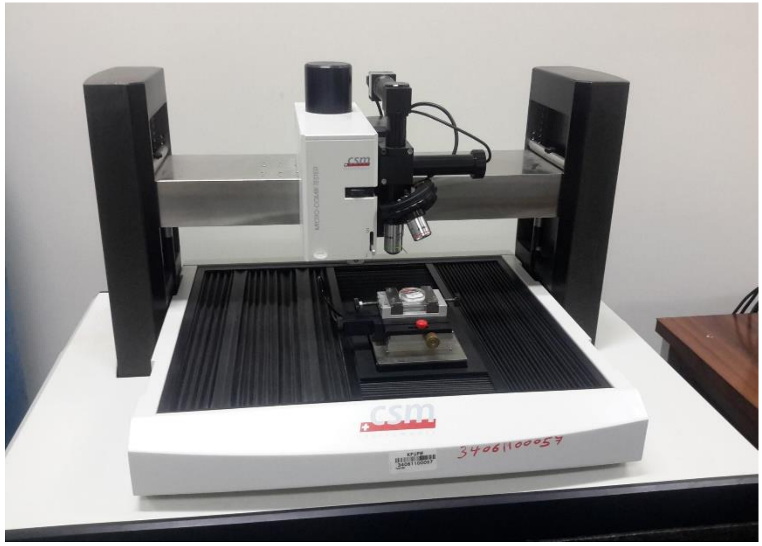

Figure 4.9. Scratching test machine

Figure 4.10. Dry mud solution samples used in scratching test

4.4 Microstructure characterization

4.4.1 Sample preparation (Specimens coating)

Sample preparation is an important issue in material characterization such as optical microscopy, scanning electron microscopy, 3Dimaging, compound analysis and elemental analysis. Generally, there are various preparation techniques that can be used. Selecting a specific technique depends on the type of information need to be analyzed. However, the common sample preparation approaches are: cutting the specimens to fit the holder size, mounting the sample, etching and coating the spacemen to prevent charging.

When using scanning electron microscope, electrically non-conductive materials such as ceramics and polymers, do absorb the electrons emitted the electron beam and hitting the surface of the sample. As a result of this, a negative charge well be formed which reduces the quality of the image [70]. Reducing either the accelerating voltage or the spot size can eliminate the charging effect to some extent, but it's limited by the tool capability. Hence, the best way to eliminate the charging effect is to coat the sample with a thin conducting layer (tenth of nanometers) of carbon or gold [71].

Dust samples are non-conductive material, so they need to be coated with a thin film of gold which cover details less than 50 nm. Surface charging plays a great role for image sharpness especially in non-conductive specimens such as polymers ceramics, and dust specimens[72]. To protect the dust samples surfaces from charging, a thin film of conductive material such as gold was used to coat the examined specimen surfaces. Conductive coating is accomplished by means of either sputtering or vacuum evaporating (using pure carbon or palladium). Sputtering cold coating was used for complex surface shapes, more sophisticated systems, targets that are available commercially. It requires short preparation time and forms a uniform film on rough specimens. Figure (4.11) shows the gold sputter coater machine used to coat the mud pellets fractured surfaces and figure (4.12) shows the mud pellet specimen fracture surface with gold coating.

A high voltage field around 3 kV was applied to the gold target (cathode) and the free electrons collided with the Ar atoms (Argon atoms) and ionized them. The positive ions knock out gold atoms and deposit on the fractured specimen surfaces of mud pellet. They formed a thin layer of gold (10 nm thickness) which made the surface conductive and eventually ready for SEM and light electron imaging.

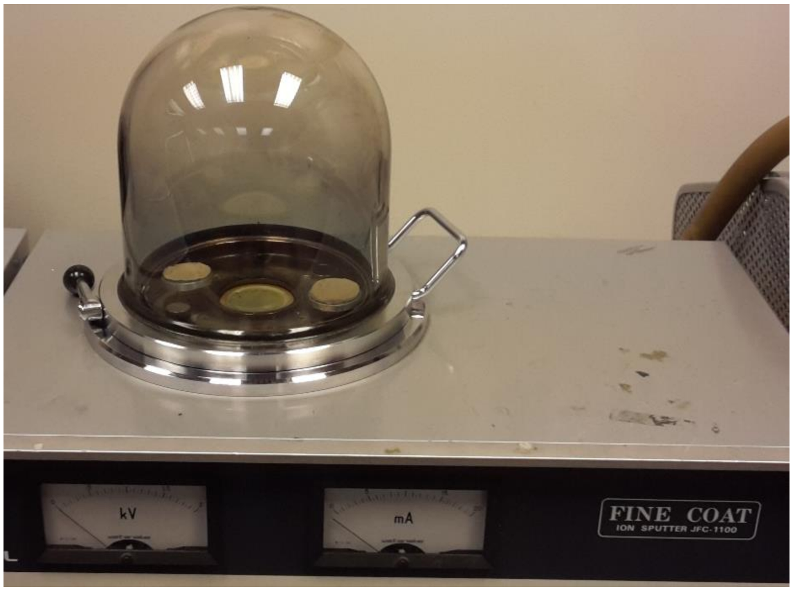

Figure 4.11. The gold sputter coater machine used to coat the mud pellets fractured

Figure 4.12. The mud specimen fracture surface with gold coating

4.4.2 Scanning electron microscopy (SEM)

One of the instrument used to examine the mud pellets fractured surface is SEM. SEM is a multipurpose device available for the microstructure identification, chemical composition and morphology exploration[72]. SEM is a technique used to create surface topography images on a microscopic level. The scanning of the specimen is carried out with a beam of high electrons energy in an electron beam column. The electrons are emitted by the beam electron filament which interact with the specimen atomic structure for topographic images generation. Numerous electrons kinds are produced from the beam emitter such as backscattered and secondary. Some microscopes contain also X-ray beam capabilities, which can create detailed information about elements specific location and the elemental structure of the specimen make-up as well [73]. Figure (4.13) shows the scanning electron microscopy components such as electron gun, electron lenses, specimen chamber and computer screen which was used to form a microscopic images in the current study.

It is very important to understand how to adjust the parameters of the SEM to best settings that will produce an image of highest resolution. For this study; the cracked mud pellets surface was examined after gold coating using SEM secondary electron imaging as shown in figure (4.12).

In such non-conductive surfaces, low accelerating voltage (5kV) for optimum sharpness and low-resolution imaging was used. But; coating the mud pellet surfaces allow the increase of accelerating voltage to 20 kV for good image resolution even in high magnification. Finally, the data obtained from SEM was analyzed thoroughly to indicate the influence of the tensile test on the mud pellets surfaces and surface topography at different magnifications.

Figure 4.13. The scanning electron microscopy components

4.4.3 X-Ray Diffraction (XRD)

X-Ray Diffraction (XRD) is an analytical technique used for phase identification and unknown solids determination of a crystalline samples in solid or powder phase[72]. It consists of three elements: a sample holder, X-ray tube, and the detector. Figure (4.14) represents the XRD machine used for the specimen quantitative analysis.

This study aims to analyze the dust and mud pellet because different behavior was expected in XRD analysis. The test was carried out for a wide range of two theta angle (between 20^o and 90^o). Three different types of samples were analyzed:

a) Fresh dust in powder form.
b) The fracture mud pallets after tensile testing
c) A thin layer of dry mud solution on a polycarbonate surface.

A typical setting of XRD was 40 kV and 30 mA and scanning angle (2θ) was ranged 20^o-90^o. For XRD test no sample preparations method took place (specimen as received). Figure (4.15) shows the samples used in XRD characterization.

4.4.4 Atomic force microscopy (AFM)

A 3D profile of the surface was provided using Atomic force microscopy (AFM) on a nano-scale. The forces were measured between the surface and sharp probe at short distance. The surface texture was analyzed using AFM/SPM Microscope, by Agilent, in contact mode. The AFM microscope tip was made of silicon nitride probes (r = 20 - 60 nm) with a manufacturer specified force constant, k, of 0.12 N/m.

Figure 4.14. The X-Ray Diffraction (XRD) machine

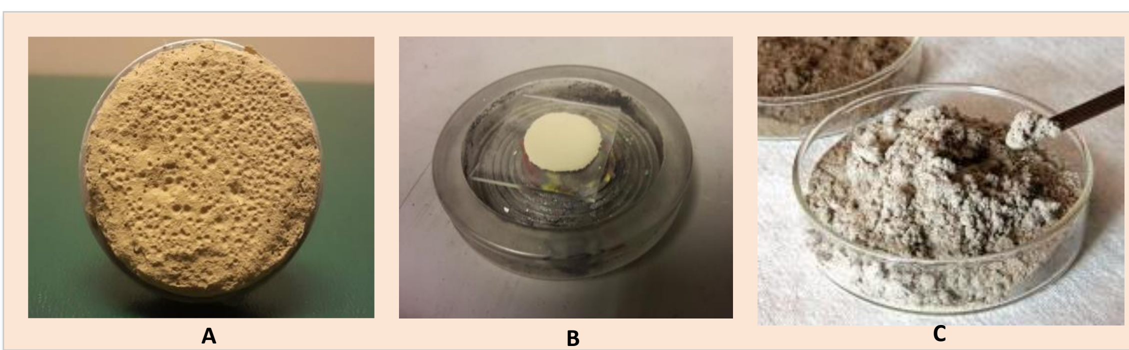

Figure 4.15. The samples used in XRD characterization: a) the fracture mud pellet sample, b) the mud pellet and c) powder sample

4.4.5 3D optical microscope

One of the instruments used to examine the mud pellets micro-structure is a 3D optical microscope. The 3D optical microscope is a light microscope based on white light interferometry that uses the light photons beam to form detailed three-dimensional images from the specimen surface. The advantage of the image taken by the light electron microscope was its accuracy and high magnification which showed more information about surface topography. Furthermore, 3D optical microscopy used for quantitative measurement, metrology applications of surfaces and providing non-contact measurement. Figure (4.16) shows a 3D optical microscope made by Bruker Company and used for this study.

4.4.5.1 Sample preparation

Similar to scanning electron microscopy, sample preparation for 3D optical microscope imaging does not require grinding, mounting, cutting and polishing of the specimens. But gold coating is primary requirement for mud pellet fractured samples to reflect the light beam coming from the microscope.

The 3D images were taken for several mud pellet fractured surface samples at more than ten different locations to ensure good surface assessments. The different heights in the 3D image (with scale bar in micrometer scale) indicated the percentage of the cohesion and the adhesion on the sample surfaces. The same specimens that used for tensile testing were prepared for 3D optical imaging and SEM. The idea of using such technique can be summarized as: The tensile testing experiment calculated the combined amount of adhesive and cohesive forces corresponding to the mud pellets area about 126 mm^2. Using SEM and elemental analysis (energy dispersive spectrometry); the microstructure of mud pellets fractured surfaces and their topography were obtained and examined. 3D optical microscopy gave detailed information about the shape and size of the features of microscopic surfaces as well as measuring surface topography. Using such data the percentage of adhesion forces to cohesion forces were estimated. The values of adhesion and cohesion forces obtained by tensile testing and the percentage of these forces for the same mud pellets provided a strong indication of final adhesive and cohesive forces assessments.

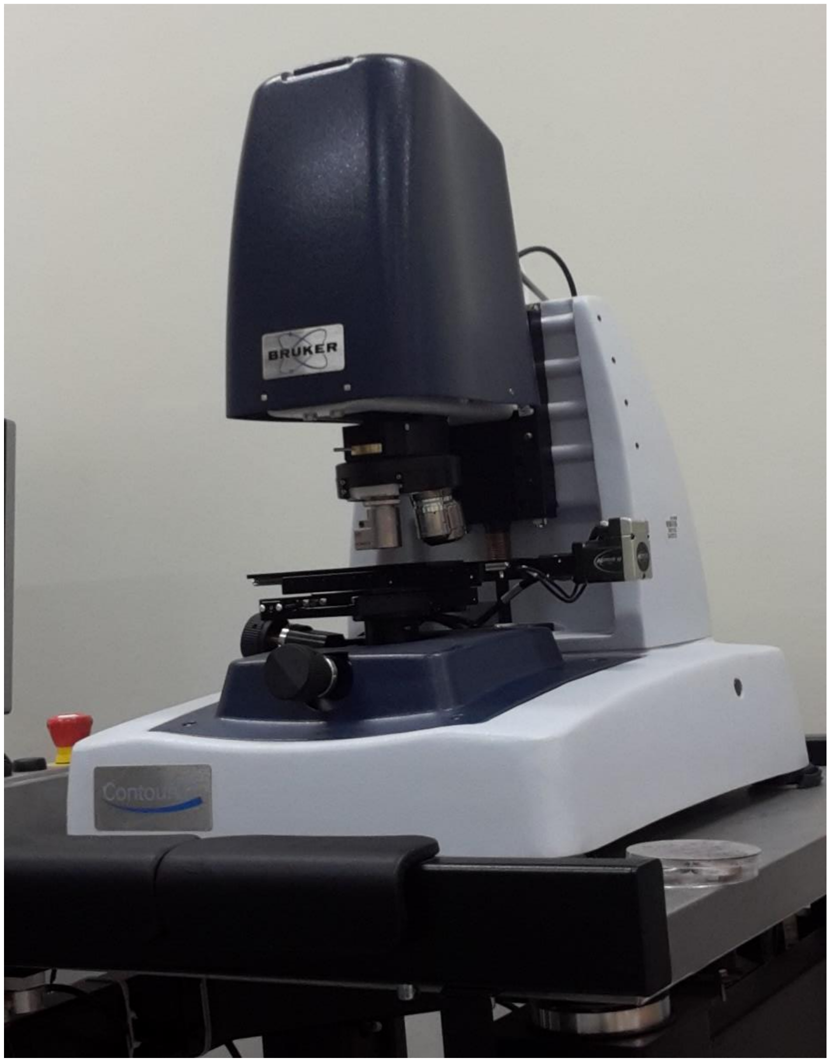

Figure 4.16. 3D optical microscope made by Bruker Company and used for this study

4.4.6 Energy Dispersive Spectroscopy (EDS)

SEM images created from Backscattered electron shows the phase contrast as a consequences of atomic number variation of the substrate elements and their spreading. Energy Dispersive Spectroscopy (EDS) permits to recognize what are those elements and the percentage of their quantities. Figure (4.17) shows the gold coated sample used for SEM and EDS analysis.

The elemental analysis software permits to get the resultant elemental data from the specimen surface. By keeping the electron beam fixed on a specified pixel or series of pixels the software can produce spectra provides elemental information for that localized area. Figure (4.18) shows the SEM image which represents the area that has been scanned (100 µm) for the elemental analysis.

Figure 4.17. The gold coated sample used for SEM and EDS analysis.

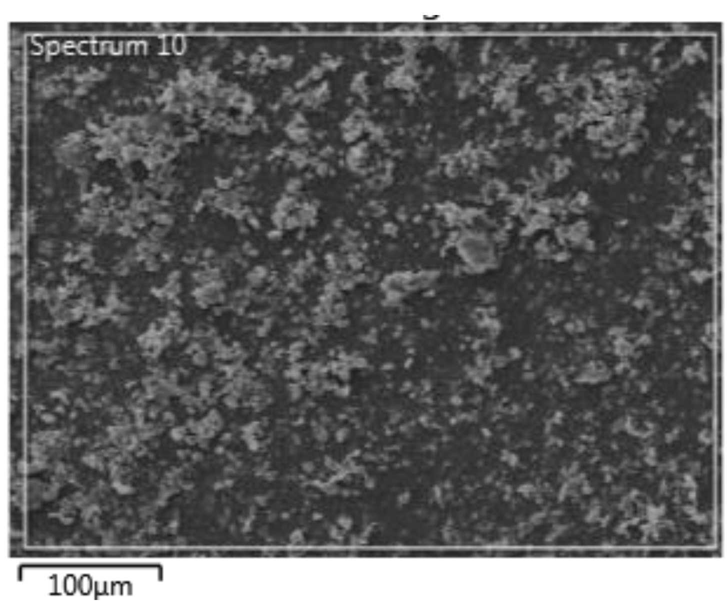

Figure 4.18. The SEM image which represents the area that has been scanned (100 µm) for the elemental analysis

4.5 Chemical investigation group

4.5.1 Fourier transform infrared spectroscopy (FTIR)

FTIR technique is used to obtain the emission or absorption infrared spectrum of gas, thin films, liquid or solid specimens. Some of infrared radiation passed through a specimen (transmitted) and other is absorbed. The final spectrum represented a molecular fingerprint of the specimen which add a strength to this type of analysis. The data of high spectral resolution were collected simultaneously with a wavelength range wider than dispersive spectrometer which consider as one of the advantages. IR spectrometry can give qualitative versus quantitative analysis (positive identification) and the spectrum peaks size represents the amount of material present. FTIR analysis provide different information:

- It can identify unknown materials
- It can determine the quality or consistency of a sample
- It can determine the amount of components in a mixture

Infrared spectrometer has infrared light source that is the baseline of energy. The dry mud solution sample is put in stage under the light path and then the absorbance of the dry mud sample is used to measure the bonds of the carbon atoms (atomic analysis) as shown in figure (4.19). The analysis process of FTIR is summarized in figure (4.20). The components and instrumental process for FTIR can be demonstrated as follows:

1. The Source: the energy is emitted from a radiant blackbody source. The radiation beam enters an aperture to control energy presented to the sample.

2. The Interferometer: where the spectral encoding takes place.

3. The dry mud pellet Sample: The beam is transmitted through or reflected off of the surface of the sample, depending on the type of analysis being accomplished.

4. The Detector: Finally the beam passes to light detector for last measurement. The detectors used are specially designed to measure the special interferogram signal.

5. The Computer: where the Fourier transformation (FT) takes place. The final IR spectrum is showed to the user for manipulation and interpretation.

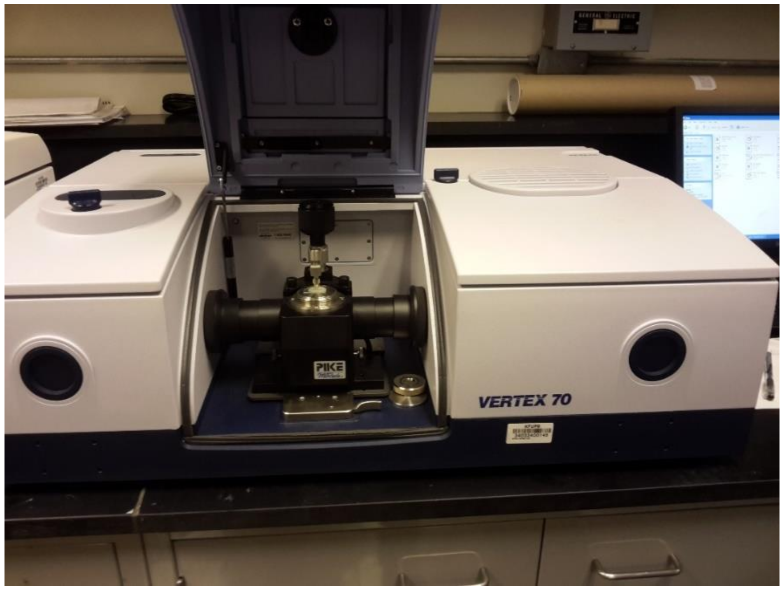

(a)

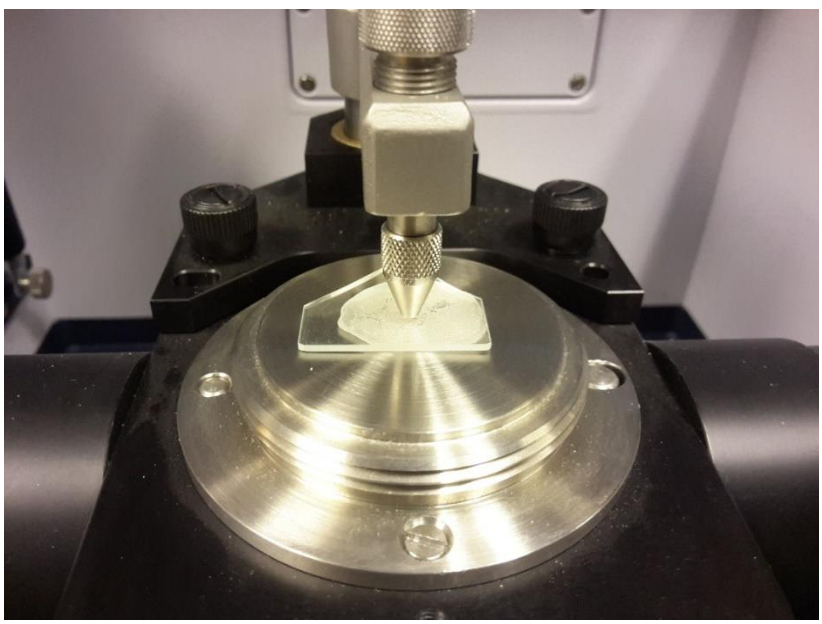

(b)

Figure 4.19. FTIR testing system: a) the FTIR device components, and b) sample placed on sample stage under IR path.

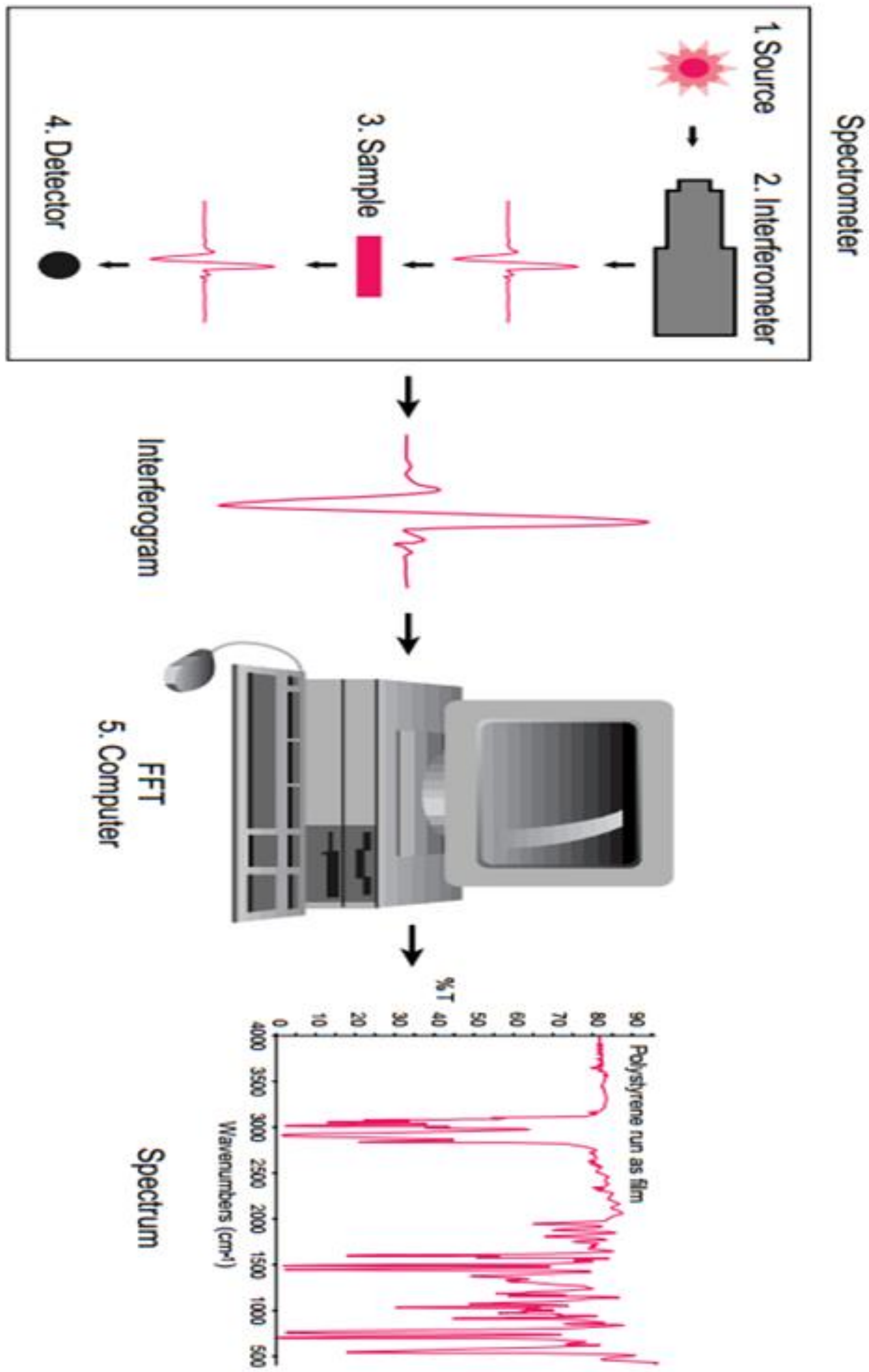

Figure 4.20. The analysis process of FTIR testing method

4.5.2 PH measurement

PH is an abbreviation of “pondus hydrogenii” and was proposed by the Danish scientist S.P.L. Sørensen in 1909 in order to express the very small concentrations of hydrogen ions. The definition based on hydrogen ion activity given as:

$$PH = -\log_{10} a_{H+}$$

Figure (4.21) shows the pH meter device used to measure the pH of mud solution. The pH is measured using a setup with two electrodes: the indicator electrode and the reference electrode. These two electrodes are often combined into one (combined electrode). PH lower than 7 means high concentration of H^+ (acid solution) and for PH greater than 7 means low concentration of H^+. The greater the PH, the higher negative charge of particle and more tendency for H^+ to attract the solution from the hydroxyl. Hydroxyls OH^- are located on the mud solution particles edges to dissociate in water. The mud solution used for PH measurement was a mixture of fresh dust and DI water with ratio 1:3. The data was recorded for different temperature during one hour time intervals.

Figure 4.21. The pH meter device used for mud solution pH measurements

CHAPTER 5

RESULTS AND DISCUSSION

Characteristics of the environmental dust and mud formed from the dust particles are examined. The adhesion among the dust particles in the dry mud is assessed using the analytical tools. The adhesion between the dry mud residues and the glass surface is assessed incorporating the micro/nano scratch tests. The findings are presented under the appropriate sub-headings.

5.1 Characterization of Dust Particles:

Figure (5.1) shows SEM micrographs of dust particles. In general, dust particles compose of various sizes and shapes. Small dust particles attach the large particles, which is associated with the electrostatic charges of small particles. Small dust particles are exposed to the solar radiation for long durations and attachment of ionic compounds to these particles in the region close to the sea areas causes static charging of these particles [29]. The shape of dust particles can be categorized through two key geometric parameters. These include the shape factor ($R_{Shape} = \frac{P^2}{4\pi A}$, where P is perimeter of the dust particle) and the aspect ratio ($A_{Aspect} = \frac{\pi (L_{proj})^2}{4A}$, where A is the cross-sectional area and L_{proj} is the longest projection length of the dust). The shape factor is related to the inverse of the particle circularity in relation to the complexity of the particle; in which case, the shape factor of unity corresponds to the perfect circle. The aspect ratio corresponds to the ratio of major to minor axes of the ellipsoid best fit to the particle, which is associated with the approximate particle roundness. Consequently, from the measured particle sizes, the equivalent circular area can be determined for the round shapes. In the case of non-circular shapes, an ellipse is considered through assuming that the longest projection as the major axis and preserving the particle cross-sectional area. The relation between the particle size and the aspect ratio or the shape factor is not simple. However, a simplified assessment can be introduced to classify dust particles in terms of their shapes. Since the inverse relation is observed in between the particle size and the aspect ratio, increasing particle sizes gives rise to low aspect ratios. However, a direct relation is present in between the particle size and the shape factor. Consequently, shape factor increases while aspect radio reduces with increasing particle size. The shape factor becomes almost unity for the small size particles (≤ 2 μm) and the median shape factor approaches almost 3 for the large size particles (≥ 10 μm). Although the particle size varies within sub-micrometer to tens of micrometer, the average particle size is in the order of 1.2 μm. Table (5.1) gives the EDS data (wt%) of dust particles. Dust particles contain various elements including Si, Ca, Mg, Na, K, Cl, S, O and Fe. In addition, presence of oxygen in the EDS data indicates the oxide compounds of these elements are present; however, Cl reveals the presence of salt compounds in dust particles. This is attributed to prolonged duration of dust in atmosphere close to the Arabian Gulf. It should be noted that dust particles are collected in the near region of Dammam, which is close to the Arabian Gulf. The existence of salt and oxide compounds in dust particles is also evident from figure (5.2), in which X-ray diffractogram is shown for dust particles. The peaks of K, Na, Ca, S, Cl, and Fe are present in the diffractogram. The peaks of Na and K are probably related to the sea salt because dust particles are gathered from Dammam region in Saudi Arabia, which is close to the Arabian Gulf. Sulphur can be associated with calcium, such as anhydrite or gypsum components ($CaSO_4$), in dust particles. Iron is likely related to the clay-aggregated hematite (Fe_2O_3).

Table 5.1. Elemental composition of the dust particles (wt%).

	Si	Ca	Na	S	Mg	K	Fe	Cl	O
Size > 2 μm	11.1	7.1	3.2	2.1	2.4	1.2	1.2	1.1	Balance
Size < 2 μm	11.7	7.9	4.9	1.8	3.7	2.5	1.1	2.4	Balance

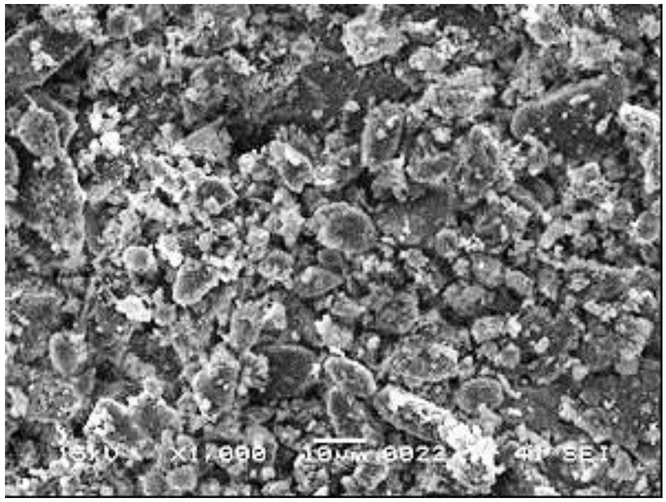

(a)

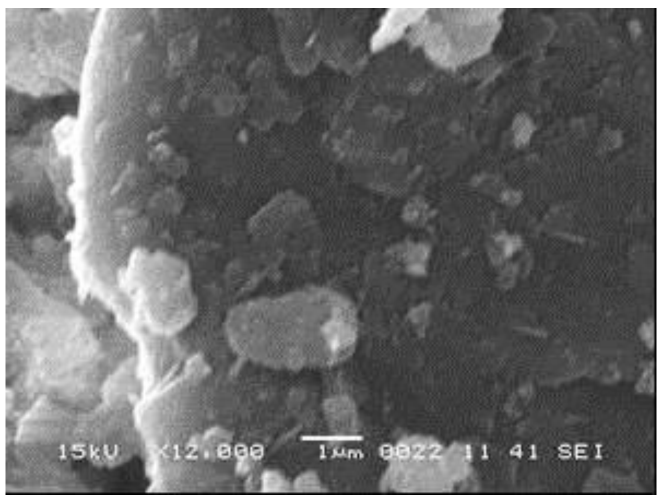

(b)

Figure 5.1. SEM micrograph of dust particles: a) various sizes of dust particles, and b) small dust particles adhere surface of large dust particles

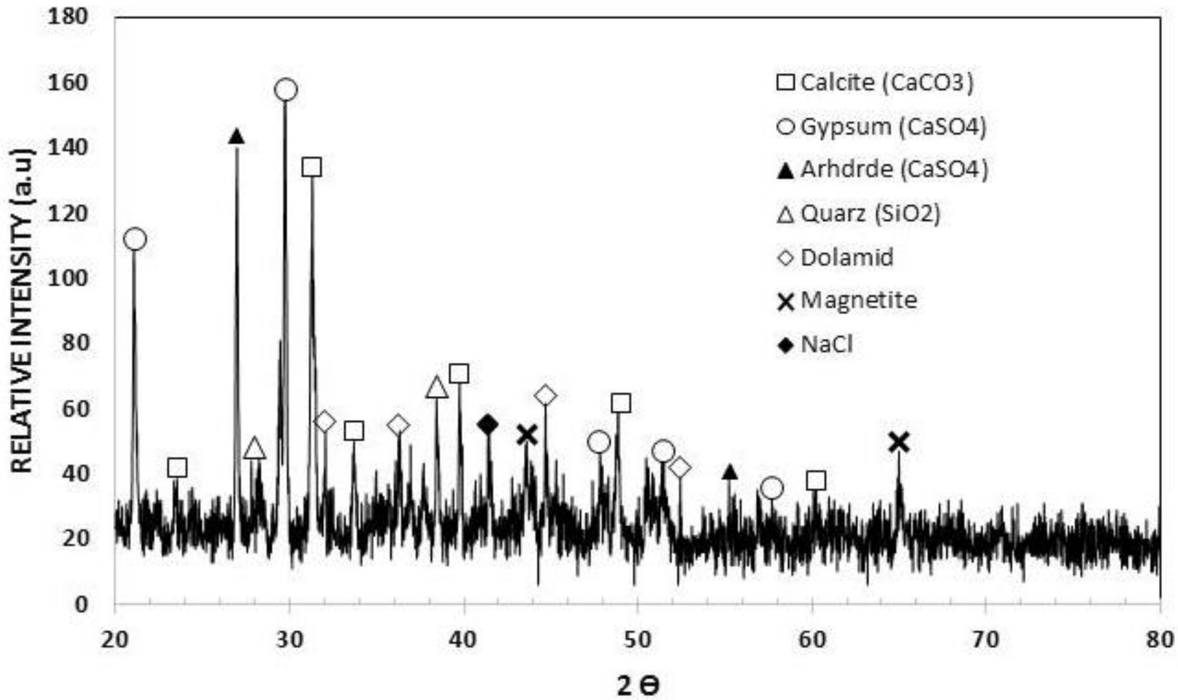

Figure 5.2. XRD diffractogram for dust particles.

5.2 Characterization of Mud Solution and Dry Mud:

Mud solution (liquid) is extracted from the mixture of dust particles and water. pH of mud liquid is measured and analyzed using inductively coupled plasma mass spectroscopy. Figure (5.3) shows temporal variation of mud liquid pH while Table (5.2) gives the data obtained from inductively coupled plasma mass analysis. It is evident that pH of mud liquid increases significantly with time and reaches almost steady after 10 days. pH of the solution demonstrates base nature and the high rate of increase pH is associated with the presence of OH^{-} ions in mud solution, which is related to the dissolution of alkaline (Na, K) and Alkaline earth (Ca) metals in dust particles. This can be also observed from Table (5.1); in which case, the presence of alkaline and alkaline earth metals are present. In order to assess dry mud solution characteristics, when dried on surfaces, mud liquid is placed on a glass surface and dried under the controlled environment (at 20 ^{o}C and 1 atmospheric pressure). Figure (5.4) shows SEM micrographs of dried mud solution on the glass surface. The various sizes of crystal structures are formed on the glass surface (figures (5.4a) and (5.4b)). It should be noted that although drying takes place under controlled environments, the local heat transfer modifies the crystal sizes on the glass surface [30]. In this case, the size of crystal structures becomes small when local cooling rates is high at the surface (figure (5.4a)). However, the opposite is true for low cooling rates where the crystal structures grow in large sizes (figure (5.4b) [30]. Appendix (C, b) shows more SEM micrographs of dried mud solution on the glass surface at different magnification. The elemental composition of crystallized structures on the glass surface is analyzed and Table 3 gives the EDS data in this regard. The crystallized layer shows that alkaline (K, Na) and alkaline earth metals (Ca), oxygen and chlorine are present in the crustal structures. The FRIR analysis was carried out for the dry mud solution on glass surface. Figure (5.5) shows the data obtained from FTIR test and hydroxyl OH^{-} peaks were observed at 3400. Appendix (A) shows the Table of Characteristic IR Absorptions used in FTIR investigation. Therefore, the compounds of alkaline and alkaline earth metals dissolve in water and form chemically active liquid at the glass surface. It should be noted that the mud solution has chemically active characteristics [31]. However, electrochemical tests are left for the future study for the assessment of chemical potential of mud solution.

Table 5.2. Inductively coupled plasma spectroscopy (ICP) data (ppb) for the mud solution after 8 hours dissolution time of dust particles in desalinated water.

Ca	Na	Mg	K	Fe	Cl
309800	44600	69950	33400	1830	37600

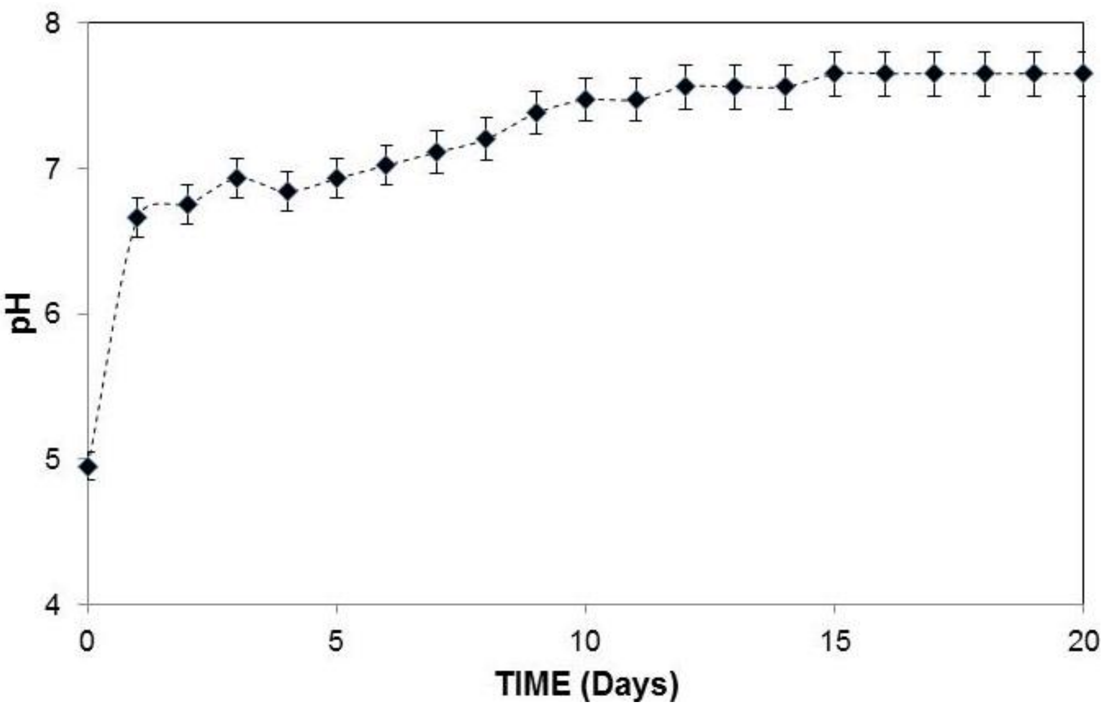

Figure 5.3. Temporal variation mud pH of mud solution.

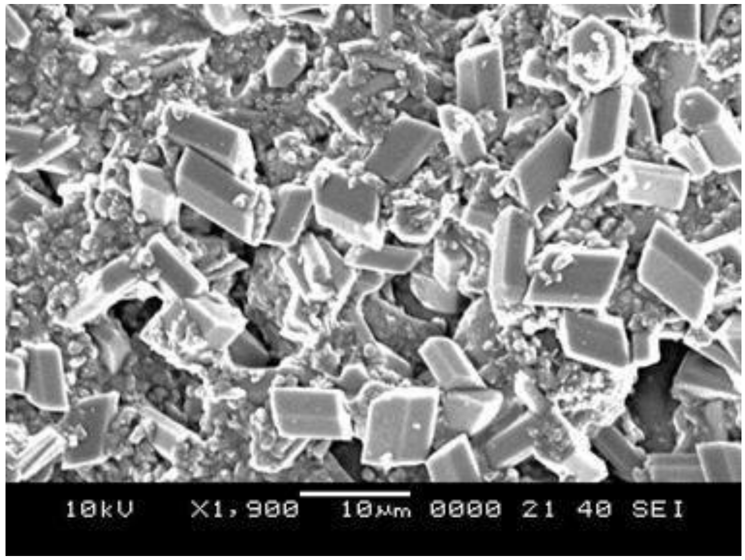

(a)

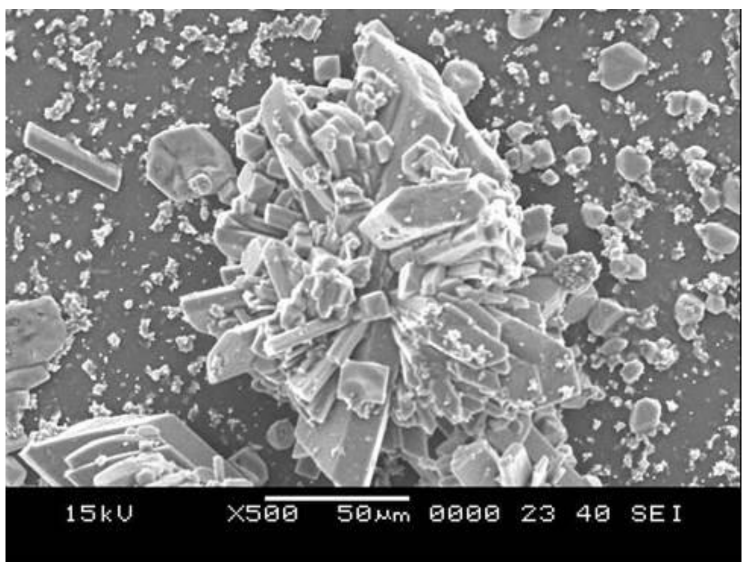

(b)

Figure 5.4. SEM micrograph of crystalized structures formed on glass surface after drying of mud solution.

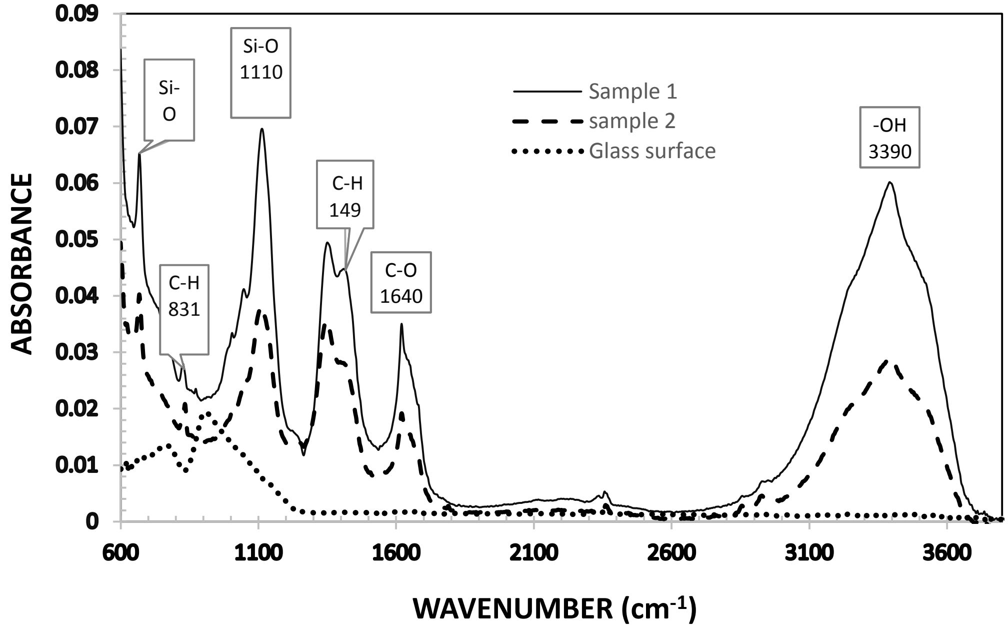

(a)

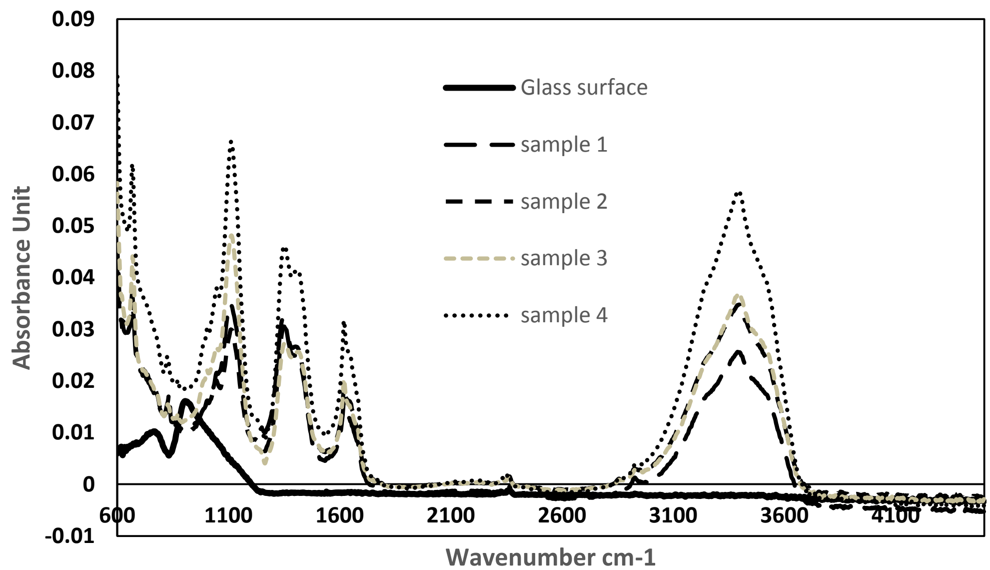

(b)

Figure 5.5. Shows the FTIR experimental test data: a) the chemical bonding stretching which indicated the hydroxyl OH- stretch peaks at 3400 cm-1 and b) The FTIR experimental test data for glass and four different samples.

Figures (5.6) and (5.7) show SEM micrographs of dry mud surface and dry mud cross-section. The large particles together with closely spaced small particles are observed at the surface of the dry mud (figures (5.6a)) while at some locations large particles some voids are observed (figure (5.6b)). In addition, some small voids occur at dry mud surface. This is mainly associated with the evaporation of water from mud surface during drying, which resulted in porous like morphology at the surface. Appendix (C, A) shows additional SEM micrograph of mud surface for three different samples with different magnifications and some voids are also observed. However, mud contains compounds of alkali and alkali earth metals (Table 5.3), these compounds dissolve in water during mud formation while forming mud solution, which flows across the mud cross-section towards the glass surface under the gravity. Mud solution accumulates at the glass surface and forms a thin liquid layer. Upon drying, a crystallized dry mud solution is formed in between dry mud and the glass surface. This situation can be observed from figure (5.7a), in which SEM micrographs of dry mud cross-section are shown. Dry mud cross-section consists of porous like structures including some small cavities across the cross-section (figure (5.7b)) because of the various dust particle sizes (0.001 – 20 μm). This arrangement enables liquid mud solution flow in between these structures. However, some of liquid mud solution is sediment in cavities across the cross-section (figure (5.7a)). This appears as bright color in SEM image (figure (5.7b)). In order to assess the effect of dry mud and its solution on the glass surface, dry mud is removed from the glass surface by a pressurized distilled water jet. Figure (5.8) shows SEM micrographs of the residues of dust particles on the glass surface. The residues of dry mud are related to dry mud solution in between dust particles and the glass surface, which increased the adhesion at the interface in between them. EDS analysis of the dry mud residues reveals that the dry mud residues composes of Ca and Si with presence of Na, K and Cl (Table 5. 4). This indicates that residues of dry mud solution together with dry mud particles are present at the glass surface (figure (5.8)). In addition, close examination of SEM micrograph (figure (5.8)) reveals that some crystallized structures are formed at the surface; in which case, dissolved alkaline and earth alkaline metals are responsible for the crystalline morphology on the dry mud removed glass surface. Figure (5.9) shows AFM image of the dry mud removed glass surface. Dry mud residues formed various texture morphologies at the glass surface, which is evident from figure (5.9a), in which 3-dimensional image of the surface is shown. The texture height due to mud residues at the surface varies, which can be observed from the line scan at the dry mud removed surface (figure (5.9b)). The maximum height varies within the range 130 nm; therefore, the average surface roughness of the glass surface increases to 80 nm. In addition, some small cavities are formed at the glass surface after dry mud removal. The formation of small cavities is associated with hydroxyl attach at the surface because of high pH of liquid mud solution prior to drying [28]. Consequently, dry mud residues modify the surface texture and surface structure of the glass through hydroxyl attacks at the surface.

Table 5.3. Elemental composition of the crystals formed after drying of mud solution on glass surface (wt%).

	Si	Ca	Na	S	Mg	K	Fe	Cl	O
40^{o}C	0.6	20	1.4	9.1	0.4	0.4	0.6	1.7	Balance

Table 5.4. Elemental composition of dry mud residues on glass surface (wt%).

	Si	Ca	Na	S	Mg	K	Fe	Cl	O
40^{o}C	1.6	24	1.2	2.2	0.4	0.5	0.8	0.9	Balance

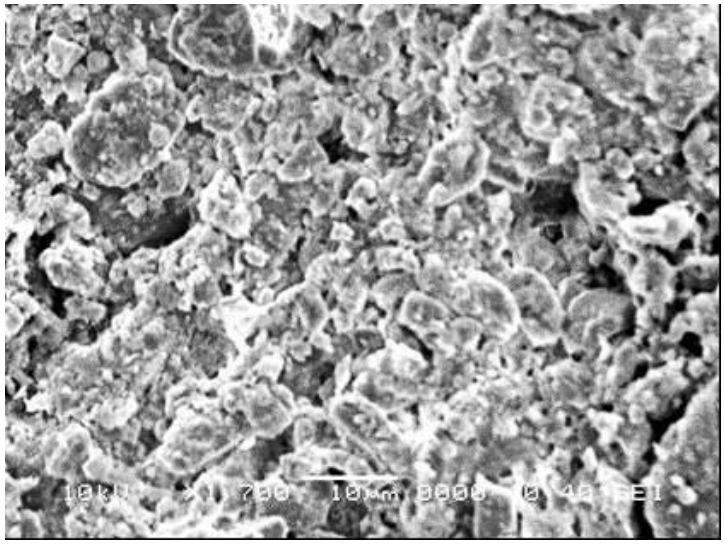

(a)

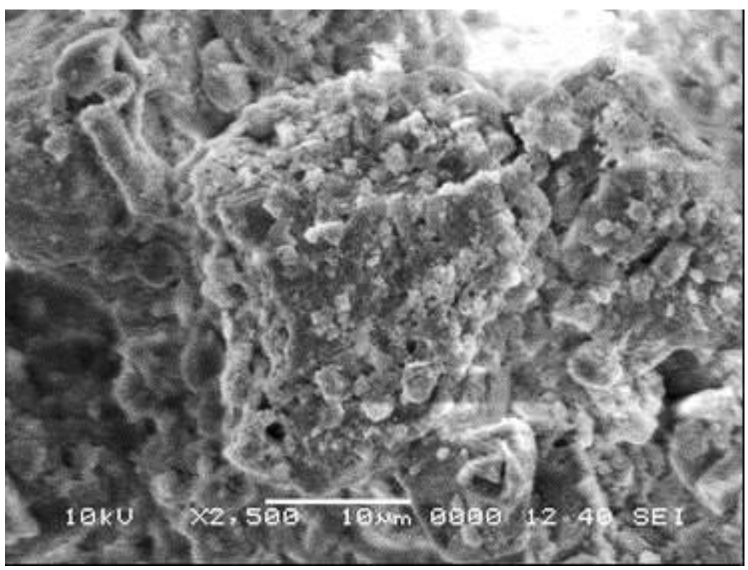

(b)

Figure 5.6. SEM micrograph of mud surface: a) voids are formed around large size dust particles, and b) dense structures are formed around small size dust particles because of mud solution.

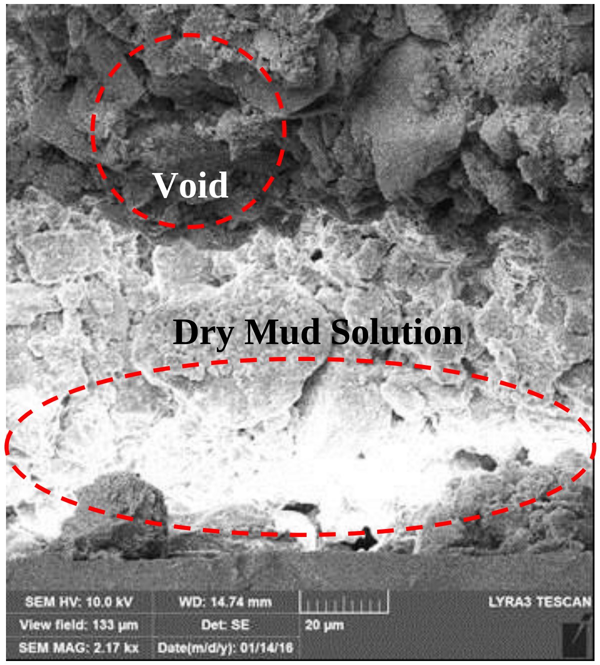

(a)

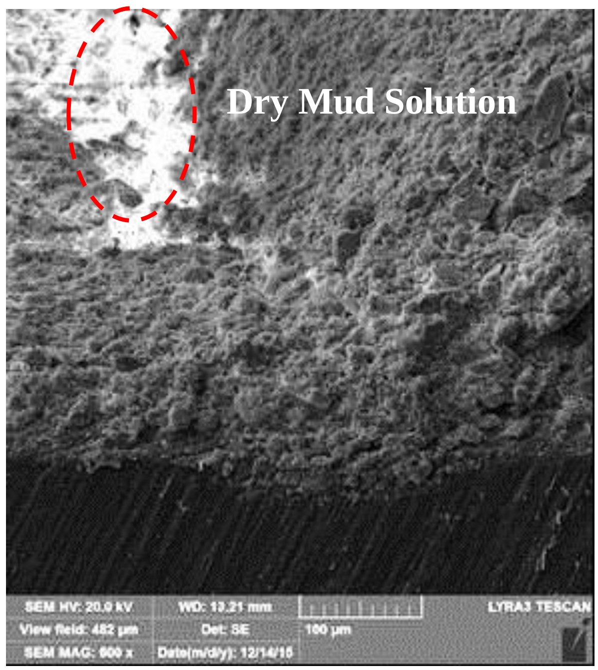

(b)

Figure 5.7. SEM micrograph of dry mud cross-section: a) Dry mud solution at dry mud-glass surface interface, and b) Dry mud solution in void.

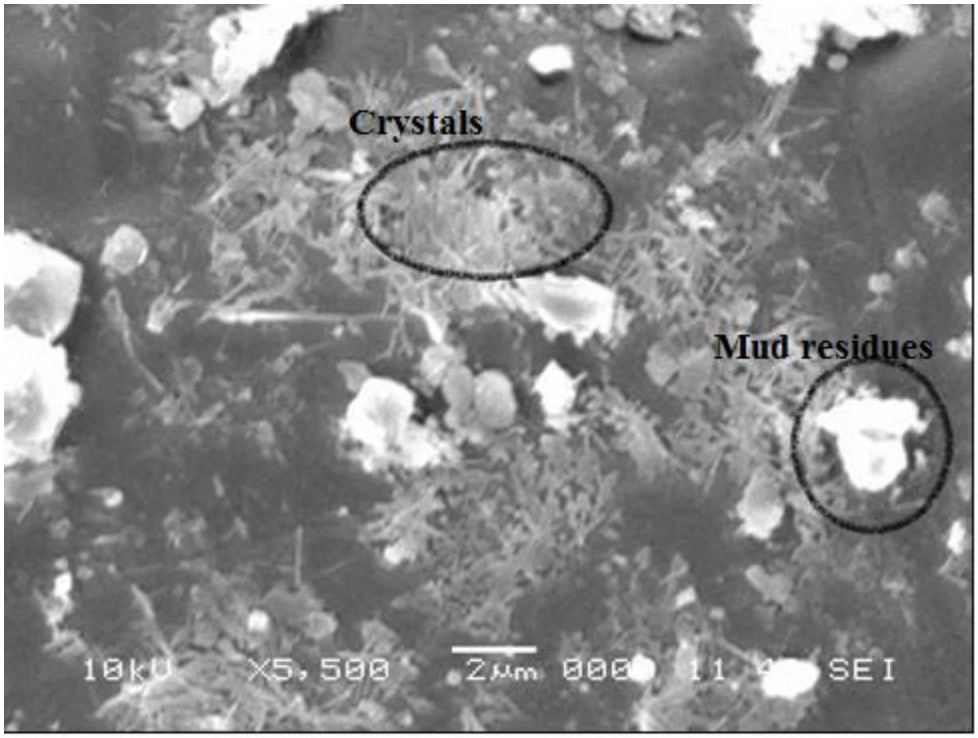

Figure 5.8. SEM micrograph of dry removed glass surface by using pressurized desalinated water jet.

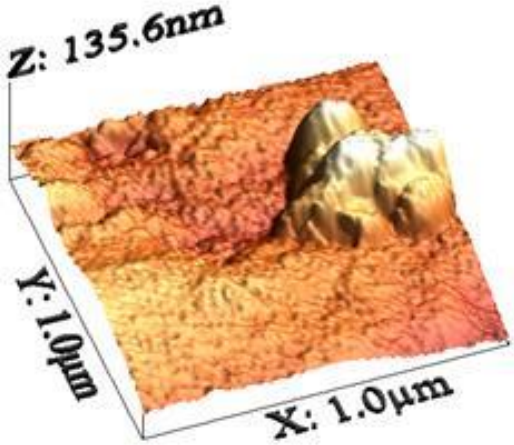

(a)

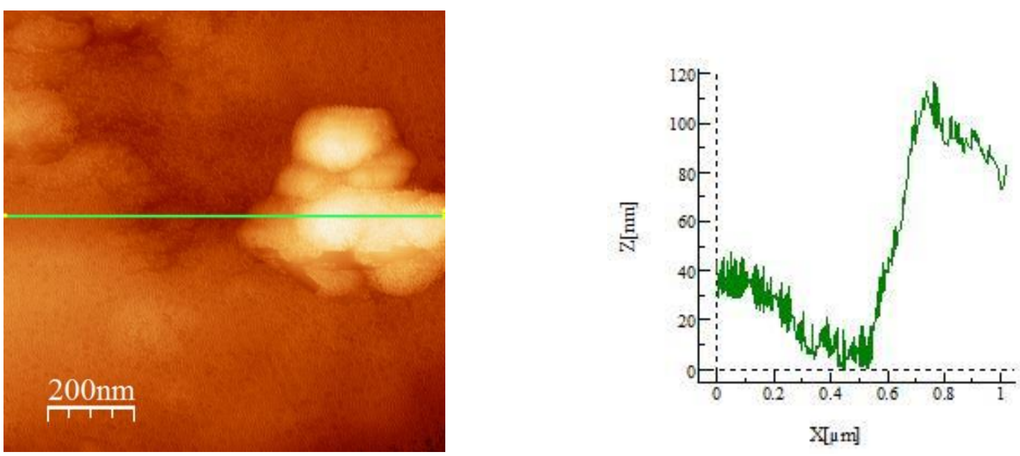

(b)

Figure 5.9. AFM micro-images of glass surface after dry mud removed by pressurized desalinated water jet a) 3-D image of surface, and b) line scan across the surface and texture height.

5.3 Mechanical Properties of Dry Mud:

Mechanical properties of dry mud are assessed via incorporating friction and tensile tests. The tangential force is monitored during friction tests to determine the adhesion work required to remove dry mud from the glass surface. Tensile tests provide combination of adhesion and cohesion forces (binding forces) in dry mud; therefore, cohesion forces due to drying of mud solution in dry mud are also assessed through comparison of tangential force and tensile test data.

Figure (5.10) shows the friction coefficient of as received, dry mud solution, and dry mud removed, by pressurized distilled water jet, samples while figure (5.11) shows the tangential force obtained during the dry mud removal from the glass surface, frictional force for the glass surface without mud deposition and tangential force corresponding to dry mud solution removal from the glass surface. It should be noted that the area below the force curves gives frictional and adhesion works. The friction coefficient attains the highest value for dry mud solution, and then follows for the surface after dry mud removal by the pressurized distilled water jet, and as received surface. Increase in the friction coefficient is the strong adhesion between the indenter tip and the dry mud solution surface, which is also seen from figure (5.11). Moreover, increased friction coefficient for dry mud removed surface is associated with the increased surface roughness because of the mud residues at the surface. It was reported that increasing surface roughness enhances the friction coefficient of the surface [32]. In addition, some small peaks in the friction curve are observed, which is related to surface roughness due to the mud residues at the surface. In addition, locally increasing friction coefficient is also related to the surface modification because of hydroxyl attacks at the surface during drying of mud solution on the glass surface. Consequently, surface roughness increase, due to mud residues and cavities formed because of hydroxyl attacks, contributes to the enhancement of friction coefficient of the surface. The scratch marks left on the as received glass surface and dry mud removed surface, by a pressurized distilled water jet, extend almost uniformly at the surface. However, some mud residues at the surface modify the scratch marks. This is attributed to the strong adhesion force between mud and the glass surface because of the thin film formed from dried mud solution at the interface. Moreover, no micro-crack is observed around the scar marks for as received and mud removed glass surfaces. This demonstrates that fracture toughness reduction due to surface modification by hydroxyl attack is not significant. In the case of tangential force (figure (5.11)), strong adhesion between dry mud and glass surface gives rise to sharp increase of tangential force. This appears locally on the force curve (figure (5.11)). Consequently, dry mud solution in between dry mud and the glass surface is responsible for increasing tangential force. Table (5.5) gives the adhesion work determined from the tangential force measured by using the scratch tester during dry mud removal. It should be noted that the adhesion work is obtained via integration of tangential force over the scratch distance. However, the adhesion work determined is corrected through subtracting the frictional work, which is obtained through integration of frictional force over the scratch distance for as received glass surface. The adhesion work determined is in the order of 0.119 mJ. The experiments for tangential force variation were repeated five times to assess the experimental error in measurements. The experimental error, based on the repeatability tests, reveals that the error is in the order of 17%.

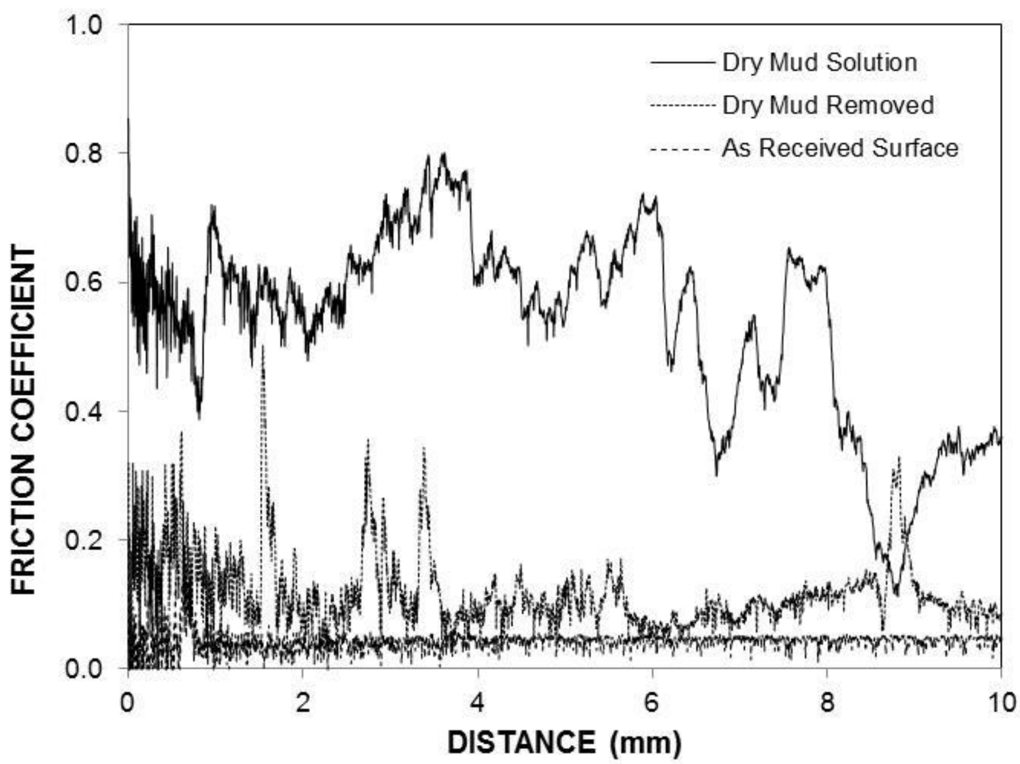

Figure 5.10. Friction coefficient for dry mud solution, as received glass surface, and dry mud removed surface by using pressurized desalinated water jet.

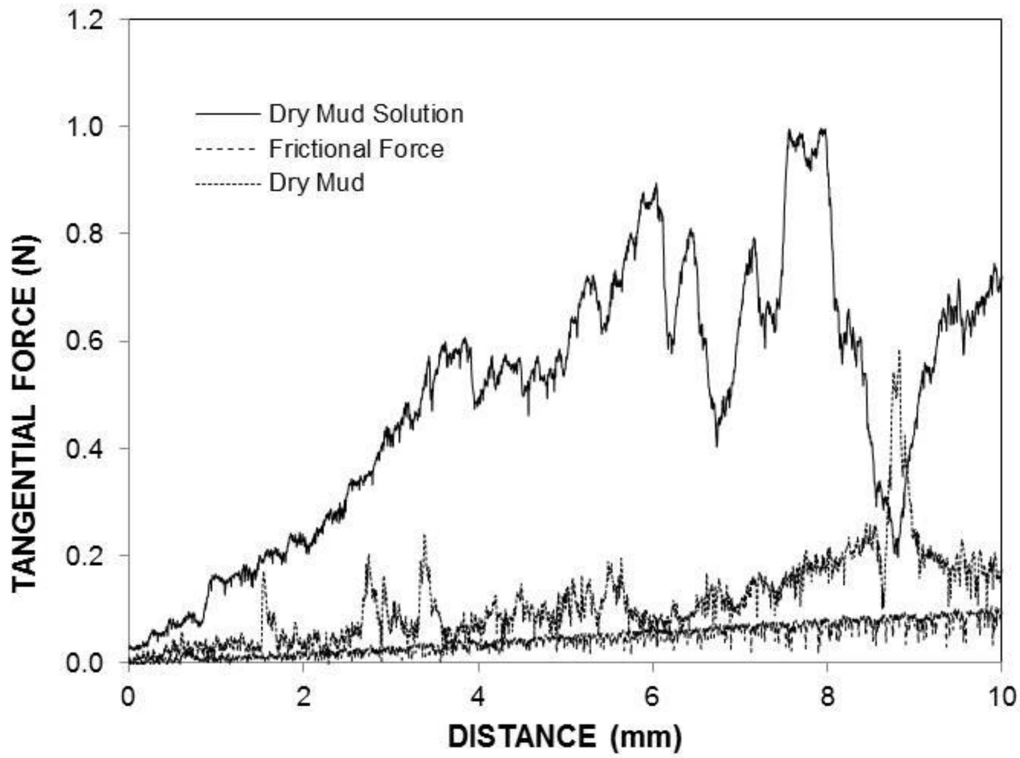

Figure 5.11. Tangential force obtained from scratch tests for dry mud solution and dry mud removed surface by using pressurized desalinated water jet, and frictional force as received glass surface is provided for comparison reason.

Figure (12) shows optical images of dry mud pellet after the tensile tests: figure (12a) is two dimensional close image of the fractured surface, figure (12b) is three-dimensional images of the fractured surface and figure (12c) corresponds to the fractured pellet. Figure (12) shows pulling force with the displacement obtained from the tensile tests. In the case of figure (13), pulling force increases to reach maximum without going through a yielding point as oppose to that observed for dense materials like metals. In addition no necking is observed in the tensile curve (figure (5.13)).It should be noted that necking is a mode of tensile deformation where relatively large amounts of strain localize disproportionately in a small region of the material; in which case; the resulting decrease in local cross-sectional area provides a form of plastic deformation where the necking occurs. The fractured facets are examined in details to determine the closely spaced mud structure where dry mud solution covers dust particle surfaces. Since mud liquid when dried causes the volume shrinkage because of evaporation of water, high strains are formed in the region where mud solution is dried. Consequently, rather closely packet mixture of dry mud solution and fine size dust particles are observed in some regions (figure (5.12a), marked as "region A" in the figure (5.12a) of the facet of fractured surface. This is also seen from figure (5.12b). However, in some other regions (marked as "region B" in the figures (5.12a) and (5.12b)), dust particles are large and are not covered completely by mud solution because of voids formed in between large dust particles. In this case, mud solution flows towards the glass surface under the gravity and the amount of mud solution present around large size dust particles remains low. Consequently, facets appear to have porous like texture (figure (5.12a)). Moreover, the coverage area of porous like fractured surface over the total area of the fractured surface is estimated from 3-dimensional images of the fractured surface (as shown in figure (5.12b)). The porous like structures appear to be blue lines where the textured height is negative (figure (5.12b)) and closely spaced dense layer appear as the brownish/reddish colors where the texture height is positive (figure (5.12b)). The area ratio of porous like faced over the total area of the faced after tensile test is found to be almost 78%. This indicates that closely spaced and dry mud solution covered faced surface is typically 22% of the total surface area of the dry mud pellet. Appendix (D) shows 3D imaging at different location and same results were observed. It is also considered that the binding force in the closely spaced and mud solution covered region is mainly the combination of cohesive and adhesive forces. However, the porous like textured region of the fractured surface is assumed to be dominated by the adhesion force. Based on this consideration, the ratio of adhesion force over the combination of the adhesion and cohesion forces is in the order of 3.55. This indicates that the adhesion force mainly governs the bindings force in dry mud pellet. The total work done during a tensile test is determined through integration of the pulling curve along the displacement, which corresponds to the area under the curve in figure (5.13). On the other hand, the tangential force is measured by the micro/nano tribometer (figure (5.13)); hence, the cohesion force can be determined from the tensile data as shown in figure (5.13). In this context, the contributions of the cohesion and adhesion forces to the binding work, which is required to separate dry mud pellet is determined using the data are given in Table 5. In this case, the total work due to adhesion and cohesion is in the order of 1.408 mJ, which corresponds to the area under the curve in figure (5.13) or per unit pellet area is 0.1121 mJ/mm^2. Since the adhesion work covers 78% of the total area and the adhesion work estimated from the tangential force is in the order of 0.119 mJ or per unit scratch area is 0.0148 mJ/mm^2, the cohesion work due to dry mud solution around the small dust particles becomes 0.0973 mJ/mm^2. Although the percentage of cohesion force based on the coverage area is small, its effect on the overall binding work is significant. Therefore, formation of a film from dry mud solution at the interface of dry mud and the solid surface plays a major role on dry mud removal from surfaces. Figure (5.14) and (5.15) shows the tensile data for another two different samples while appendix (B) shows the numerical raw data used to draw these figures.

Table 5.5. Adhesion work obtained from the tangential force measurements.

	Adhesion Work (mJ)
Dry Mud	0.119±0.008
Mud Solution	0.536.1±0.01

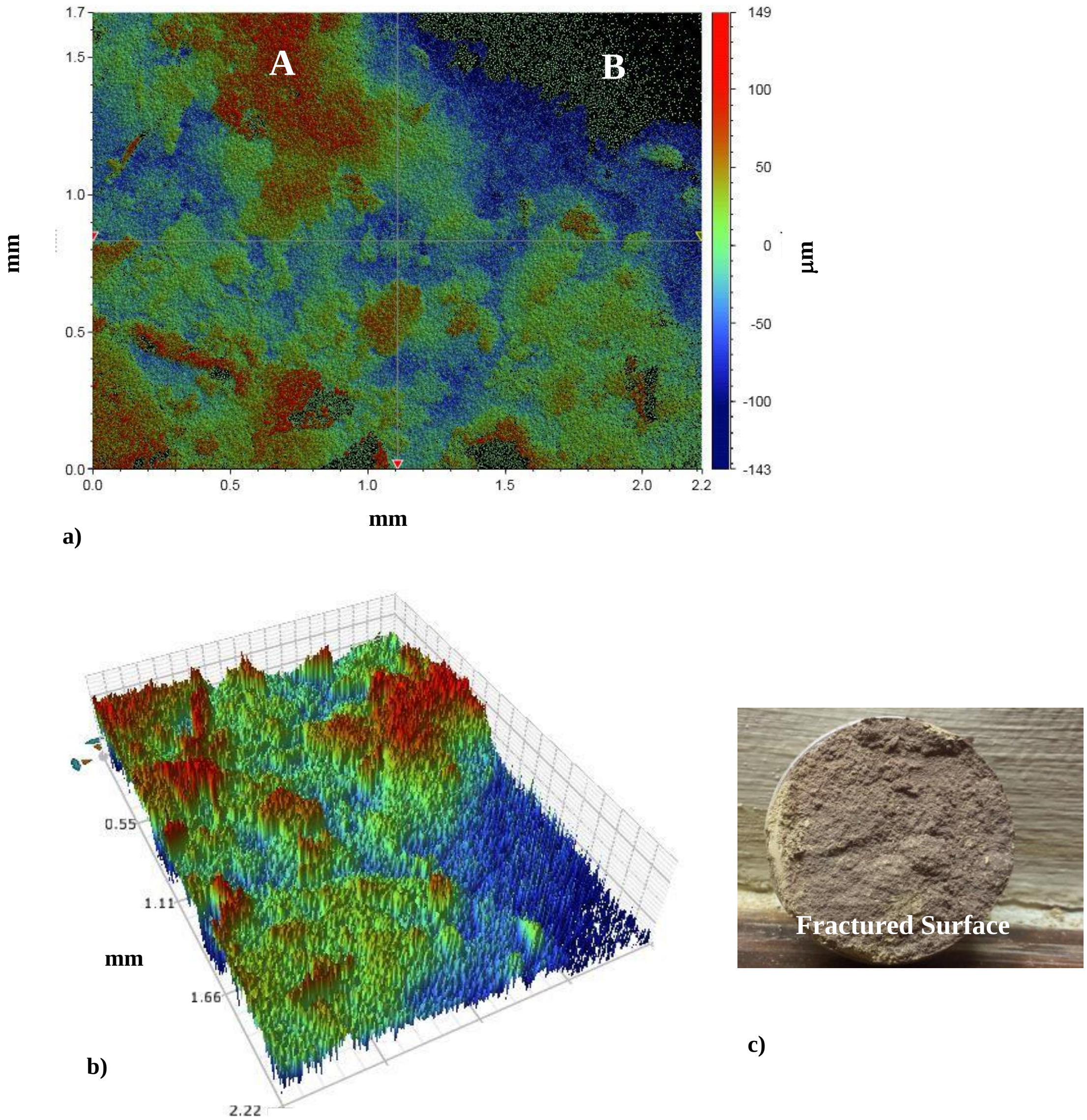

Figure 5.12. Optical image of the fractured pellet surface after tensile tests: a) 2-dimensional image showing texture height distribution, b) 3-dimensional view of texture of fractured surface, and c) optical image of fractured surface (pellet diameter is 4 mm).

(a)

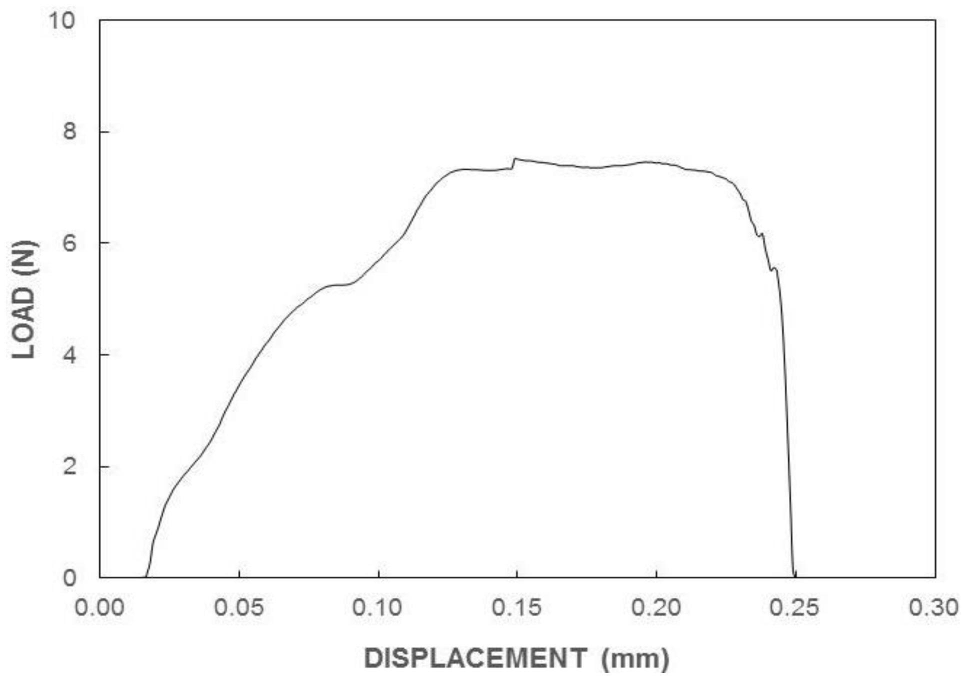

(b)

Figure 5.13. The data obtained from tensile testing for sample (1): a) the fractured tested sample, the circles show closely packet mixture of dry mud solution and fine size dust particles b) Load-displacement curve for tensile test of dry mud pellet

(a)

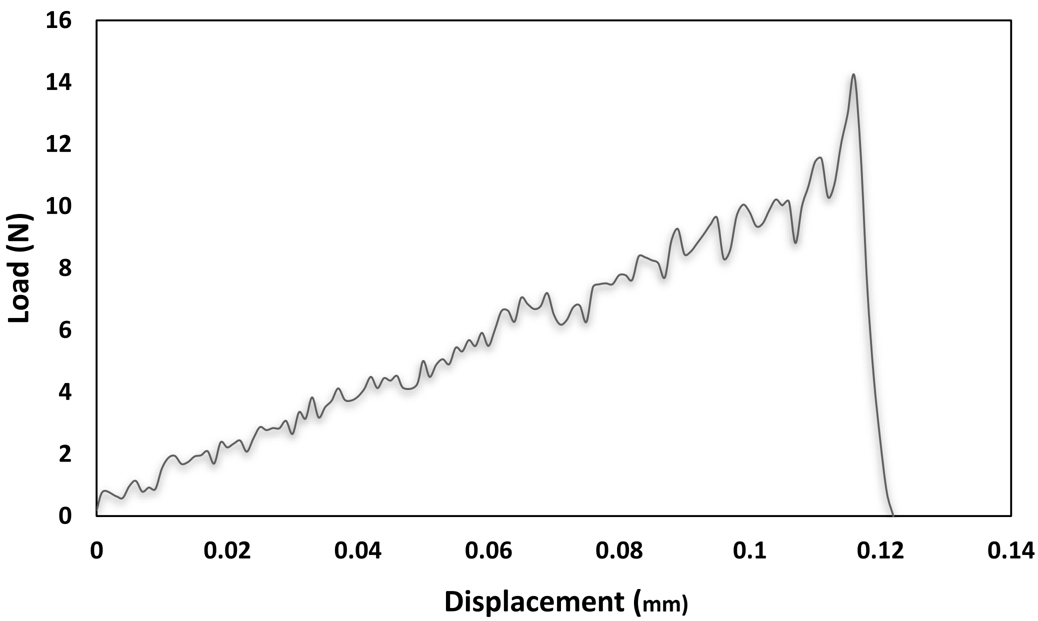

(b)

Figure 5.14. The data obtained from tensile testing for sample (2): a) the fractured tested sample, the circles show closely packet mixture of dry mud solution and fine size dust particles b) Load-displacement curve for tensile test of dry mud pellet.

(a)

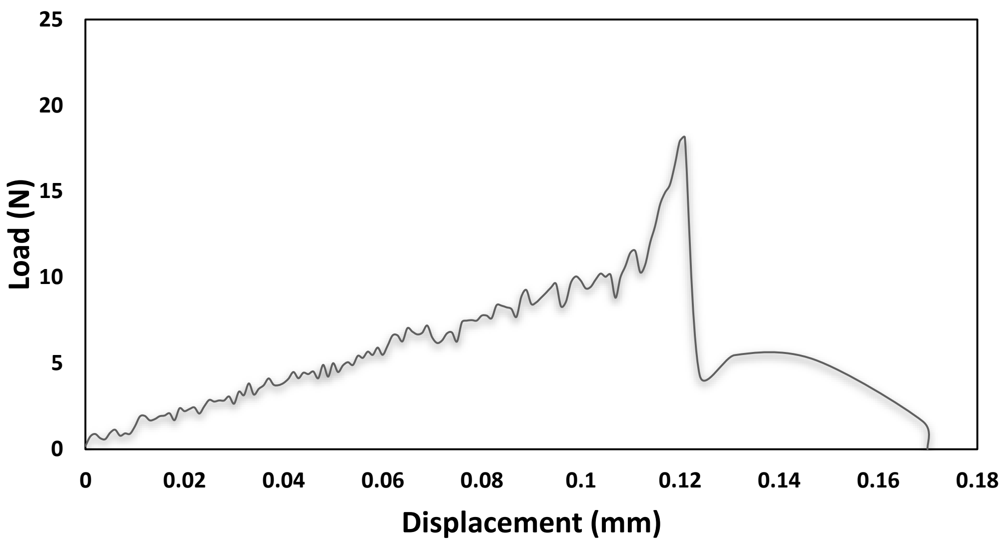

(b)

Figure 5.15. The data obtained from tensile testing for sample (3): a) the fractured tested sample , the circles show the closely packet mixture of dry mud solution and fine size dust particles b) Load-displacement curve for tensile test of dry mud pellet.

CHAPTER 6

CONCLUSIONS AND RECOMMENDATION

6.1 Conclusions

Glasses are used as protective cover for photovoltaic panels to protect photo-active surfaces from environmental effects such as dusts and humidity. Environmental dust particles settle at surfaces and form mud in humid air conditions because of condensation of water vapor on dust particles. Since dust particles contain alkaline and alkaline earth metal compounds, they dissolve in water and form mud solution, which flows in between dust particles under the gravity and sediments at solid surfaces. Therefore, a thin film of mud solution is formed in between dry mud and solid surface once mud is dried. This alters the characteristics of solid surface and binding forces at the dry mud solid interface. Consequently, in the present study, chemo-mechanical characteristics of dry mud formed from environmental dust particles are examined in relation to dry mud adhesion on glass surfaces. Dust particles, mud solution, and dry mud are analyzed using analytical tools including scanning electron and atomic force microscopes, energy dispersive spectroscopy, X-ray diffraction, and plasma mass spectroscopy. Friction coefficient of glass surface after dry mud removal is measured and adhesion and cohesion works required removing dry mud from glass surface are determined by tangential force measurements and tensile test data. It is found that dust particles have various sizes and small dust particles do attach on large size particle surfaces because of electrostatic charges. Alkaline and alkaline earth metals dissolve in water creating a mud solution, which has a base character (pH = 7.5). Mud solution forms crystals at solid surface upon drying. Some dry mud residues are left on glass surface after pressurized distilled water jet cleaning. The presence of dry mud residues is associated with strong adhesion of dry mud occurring locally on glass surface. Dried liquid film formed by mud solution at the interface of dry mud and glass surface is responsible for improved adhesion. Measurement of adhesion work from tangential force component during mechanical removal of dry mud from glass surface demonstrates that adhesion work is significantly higher than the frictional work. Tensile test data shows that binding forces for dry mud consists of cohesion and adhesion forces. Based on the consideration of the area ratio of closely spaced small dust particles covered by dry mud solution on fractured surface over the total area of test samples fractured surface, the cohesion force acts on 22% of the fractured pellet surface. Although the coverage fractured area is small for cohesive forces, the cohesion work associated with binding of dry mud is larger than that of adhesion work.

6.2 Recommendation

The below list provides possible future study on the extension of the current study:

- Inclusion of chemicals such as solvents, to reduce dust adhesion and dry mud solution adhesion to the surface.
- Minimizing of dust accumulation and settlement prior to mud formation on surfaces with use of external electro-static efforts.
- Surface texturing lead to self-cleaning of active surfaces while minimizing dust accumulation.

References

[1] I. Dincer, “Renewable energy and sustainable development : a crucial review,” vol. 4, pp. 157–175, 2000.

[2] J. E. Cohen, “Human population: the next half century,” *Science (80-.).*, vol. 302, no. 5648, pp. 1172–1175, 2003.

[3] A. A. and L. El Chaar, “EFFECT OF WIND BLOWN SAND AND DUST ON PHOTOVOLTAIC ARRAYS,” *J. Chem. Inf. Model.*, vol. 53, no. September, pp. 1689–1699, 2013.

[4] N. N. Shinde, “Performance & Evaluation of Industrial Solar Cell w . r . t . Temperature and Humidity,” vol. 5762, pp. 69–73, 2011.

[5] R. Appels, B. Lefevre, B. Herteleer, H. Goverde, A. Beerten, R. Paesen, K. De Medts, J. Driesen, and J. Poortmans, “Effect of soiling on photovoltaic modules,” *Sol. Energy*, vol. 96, pp. 283–291, 2013.

[6] J. T. Mccarthy, O. F. Canziani, N. A. Leary, and D. D. Dokken, “Book Reviews,” vol. 95, pp. 321–323, 2003.

[7] S. a M. Said and H. M. Walwil, “Fundamental studies on dust fouling effects on PV module performance,” *Sol. Energy*, vol. 107, pp. 328–337, 2014.

[8] R. a Sims, a S. Biris, J. D. Wilson, C. U. Yurteri, M. K. Mazumder, C. I. Calle, and C. R. Buhler, “Development of a transparent self-cleaning dust shield for solar panels,” *Proc. ESA-IEEE Jt. Meet. Electrost.*, no. 1, pp. 814–821, 2003.

[9] L. K. Verma, M. Sakhuja, J. Son, a. J. Danner, H. Yang, H. C. Zeng, and C. S. Bhatia, “Self-cleaning and antireflective packaging glass for solar modules,” *Renew. Energy*, vol. 36, no. 9, pp. 2489–2493, 2011.

[10] P. G. C. Petean and M. L. Aguiar, “Determining the adhesion force between particles and rough surfaces,” *Powder Technol.*, vol. 274, pp. 67–76, 2015.

[11] A. Kumar, T. Staedler, and X. Jiang, “Role of relative size of asperities and adhering particles on the adhesion force,” *J. Colloid Interface Sci.*, vol. 409, pp. 211–218, 2013.

[12] D. C. Jordan, J. H. Wohlgemuth, and S. R. Kurtz, “Technology and Climate Trends in PV Module Degradation Preprint,” no. October, 2012.

[13] S. Mekhilef, R. Saidur, and M. Kamalisarvestani, “Effect of dust , humidity and air velocity on efficiency of photovoltaic cells,” *Renew. Sustain. Energy Rev.*, vol. 16, no. 5, pp. 2920–2925, 2012.

[14] M. Mani and R. Pillai, “Impact of dust on solar photovoltaic (PV) performance: Research status, challenges and recommendations,” *Renew. Sustain. Energy Rev.*, vol. 14, no. 9, pp. 3124–3131, 2010.

[15] F. Kurokawat, T. Satot, and H. Matsuot, “Degradation of Output Characteristics of a Small Photovoltaic Module Due to Dirt Spots,” no. 5, pp. 421–426, 2005.

[16] H. K. Elminir, A. E. Ghitas, R. H. Hamid, F. El-Hussainy, M. M. Beheary, and K. M. Abdel-Moneim, “Effect of dust on the transparent cover of solar collectors,” *Energy Convers. Manag.*, vol. 47, no. 18–19, pp. 3192–3203, 2006.

[17] H. Jiang, L. Lu, and K. Sun, “Experimental investigation of the impact of airborne dust deposition on the performance of solar photovoltaic (PV) modules,” *Atmos. Environ.*, vol. 45, no. 25, pp. 4299–4304, 2011.

[18] K. Brown, T. Narum, N. Jing, and S. Paul, “Soiling Test Methods and their Use in Predicting Performance of Photovoltaic Modules in Soiling Environments,” *Photovolt. Spec. Conf. (PVSC), 2012 38th IEEE*, pp. 1881–1885, 2012.

[19] F. Touati, M. Al-Hitmi, and H. Bouchech, “Towards understanding the effects of climatic and environmental factors on solar PV performance in arid desert regions (Qatar) for various PV technologies,” *2012 First Int. Conf. Renew. Energies Veh. Technol.*, pp. 78–83, 2012.

[20] D. S. Rajput and K. Sudhakar, “Effect of dust on the performance of solar PV panel,” *Int. J. ChemTech Res.*, vol. 5, no. 2, pp. 1083–1086, 2013.

[21] S. Ghazi, A. Sayigh, and K. Ip, “Dust effect on flat surfaces – A review paper,” *Renew. Sustain. Energy Rev.*, vol. 33, pp. 742–751, 2014.

[22] A. A. Kazem, M. T. Chaichan, and H. A. Kazem, “Dust effect on photovoltaic utilization in Iraq: Review article,” *Renew. Sustain. Energy Rev.*, vol. 37, pp. 734–749, 2014.

[23] L. Boyle, H. Flinchpaugh, and M. P. Hannigan, “Natural soiling of photovoltaic cover plates and the impact on transmission,” *Renew. Energy*, vol. 77, pp. 166–173, 2015.

[24] S. A. M. Said, “Effects of dust accumulation on performances of thermal and photovoltaic flat-plate collectors,” *Appl. Energy*, vol. 37, no. 1, pp. 73–84, 1990.

[25] M. J. Adinoyi and S. a M. Said, “Effect of dust accumulation on the power outputs of solar photovoltaic modules,” *Renew. Energy*, vol. 60, pp. 633–636, 2013.

[26] S. A. M. Said, N. Al-Aqeeli, and H. M. Walwil, “The potential of using textured and anti-reflective coated glasses in minimizing dust fouling,” *Sol. Energy*, vol. 113, pp. 295–302, 2015.

[27] M. M. Rahman, M. Hasanuzzaman, and N. A. Rahim, “Effects of various parameters on PV-module power and efficiency,” *Energy Convers. Manag.*, vol. 103, pp. 348–358, 2015.

[28] B. M. A. Mohandes and L. A. Lamont, “Application Study of 500 W Photovoltaic (PV) System in the UAE 1,” vol. 45, no. 4, pp. 242–247, 2009.

[29] E. Boykiw, "The Effect of Settling Dust in the Arava Valley on the Performance of Solar Photovoltaic Panels," pp. 1–36, 2011.

[30] F. Touati, a. Massoud, J. Abu-Hamad, and S. a. Saeed, "Effects of Environmental and Climatic Conditions on PV Efficiency in Qatar," *Renew. Energy Power Qual. J.*, no. 11, p. 275, 2013.

[31] L. Chaar, A. Jamaleddine, F. Ajmal, and H. Khan, "Effect of wind blown sand and dust on PV arrays especially in UAE," in *Power Systems Conference (PSC)*, 2008.

[32] A. A. Hegazy, "Effect of dust accumulation on solar transmittance through glass covers of plate-type collectors," vol. 22, pp. 525–540, 2001.

[33] L. Clarke, M. S. Elatrash, and S. L. O. H. Ã, "Field measurements of desert dust deposition in Libya," vol. 40, pp. 3881–3897, 2006.

[34] D. Goossens, Z. Y. Offer, and A. Zangvil, "WIND TUNNEL EXPERIMENTS AND FIELD INVESTIGATIONS OF EOLIAN DUST DEPOSITION ON PHOTOVOLTAIC SOLAR COLLECTORS," vol. 50, no. 1, pp. 75–84, 1993.

[35] D. Goossens and E. V. A. N. Kerschaever, "AEOLIAN DUST DEPOSITION ON PHOTOVOLTAIC SOLAR CELLS : THE EFFECTS OF WIND VELOCITY AND AIRBORNE DUST CONCENTRATION ON CELL PERFORMANCE," vol. 66, no. 4, pp. 277–289, 1999.

[36] J. R. Gaier and M. E. Perez-davis, "Effect of Particle Size of Martian Dust on the Degradation of Photovoltaic Cell Performance," 1992.

[37] H. A. AlBusairi, 1, * and Hans Joachim Möller, and 2, "PERFORMANCE EVALUATION OF CdTe PV MODULES UNDER NATURAL OUTDOOR CONDITIONS IN KUWAIT," 2010, no. September, pp. 3468–3470.

[38] M. Piliougine, C. Cañete, R. Moreno, J. Carretero, J. Hirose, S. Ogawa, and M. Sidrach-de-cardona, "Comparative analysis of energy produced by photovoltaic modules with anti-soiling coated surface in arid climates," *Appl. Energy*, vol. 112, pp. 626–634, 2013.

[39] S. Ghazi and K. Ip, "The effect of weather conditions on the efficiency of PV panels in the southeast of UK," *Renew. Energy*, vol. 69, pp. 50–59, 2014.

[40] K. Brown, T. Narum, and N. Jing, "Soiling test methods and their use in predicting performance of photovoltaic modules in soiling environments," in *Photovoltaic Specialists Conference (PVSC), 2012 38th IEEE*, 2012, pp. 1881–1885.

[41] C. Ming, B. Khai, E. Chen, and K. Peng, "Microelectronics Reliability Humidity study of a-Si PV cell," *Microelectron. Reliab.*, vol. 50, no. 9–11, pp. 1871–1874, 2010.

[42] A. Ibrahim, "Effect of Shadow and Dust on the Performance of Silicon Solar Cell," vol. 1, no. 3, pp. 222–230, 2011.

[43] E. Photovoltaic, S. Energy, P. Tecnol, and S. Ochoa, “COMPARATIVE ANALYSIS OF THE DUST LOSSES IN PHOTOVOLTAIC,” no. September, pp. 2698–2700, 2008.

[44] H. Pang, J. Close, and K. Lam, “Study on effect of urban pollution to performance of commercial copper indium diselenide modules,” in *Photovoltaic Energy Conversion, Conference Record of the 2006 IEEE 4th World Conference on*, 2006, vol. 2, pp. 2195–2198.

[45] J. K. Kaldellis and A. Kokala, “Quantifying the decrease of the photovoltaic panels ’ energy yield due to phenomena of natural air pollution disposal,” *Energy*, vol. 35, no. 12, pp. 4862–4869, 2010.

[46] L. I. N. Jing, Z. Zhi-jun, Y. U. Ji-lin, and B. A. I. Yi-long, “My IOPscience A Thin Liquid Film and Its Effects in an Atomic Force Microscopy Measurement A Thin Liquid Film and Its Effects in an Atomic Force Microscopy Measurement,” vol. 086802, pp. 8–12.

[47] M. D. K. Ã, “Modeling of rates of moisture ingress into photovoltaic modules,” vol. 90, pp. 2720–2738, 2006.

[48] M. Corn, “*The* Adhesion *of Solid* Particles *to Solid* Surfaces, I. *a* Review,” *J. Air Pollut. Control Assoc.*, vol. 11, no. 11, pp. 523–528, 1961.

[49] G.W.Penny & E.H.Kilingler, “Contact Potentials and the Adhesion of Dust,” pp. 200–204, 1962.

[50] K. J. McLean, “Cohesion of Precipitated Dust Layer in Electrostatic Precipitators,” *J. Air Pollut. Control Assoc.*, vol. 27, no. 11, pp. 1100–1103, 1977.

[51] F. Podczeck, J. M. Newton, and M. B. James, “The influence of constant and changing relative humidity of the air on the autoadhesion force between pharmaceutical powder particles,” *Int. J. Pharm.*, vol. 145, no. 1–2, pp. 221–229, 1996.

[52] P. Somasundaran, H. K. Lee, E. D. Shchukin, and J. Wang, “Cohesive force apparatus for interactions between particles in surfactant and polymer solutions,” *Colloids Surfaces A Physicochem. Eng. Asp.*, vol. 266, no. 1–3, pp. 32–37, 2005.

[53] A. Fukunishi and Y. Mori, “Adhesion force between particles and substrate in a humid atmosphere studied by atomic force microscopy,” *Adv. Powder Technol.*, vol. 17, no. 5, pp. 567–580, 2006.

[54] Y. Zhong, Z. Wang, Z. Guo, and Q. Tang, “Defluidization behavior of iron powders at elevated temperature: Influence of fluidizing gas and particle adhesion,” *Powder Technol.*, vol. 230, pp. 225–231, 2012.

[55] a. Duri, M. George, M. Saad, E. Gastaldi, M. Ramonda, and B. Cuq, “Adhesion properties of wheat-based particles,” *J. Cereal Sci.*, vol. 58, no. 1, pp. 96–103, 2013.

[56] D. M. Jarząbek, M. Chmielewski, and T. Wojciechowski, “The measurement of the

adhesion force between ceramic particles and metal matrix in ceramic reinforced-metal matrix composites,” *Compos. Part A Appl. Sci. Manuf.*, vol. 76, pp. 124–130, 2015.

[57] J. Knoll, S. Knott, and H. Nirschl, “Characterization of the adhesion force between magnetic microscale particles and the influence of surface-bound protein,” *Powder Technol.*, vol. 283, pp. 163–170, 2015.

[58] R. Giovanol, J. L. Schnoor, L. Sigg, W. Stumm, and J. Zobrist, “CHEMICAL W E A T H E R I N G OF CRYSTALLINE ROCKS IN THE C A T C H M E N T A R E A OF ACIDIC TICINO LAKES , SWITZERLAND,” vol. 36, no. 6, pp. 521–529, 1988.

[59] S.-J. Park, D.-I. Seo, and C. Nah, “Effect of acidic surface treatment of red mud on mechanical interfacial properties of epoxy/red mud nanocomposites.,” *J. Colloid Interface Sci.*, vol. 251, no. 1, pp. 225–229, 2002.

[60] F. Pacheco-Torgal and S. Jalali, “Influence of sodium carbonate addition on the thermal reactivity of tungsten mine waste mud based binders,” *Constr. Build. Mater.*, vol. 24, no. 1, pp. 56–60, 2010.

[61] R. W. Style, S. S. L. Peppin, and A. C. F. Cocks, “Mud peeling and horizontal crack formation in drying clays,” *J. Geophys. Res. Earth Surf.*, vol. 116, no. 1, pp. 1–8, 2011.

[62] L. Goehring, R. Conroy, A. Akhter, W. J. Clegg, and A. F. Routh, “Evolution of mud-crack patterns during repeated drying cycles,” *Soft Matter*, vol. 6, no. 15, p. 3562, 2010.

[63] E. Santanach Carreras, F. Chabert, D. E. Dunstan, and G. V. Franks, “Avoiding ‘mud’ cracks during drying of thin films from aqueous colloidal suspensions,” *J. Colloid Interface Sci.*, vol. 313, no. 1, pp. 160–168, 2007.

[64] L. Pauling, *The nature of the chemical bond and the structure of molecules and crystals: an introduction to modern structural chemistry*, vol. 18. Cornell university press, 1960.

[65] D. Eisenberg and W. Kauzmann, “The structure and properties of water, Clarendon.” Oxford, 1969.

[66] H. S. Frank and W.-Y. Wen, “Ion-solvent interaction. Structural aspects of ion-solvent interaction in aqueous solutions: a suggested picture of water structure,” *Discuss. Faraday Soc.*, vol. 24, pp. 133–140, 1957.

[67] P. F. Low, “Physical chemistry of clay-water interaction,” *Adv. Agron.*, vol. 13, pp. 269–327, 1961.

[68] E. Materials, “Chapter 12 Weathering , sediment production and soils,” .

[69] W. Chiu and A. B. Wolbarst, “py rig hte d M ate ria l Co py rig hte d M ate ria l,” *Environ. Prot.*, no. 8, p. 2003, 2003.

[70] M. T. Postek, “The scanning electron microscope,” *Handb. Charg. Part. Opt.*, pp.

363–399, 1997.

[71] C. J. D. Catto and K. C. A. Smith, “Resolution limits in the surface scanning electron microscope,” *J. Microsc.*, vol. 98, no. 3, pp. 417–435, 1973.

[72] C. M. Lewandowski, *Introduction to Microscopic and Spectroscopic Methods Second Edition*, vol. 1. 2015.

[73] E. S. Velasco, “Scanning Electron Microscope (SEM) images as a means to determine dispersibility,” 2013.

APPENDIX

Appendix A

Table of Characteristic IR Absorptions used

Frequency, cm–1	Bond	Functional group
3640–3610 (s, sh)	O–H stretch, free hydroxyl	Phenols
3500–3200 (s,b)	O–H stretch, H–bonded	Alcohols, phenols
3400–3250 (m)	N–H stretch	1°, 2° amines, amides
3300–2500 (m)	O–H stretch	Carboxylic acids
3330–3270 (n, s)	–C≡C–H: C–H stretch	Alkynes (terminal)
3100–3000 (s)	C–H stretch	Aromatics
3100–3000 (m)	=C–H stretch	Alkenes
3000–2850 (m)	C–H stretch	Alkanes
2830–2695 (m)	H–C=O: C–H stretch	Aldehydes
2260–2210 (v)	C≡N stretch	Nitriles
2260–2100 (w)	–C≡C– stretch	Alkynes
1760–1665 (s)	C=O stretch	Carbonyls (general)
1760–1690 (s)	C=O stretch	Carboxylic acids
1750–1735 (s)	C=O stretch	Esters, saturated aliphatic
1740–1720 (s)	C=O stretch	Aldehydes, saturated aliphatic
1730–1715 (s)	C=O stretch	α, β–unsaturated esters
1715 (s)	C=O stretch	Ketones, saturated aliphatic
1710–1665 (s)	C=O stretch	α, β–unsaturated aldehydes, ketones

1680–1640 (m)	–C=C– stretch	Alkenes
1650–1580 (m)	N–H bend	1° amines
1600–1585 (m)	C–C stretch	(in–ring) aromatics
1550–1475 (s)	N–O asymmetric stretch	Nitro compounds
1500–1400 (m)	C–C stretch	(in–ring) aromatics
1470–1450 (m)	C–H bend	Alkanes
1370–1350 (m)	C–H rock	Alkanes
1360–1290 (m)	N–O symmetric stretch	Stretch nitro compounds
1335–1250 (s)	C–N stretch	Aromatic amines
1320–1000 (s)	C–O stretch	Alcohols, carboxylic acids, esters, ethers
1300–1150 (m)	C–H wag (–CH2X)	Alkyl halides
1250–1020 (m)	C–N stretch	Aliphatic amines
1000–650 (s)	=C–H bend	Alkenes
950–910 (m)	O–H bend	Carboxylic acids
910–665 (s, b)	N–H wag	1°, 2° amines
900–675 (s)	C–H	Aromatics
850–550 (m)	C–Cl stretch	Alkyl halides
725–720 (m)	C–H rock	Alkanes
700–610 (b, s)	–C≡C–H: C–H bend	Alkynes
690–515 (m)	C–Br stretch	Alkyl halides

s=strong, b=broad, m=medium, n=narrow, sh=sharp, w=weak,

Appendix B

The raw data extracted from tensile testing machine for dry mud specimens. The following table shows the load, relative displacement and scanning time for one sample.

Points	Scan Time sec	Displacement mm	Load N	Relative Displacement	Movers Axial &Temp
1	0	0	0.1881788	0	0
2	0.01	0.001	0.7471351	0.001	0
3	0.02	0.002	0.8868627	0.002	0
4	0.03	0.003	0.6459589	0.003	0
5	0.04	0.004	0.5867143	0.004	0
6	0.05	0.005	0.9598052	0.005	0
7	0.06	0.006	1.1355556	0.006	0
8	0.07	0.007	0.7894186	0.007	0
9	0.08	0.008	0.9242857	0.008	0
10	0.09	0.009	0.898843	0.009	0
11	0.1	0.01	1.3343318	0.01	0
12	0.11	0.011	1.9053414	0.011	0
13	0.12	0.012	1.9395154	0.012	0
14	0.13	0.013	1.6810615	0.013	0
15	0.14	0.014	1.7515766	0.014	0
16	0.15	0.015	1.9214516	0.015	0
17	0.16	0.016	1.962551	0.016	0
18	0.17	0.017	2.0924691	0.017	0
19	0.18	0.018	1.6933735	0.018	0
20	0.19	0.019	2.3813559	0.019	0
21	0.2	0.02	2.2160825	0.02	0
22	0.21	0.021	2.3378333	0.021	0
23	0.22	0.022	2.434329	0.022	0
24	0.23	0.023	2.0778182	0.023	0
25	0.24	0.024	2.4995238	0.024	0
26	0.25	0.025	2.8682845	0.025	0
27	0.26	0.026	2.7739286	0.026	0
28	0.27	0.027	2.8393893	0.027	0
29	0.28	0.028	2.8354585	0.028	0
30	0.29	0.029	3.0724091	0.029	0
31	0.3	0.03	2.6487574	0.03	0
32	0.31	0.031	3.3521081	0.031	0
33	0.32	0.032	3.1449327	0.032	0
34	0.33	0.033	3.8299359	0.033	0
35	0.34	0.034	3.1799111	0.034	0
36	0.35	0.035	3.5132967	0.035	0
37	0.36	0.036	3.7245355	0.036	0
38	0.37	0.037	4.1196721	0.037	0
39	0.38	0.038	3.7514674	0.038	0
40	0.39	0.039	3.729011	0.039	0
41	0.4	0.04	3.8523039	0.04	0
42	0.41	0.041	4.1046569	0.041	0
43	0.42	0.042	4.4929412	0.042	0
44	0.43	0.043	4.1304739	0.043	0
45	0.44	0.044	4.4502212	0.044	0
46	0.45	0.045	4.3711029	0.045	0
47	0.46	0.046	4.5242308	0.046	0
48	0.47	0.047	4.1284716	0.047	0
49	0.48	0.048	4.9091011	0.048	0
50	0.49	0.049	4.2255618	0.049	0
51	0.5	0.05	5.0044131	0.05	0
52	0.51	0.051	4.490973	0.051	0
53	0.52	0.052	4.8808134	0.052	0
54	0.53	0.053	5.0614286	0.053	0
55	0.54	0.054	4.9012941	0.054	0
56	0.55	0.055	5.4352402	0.055	0
57	0.56	0.056	5.3156707	0.056	0
58	0.57	0.057	5.677907	0.057	0
59	0.58	0.058	5.4872195	0.058	0
60	0.59	0.059	5.912757	0.059	0
61	0.6	0.06	5.4904511	0.06	0

62	0.61	0.061	6.0234221	0.061	0
63	0.62	0.062	6.6169683	0.062	0
64	0.63	0.063	6.6266292	0.063	0
65	0.64	0.064	6.2744503	0.064	0
66	0.65	0.065	7.0412451	0.065	0
67	0.66	0.066	6.8410556	0.066	0
68	0.67	0.067	6.6820192	0.067	0
69	0.68	0.068	6.7759459	0.068	0
70	0.69	0.069	7.1971905	0.069	0
71	0.7	0.07	6.508961	0.07	0
72	0.71	0.071	6.1806803	0.071	0
73	0.72	0.072	6.3288333	0.072	0
74	0.73	0.073	6.7411111	0.073	0
75	0.74	0.074	6.7877957	0.074	0
76	0.75	0.075	6.2640964	0.075	0
77	0.76	0.076	7.3868421	0.076	0
78	0.77	0.077	7.4809735	0.077	0
79	0.78	0.078	7.5090345	0.078	0
80	0.79	0.079	7.4832432	0.079	0
81	0.8	0.08	7.7715525	0.08	0
82	0.81	0.081	7.7738286	0.081	0
83	0.82	0.082	7.620197	0.082	0
84	0.83	0.083	8.3785714	0.083	0
85	0.84	0.084	8.3501786	0.084	0
86	0.85	0.085	8.2561215	0.085	0
87	0.86	0.086	8.1590041	0.086	0
88	0.87	0.087	7.6976796	0.087	0
89	0.88	0.088	8.874633	0.088	0
90	0.89	0.089	9.2659563	0.089	0
91	0.9	0.09	8.4525414	0.09	0
92	0.91	0.091	8.5414732	0.091	0
93	0.92	0.092	8.8179641	0.092	0
94	0.93	0.093	9.1035519	0.093	0
95	0.94	0.094	9.4113866	0.094	0
96	0.95	0.095	9.6231111	0.095	0
97	0.96	0.096	8.3150829	0.096	0
98	0.97	0.097	8.5780526	0.097	0
99	0.98	0.098	9.6836036	0.098	0
100	0.99	0.099	10.048939	0.099	0
101	1	0.1	9.8043939	0.1	0
102	1.01	0.101	9.3561694	0.101	0
103	1.02	0.102	9.4435965	0.102	0
104	1.03	0.103	9.8689552	0.103	0
105	1.04	0.104	10.215714	0.104	0
106	1.05	0.105	10.029045	0.105	0
107	1.06	0.106	10.153371	0.106	0
108	1.07	0.107	8.8117391	0.107	0
109	1.08	0.108	9.9957005	0.108	0
110	1.09	0.109	10.648152	0.109	0
111	1.1	0.11	11.425291	0.11	0
112	1.11	0.111	11.529659	0.111	0
113	1.12	0.112	10.291092	0.112	0
114	1.13	0.113	10.735565	0.113	0
115	1.14	0.114	12.011097	0.114	0
116	1.15	0.115	12.979732	0.115	0
117	1.16	0.116	14.232959	0.116	0
118	1.17	0.117	14.920946	0.117	0
119	1.18	0.118	15.393717	0.118	0
120	1.19	0.119	16.564741	0.119	0
121	1.2	0.12	17.931071	0.12	0
122	1.21	0.121	18.135	0.121	0
123	1.22	0.124	4.31	0.124	0
124	1.23	0.131	5.47	0.131	0
125	1.24	0.147	5.23	0.147	0
126	1.25	0.169	1.63	0.169	0
127	1.26	0.17	0	0.17	0

Appendix C

A: The SEM images for the mud fracture surfaces after tensile testing.

<u>Sample 1</u>

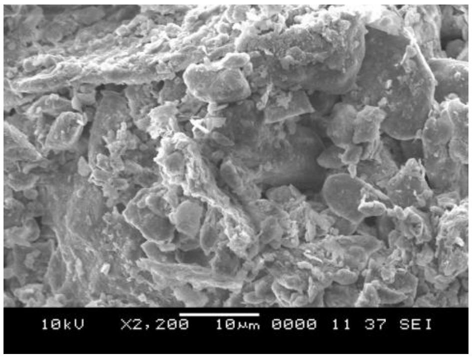

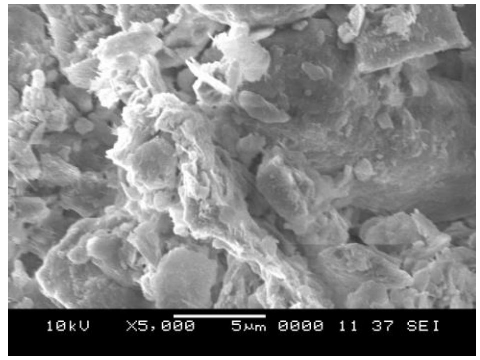

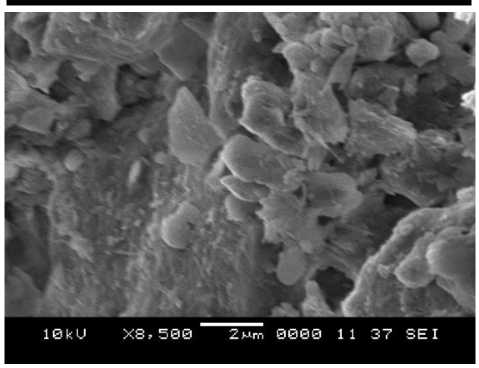

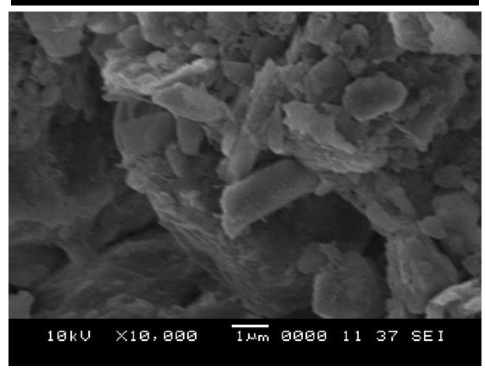

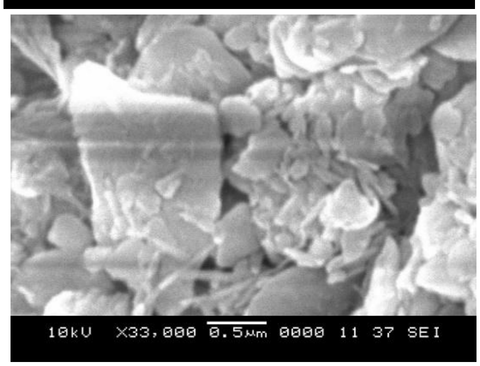

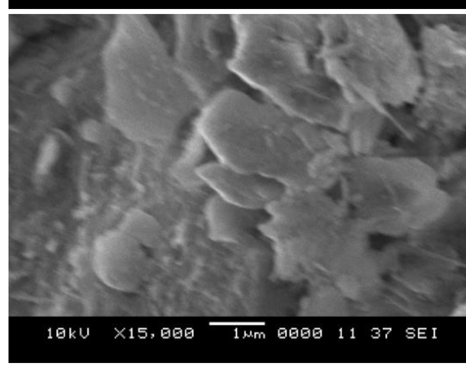

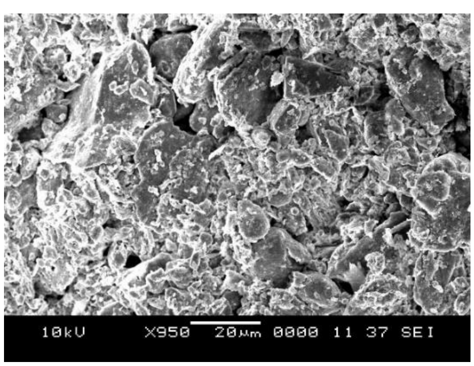

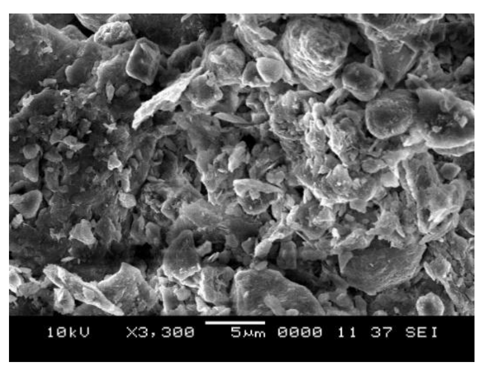

<u>Sample 2</u>

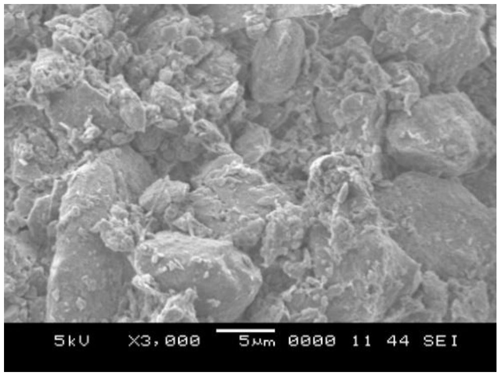
5kV X3,000 5µm 0000 11 44 SEI

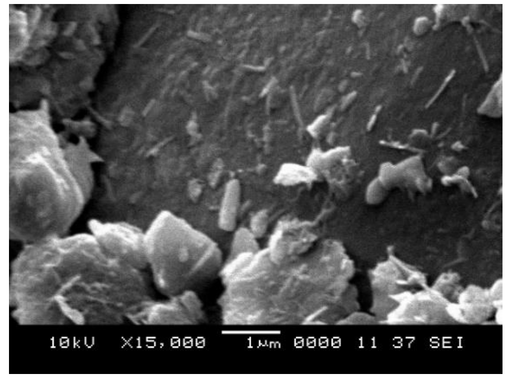
10kV X15,000 1µm 0000 11 37 SEI

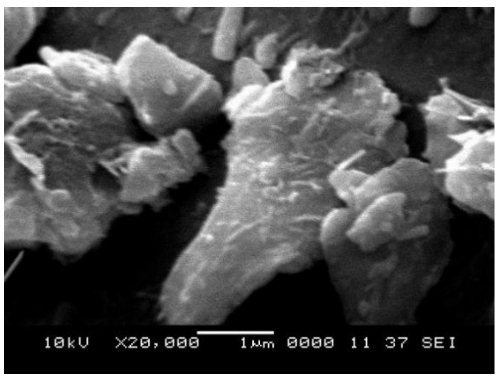
10kV X20,000 1µm 0000 11 37 SEI

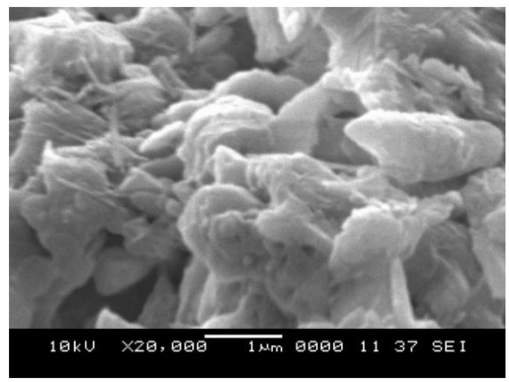
10kV X20,000 1µm 0000 11 37 SEI

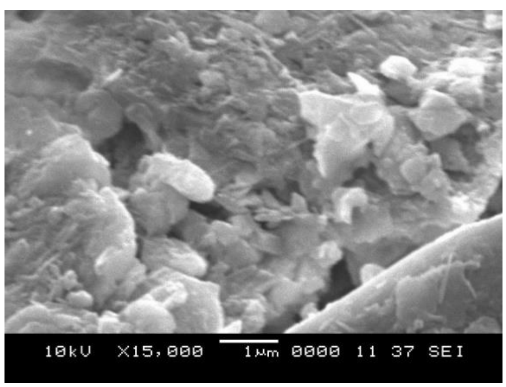
10kV X15,000 1µm 0000 11 37 SEI

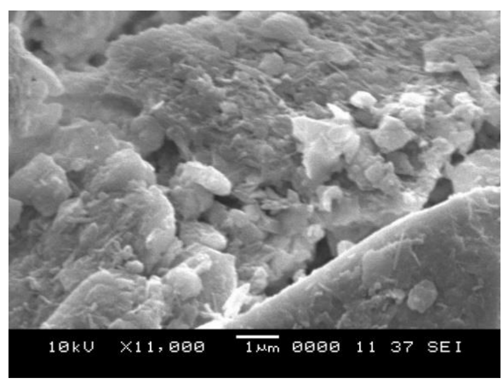
10kV X11,000 1µm 0000 11 37 SEI

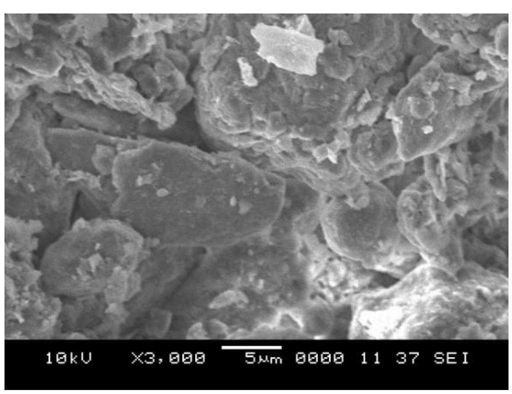
10kV X3,000 5µm 0000 11 37 SEI

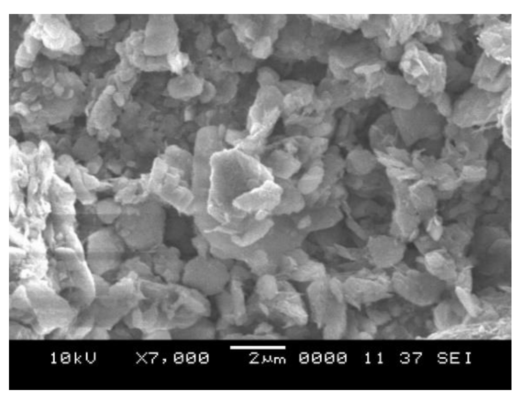
10kV X7,000 2µm 0000 11 37 SEI

Sample 3

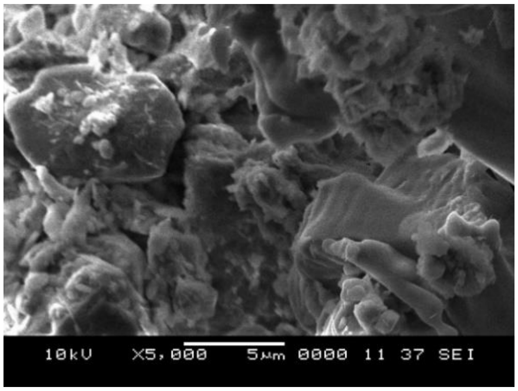
10kV X5,000 5µm 0000 11 37 SEI

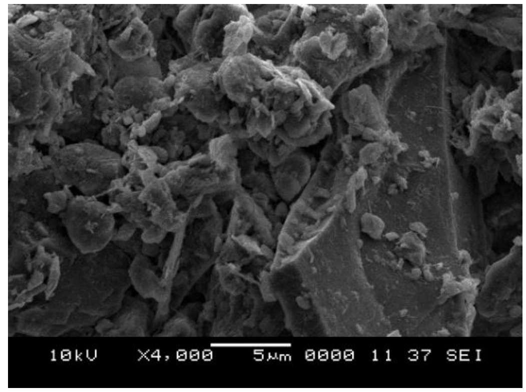
10kV X4,000 5µm 0000 11 37 SEI

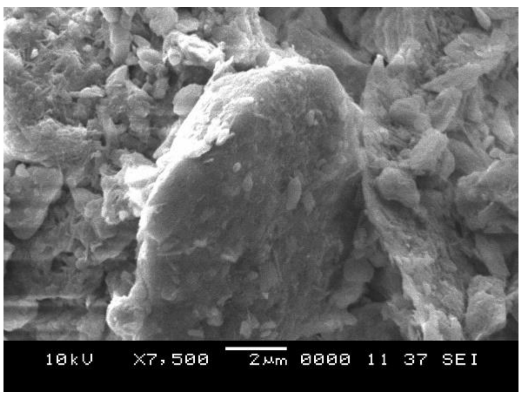
10kV X7,500 2µm 0000 11 37 SEI

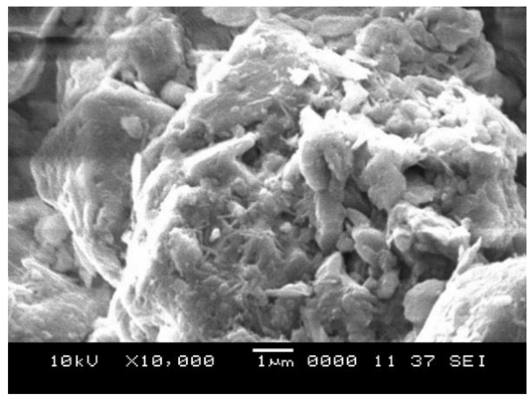
10kV X10,000 1µm 0000 11 37 SEI

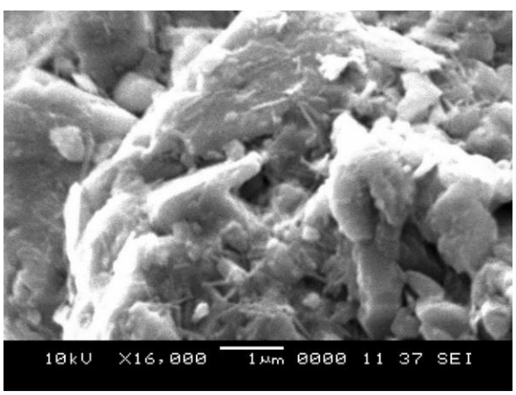
10kV X16,000 1µm 0000 11 37 SEI

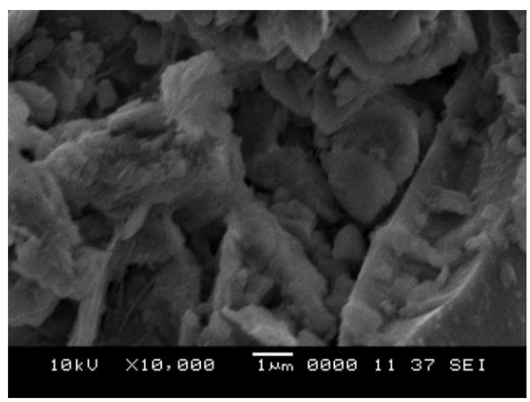
10kV X10,000 1µm 0000 11 37 SEI

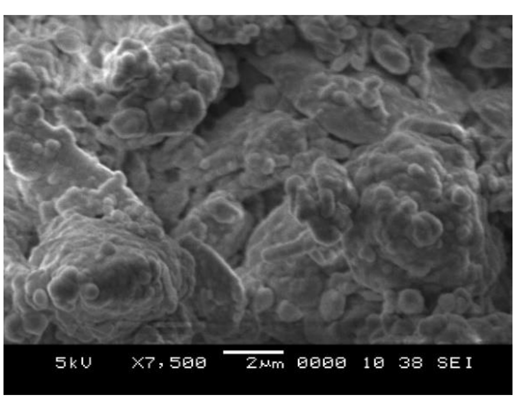
5kV X7,500 2µm 0000 10 38 SEI

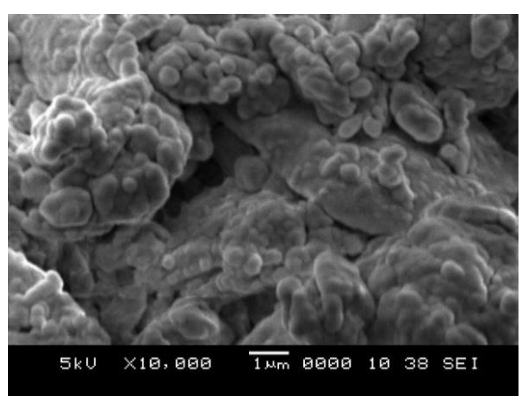
5kV X10,000 1µm 0000 10 38 SEI

B: The SEM images at different locations and magnifications for the dry mud solution specimens on the glass surfaces.

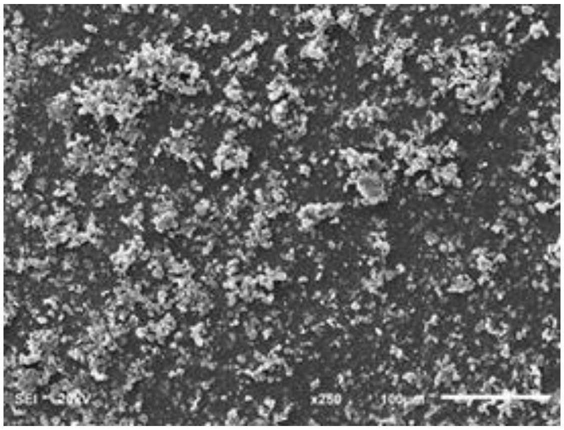

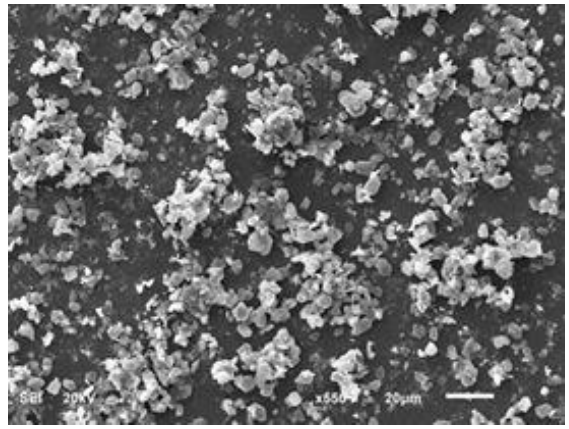

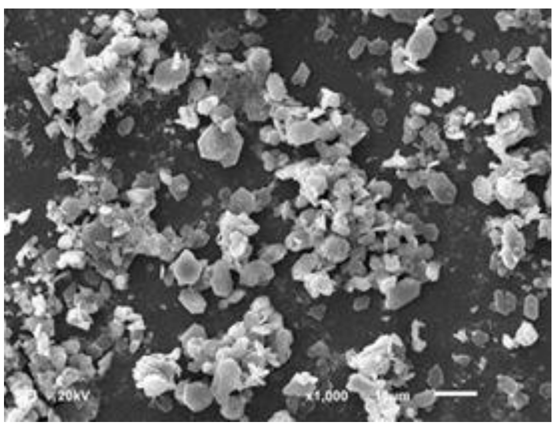

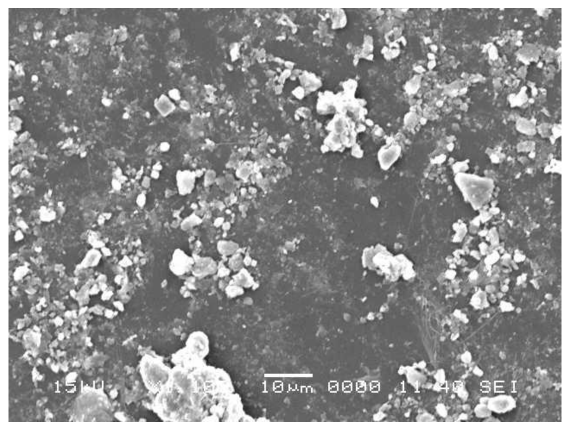

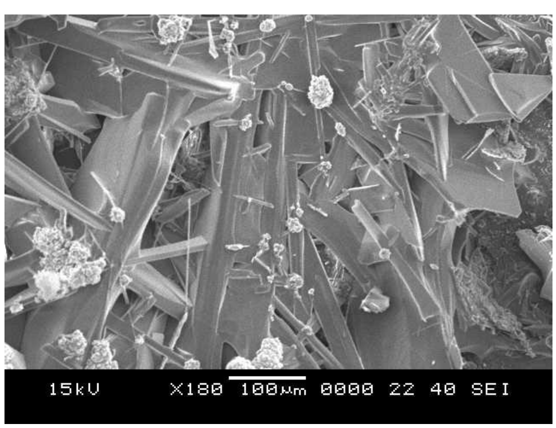

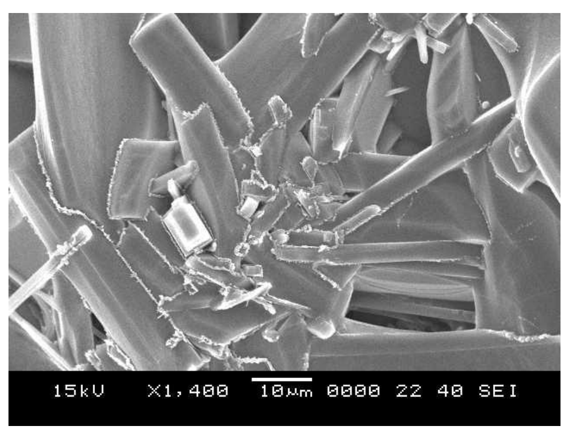

Appendix D

The 3D images for the mud fracture surfaces samples after tensile testing at different locations.

<u>Sample 1</u>

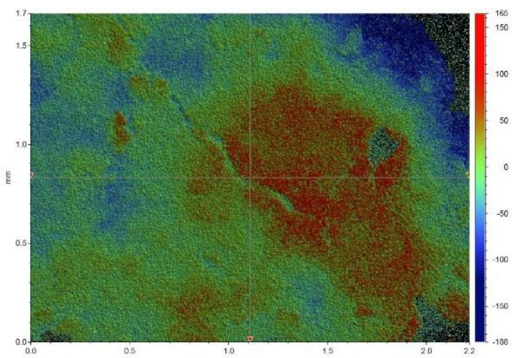

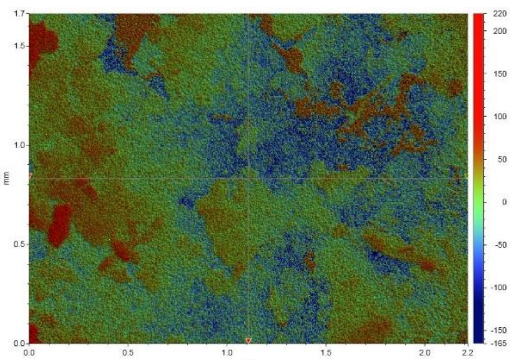

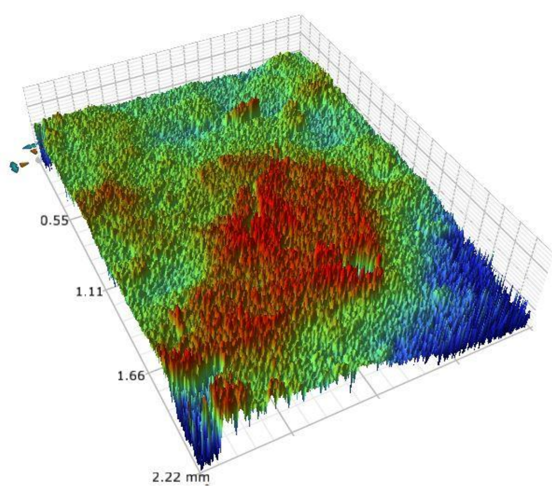

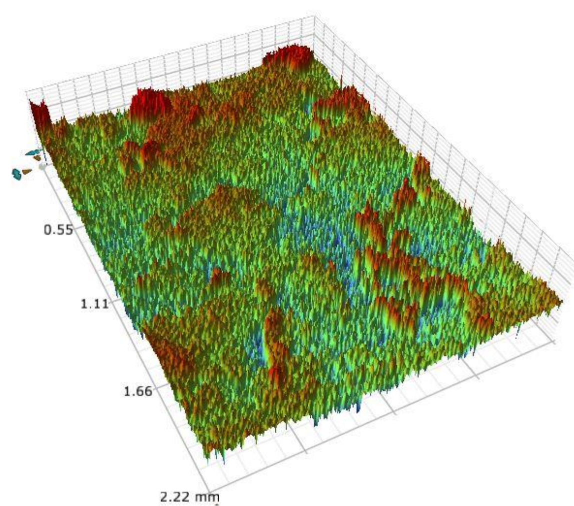

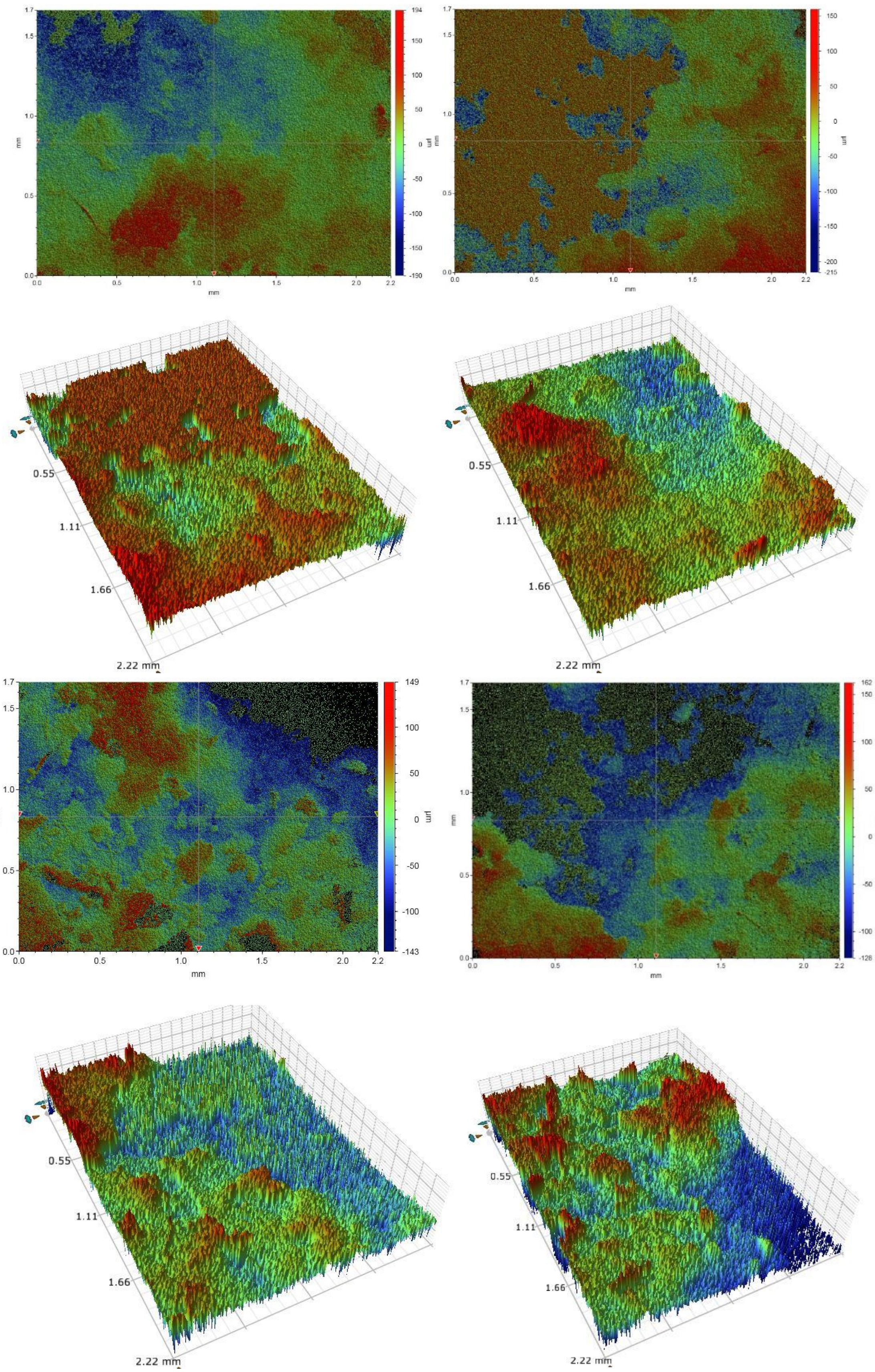
mm
0.55
1.11
1.66
2.22 mm

Sample 2

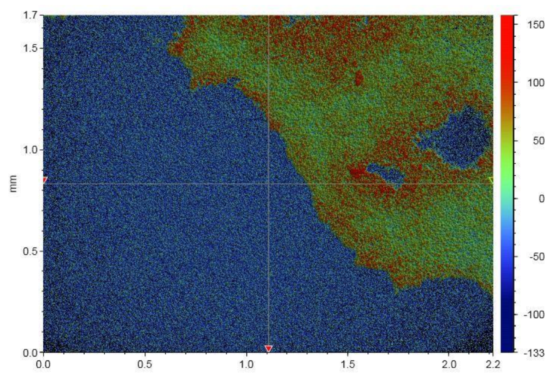
mm
µm
0.0
0.5
1.0
1.5
1.7
2.0
2.2
150
100
50
0
-50
-100
-133

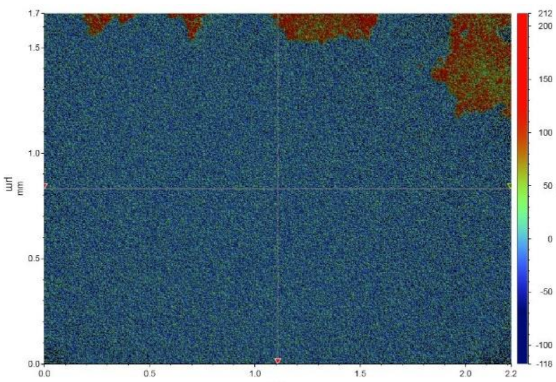
mm
µm
0.0
0.5
1.0
1.5
1.7
2.0
2.2
212
200
150
100
50
0
-50
-100
-118

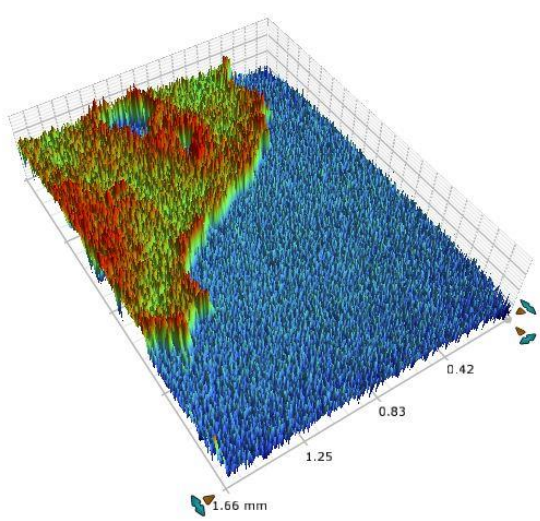
0.42
0.83
1.25
1.66 mm

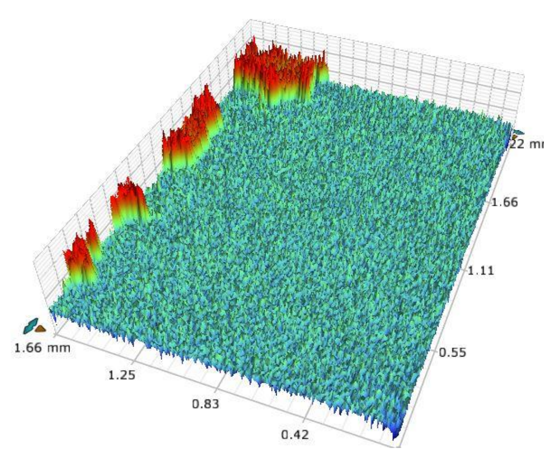
1.66 mm
1.25
0.83
0.42
0.55
1.11
1.66

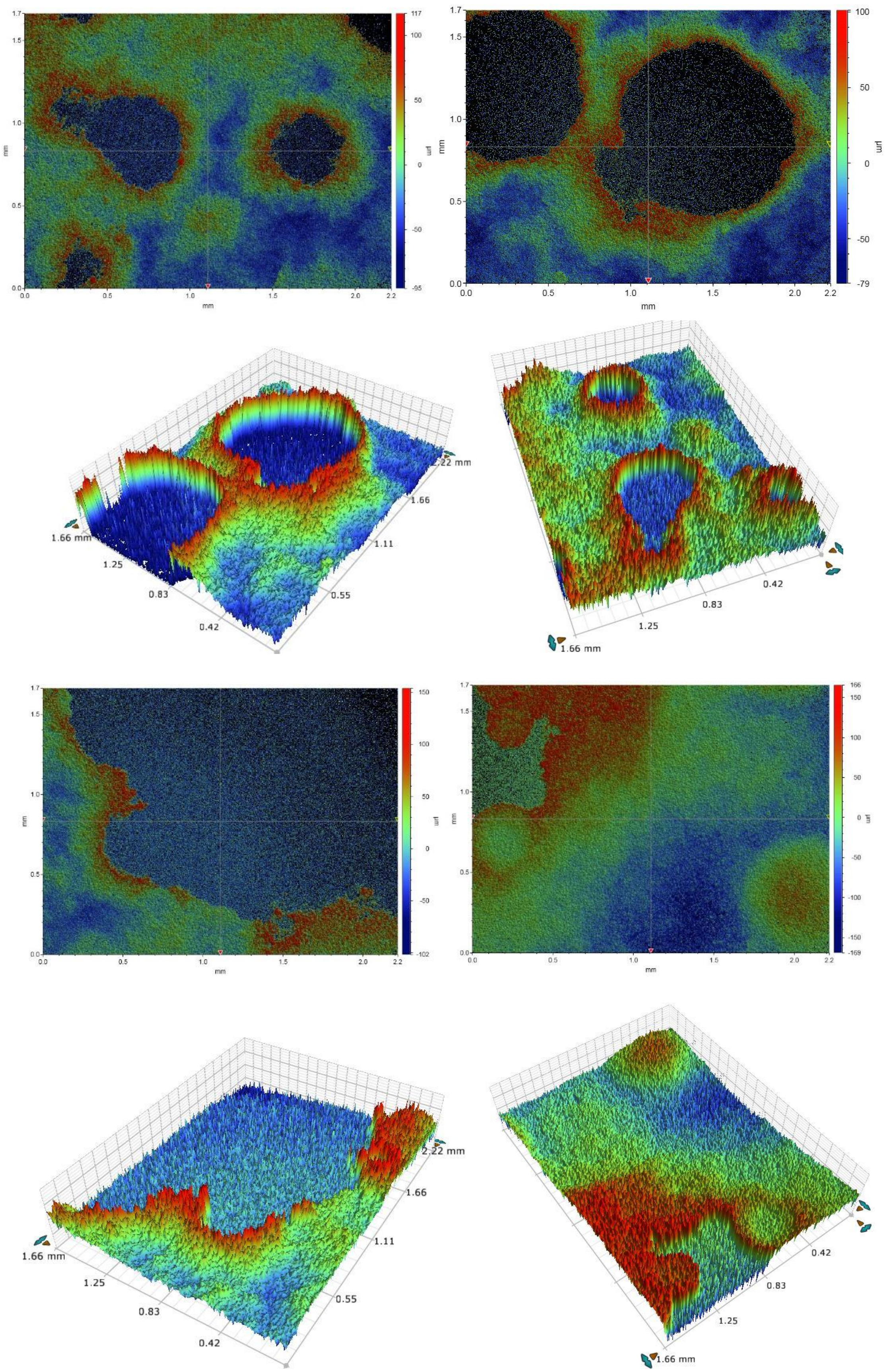

Vitae

Name	: Ghassan Hassan Hajhamed Abdelmajid
Nationality	: Sudanese
Date of Birth	: July 15, 1992
Email	: ghassanhassan93@hotmail.com
Address	: Kassala, Sudan
Academic Background	: **M.S (Mechanical Engineering)** May, 2016 King Fahd University of Petroleum and Minerals Dhahran, Saudi Arabia **B.Sc. (Mechanical Engineering)** September 2013 University of Khartoum Khartoum, Sudan